RAMAN AND PHOTOLUMINESCENCE STUDIES OF POLY (P-PHENYLENE SULFIDE) FILMS

By

ZHENGDA PAN

Bachelor of Science
Tsing Hua University
Beiging, China
1968

Master of Science
Oklahoma State University
Stillwater, Oklahoma
1989

Submitted to the Faculty of the
Graduate College of the
Oklahoma State University
in partial fulfillment of
the requirements for
the Degree of
DOCTOR OF PHILOSOPHY
December, 1992

RAMAN AND PHOTOLUMINESCENCE STUDIES OF POLY

(P-PHENYLENE SULFIDE) FILMS

Thesis Approved:

Thesis Adviser

Dean of the Graduate College

ACKNOWLEDGMENTS

I wish to express my sincere gratitude and appreciation to my dissertation advisor, Dr. J.P. Wicksted, for his guidance, support, and help throughout the entire research.

Appreciation is also acknowledged to Dr. R.C. Powell, Dr. H.L. Scott, Dr. J.P. Devlin, and Dr. J. Krasinski for serving on my dissertation committee.

Thanks are extended to Dr. W.T. Ford and Dr. Huimin Liu for their helpful discussions and to Dr. J.P. Devlin for helpful discussion and conducting IR measurements.

Finally, I want to thank my parents, my uncle, my wife, and my son for their love and encouragement throughout my student years at Oklahoma State University.

Financial support for this work was provided by the Oklahoma Center for the Advancement of Science and Technology (OCAST) under Contract No. 3757.

TABLE OF CONTENTS

LIST OF TABLES

LIST OF FIGURES

Figures Page

Figure Page

Figure Page

CHAPTER I

INTRODUCTION

Conducting Polymers

In 1977, the discovery of highly conducting polyacetylene [1], the prototype organic one-dimensional conducting polymer, touched off a flurry of research activity directed toward the study and discovery of new conducting polymeric systems. Shortly thereafter, highly conducting poly (p-phenylene) (PPP) was reported [2]. PPP is one of the highly conducting polymers derived from polyaromatics. The most striking property of these conducting polymers is that they become conductive upon "doping". The promise these materials may hold as synthetic replacements for metals or semiconductors in a variety of applications such as in high-energy density batteries, solar cells, and novel electronic devices, spurred an exponential rise in research activity around the world in both academic and industrial circles. Figure 1 shows the chemical formulas of the most important polymers which are known today to become conductive upon doping [3]. These conducting polymers can be classified as two classes [4]. Polymers which belong to class I are those which simply undergo electron transfer upon doping to produce the conducting complex. Polyacetylene, polyphenylene, and polypyrrole are examples of class I

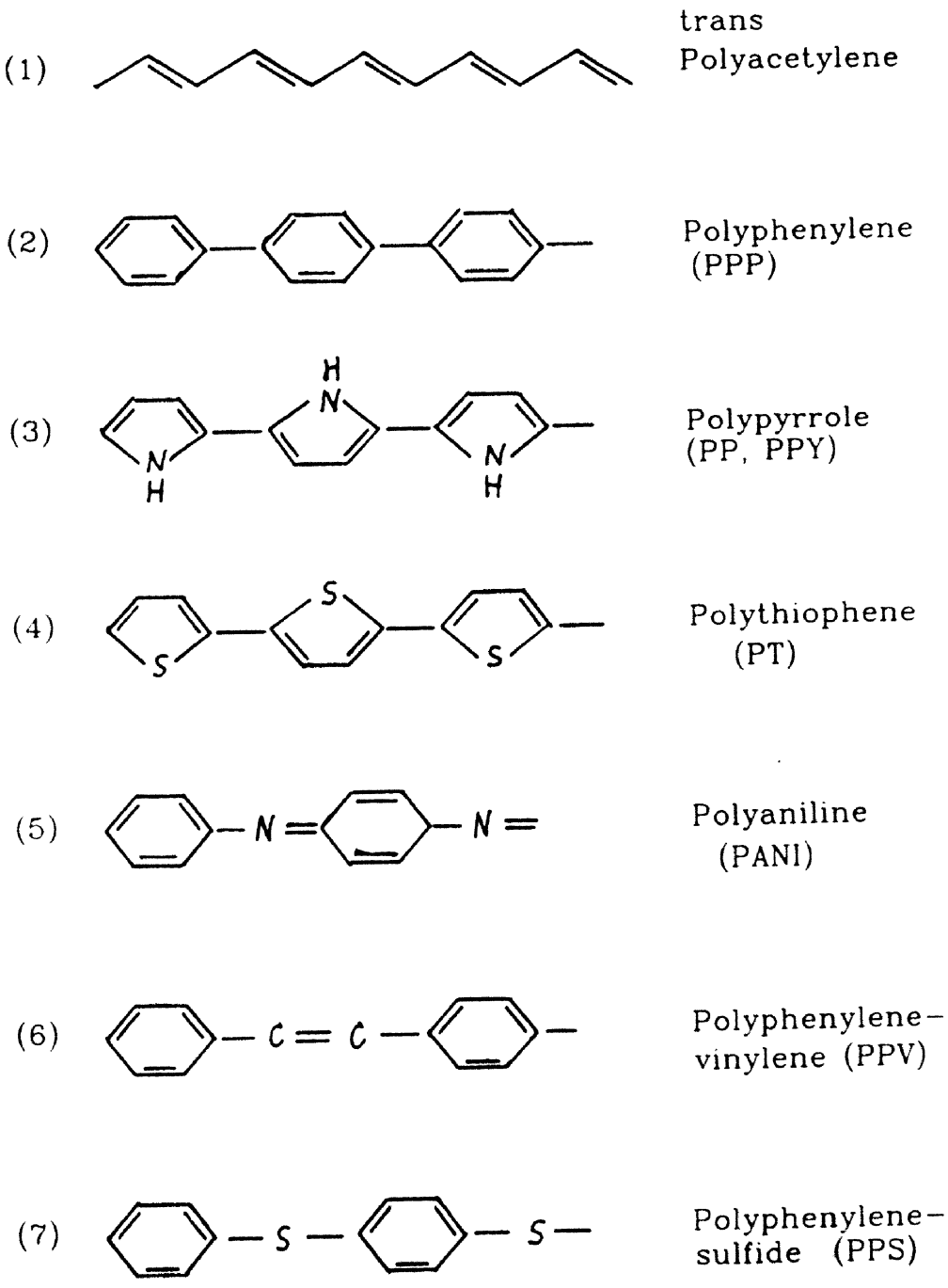

Figure 1. Chemical Structure of the Most Important Polymers Which Become Conducting Upon Doping (Ref.3).

polymers. Class II polymers are those which undergo chemical modification (carbon-carbon bond formation, for example) upon doping, which results in the formation of a new, highly conducting polymer complex. Poly (p-phenylene sulfide) falls into the second class.

All polymers in the first class have one feature in common: they possess conjugated double bonds (segments of the polymer chain where single and double bonds alternate regularly). Polyacetylene is the most thoroughly investigated in this area and very often it is considered a prototype of conductive polymers. At room temperature, the conductivity of the heavy doped polyacetylene ($[(CH)^{+y}(I_3)_y]_x$ with $y \approx 0.08$) is greater than 20,000 S/cm [5]. Even more recent improvements in synthesis and orientation have resulted in $\sigma = 1.5 \times 10^5$ S/cm [6]. It now appears quite clear that the intrinsic conductivity for doped polyacetylene is greater than that of copper (Copper has a conductivity of $\sigma \approx 590{,}000$ S/cm) [7]. This doping-induced conductivity change is a remarkable physical phenomenon.

The studies of polyacetylene have stimulated an awareness of the potential importance of the general class of conducting polymers, and they have stimulated the generation of new concepts [7,8] which are of broad interest to physics and chemistry.

However, there are two main problems in commercialization of polyacetylene. Instability is the chief obstacle to the

commercialization of polyacetylene. The undoped material is not stable in air and decomposes quite rapidly. An acceptable useful lifetime (10 years or longer) has not been achieved because the conductivity of the doped polymeric component decays. Additionally, polyacetylene is difficult to process even beyond the requirement that it be processed in an inert atmosphere [9]. The polyacetylene, as well as poly (p-phenylene), polypyrole, and poly (phenylene vinylene) are not melt or solution processible [10]. On the other hand, poly (p-phenylene sulfide) is easily melt processible, an important property for potentially obtaining commercial applications of the conducting polymers.

Poly (p-Phenylene Sulfide) (PPS)

Poly (phenylene sulfide), PPS, has a long history in the chemical literature. Reported syntheses of PPS or PPS-related resins date back almost 100 years. Commercial development activities began approximately 40 years ago, ultimately leading to the first commercial production of PPS in 1973 [11,12].

The structure of PPS consists of a series of alternating disubstituted aromatic ring (p-phenylene units) and divalent sulfur atoms (sulfide linkages), as shown in Figure 2. PPS is a semi-crystalline thermoplastic polymer which possesses excellent mechanical, electrical, thermal, and chemical resistance properties in addition to the polymer being inherently self-extinguishing. Because of this unique

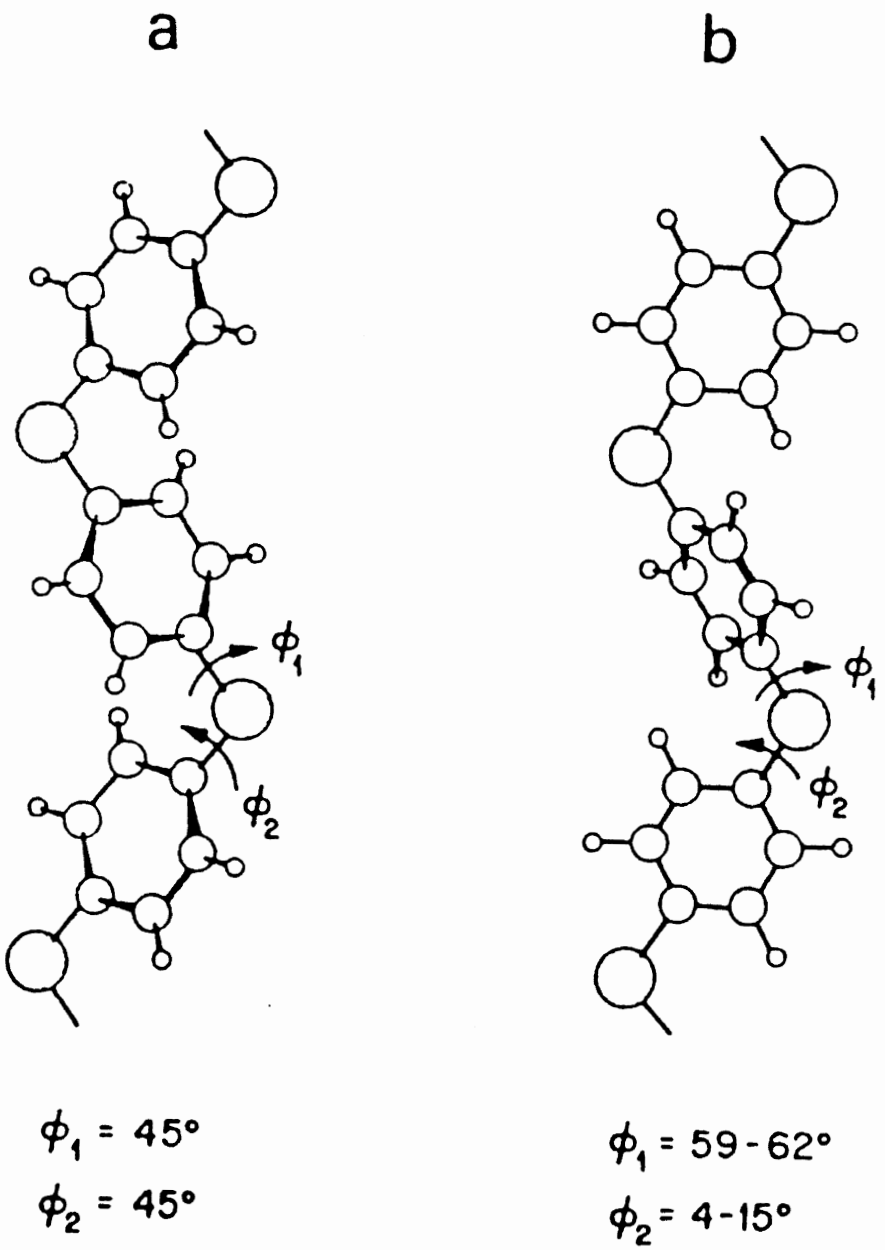

Figure 2. Two Molecular Models of the Conformation of PPS. The Three Types of Circles Represent S, C, and H Atoms in Decreasing Order of Size (Ref. 14).

combination of properties, PPS is referred to as one of the "engineering thermoplastics" [13].

The thermal transitions of PPS are appropriate for melt processing of material into finished parts. As defined by differential scanning calorimetry (DSC), PPS possesses a high crystalline melting point (T_m, 285^{0}C) and a modest glass transition temperature (T_g, 85^{0}C). The ability to mold PPS in a crystalline form is critical in order to achieve dimensional stable parts and to allow those parts to be used at elevated temperatures. According to an X-ray diffraction method described by Brady, fully crystallized PPS has a crystallinity index of about 65% [14].

The sulfur link in PPS plays a unique role. It provides both the flexible link between the aromatic rings necessary for processibility and the p orbitals on the sulfur atom for continuous orbital overlap along the polymer chain. Calculations on both the oligomers and the polymer show that even though the phenyl rings are orthogonal to one another, substantial orbital overlap occurs along the chain via participation of the lone pairs on the sulfur atoms [13].

PPS was the first nonrigid, not fully carbon-backbone-linked polymer made highly conducting upon doping [14,15]. This discovery was particularly exciting, because the pristine polymer is a commercially available melt and solution-processible polymer (Ryton, Phillips Petroleum Co.), and it provided precedent for potentially obtaining commercially

viable conducting plastics. PPS was not only the first processible polymer to be made highly conducting, but also the first system discovered to be processible in its conductive form. Furthermore, PPS is just one of what is now recognized as a general class of processible conducting polymers, namely, the polyphenylene chalcogenides [9].

Because of its high ionization potential (6.0 ev), only very aggressive (strongly oxidizing) agents such as AsF_5, SbF_5, NO^+ salts, SO_3, and the like are capable of forming doped, conductive complexes with PPS. Conductivities of around 1 S/cm are routinely obtained with AsF_5 doped compacted powder pellets or melt-molded films. Film produced from AsF_3 solution of PPS has a remarkably high conductivity of 200 S/cm after doping with AsF_5 [16].

AsF_5 doped PPS conducting complex differs in many ways from that obtained upon doping PPP. Both the IR and elemental analysis support the contention that the polymer has undergone some irreversible chemical modification upon doping. This modification was found to be predominantly intramolecular "crosslinking" (cyclization) whereby adjacent phenyl rings couple to form dibenzothiophene units along the polymer chain (Fig. 3). Studies [17] show that continuous π-orbital overlap along the polymer backbone plays an important role in obtaining conductive complexes.

The biggest markets for the PPS resin are in the electrical and electronics markets. Target development markets

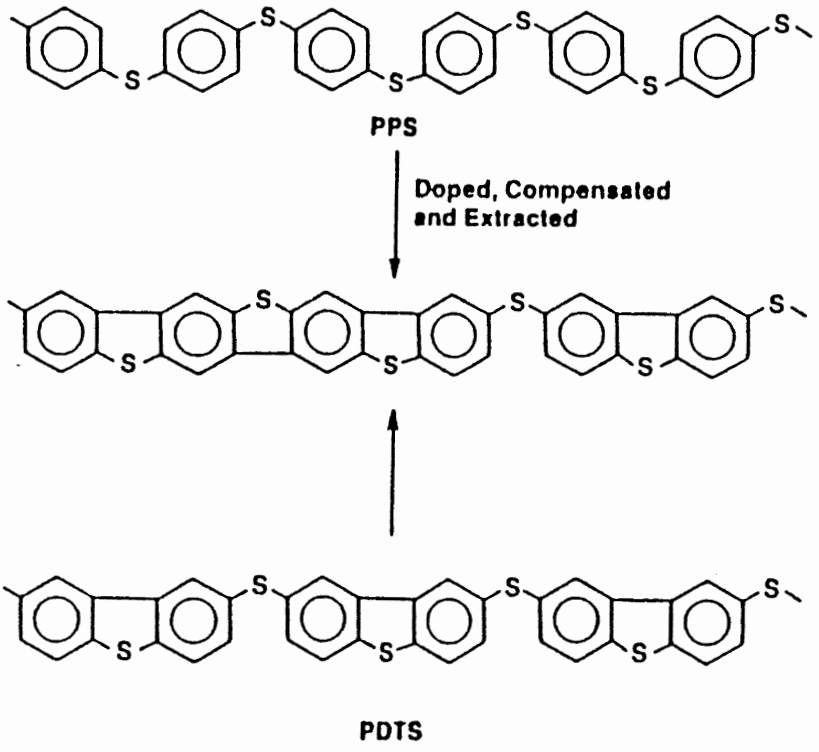

Figure 3. The Intramolecular Crosslinking upon Doping in PPS. (from Ref. 14)

include chemical process industry parts, fuel-line systems, gears, fittings, and other industrial parts. The market future for PPS is bright, forecasting that current worldwide PPS production of 22 million to 23 million Lbs will grow 10% annually through the late 1990s. PPS prices are a good deal lower than many of the other high-performance resins since their production volume is much higher than most others. Mineral-filled grades of PPS sell for between $1.60 and $2.00 a Lb, and glass-filled grades sell for more than $3.30. PPS's strongest market is as a backing for electrical connection because the plastic not only withstands the high-temperature exposures of vapor-phase soldering, but also chemically resists the solvents used to wash circuit boards.

Both the current applications as one of "engineering thermoplastics" and the potential applications as a prossesible conducting polymer spurred some extensive studies on PPS in the last decade. The crystalline structure of PPS was determined by X-ray and electron diffraction experiments [18,19]. The valence electronic structure of PPS was investigated by X-ray photoelectron spectroscopy (XPS) [20], UV photoelectron spectroscopy(UVS) [21], Electro-energy-loss spectroscopy (EELS)[22] and calculated by Bredas et al using the valence effective Hamiltonian (VEH) method [23]. The results of these investigations indicate that PPS has a ionization potential of 6.0 ev, a well-defined π-π^* gap of 3.4 ev, and a width of the highest occupied π band of 1.2 ev which

is the evidence of the delocalization of the π electrons along the PPS chain. The electrical conductivity and photoconductivity measurements on pristine, heat-treated, and doped PPS films were carried out by several research groups [24-26] in Japan. They reported that a biaxially stretched PPS film annealed in oxygen at around 285^0 C showed extremely high photoconductivity, four orders of magnitude larger than that of conventional pristine PPS. Extensive IR or FTIR [27-29] absorption measurements were carried out to investigate the PPS morphology and its change upon doping. Some Raman measurements have also been conducted on PPS [30-31] although a certain lack of clarity in the mode assignment remained. Other recent investigations on PPS include the studies on rheological and morphological properties of thermal-aged PPS resin by FTIR and solid-state C-NMR [32]; chemiluminescence studies of the low temperature thermooxidation of PPS [33], and absorption study [34].

However, because of its chemical complexity and the lack of an attractive physical model such as the soliton in conjugated polymers, the research on the electronic properties of the PPS still lags behind that of conjugated polymers. Many electronic and lattice dynamical properties of PPS remain to be studied. Little data on PPS photoluminescence (PL) have been reported.

The Outline of This Study

This dissertation presents the results of Raman and Photoluminescence studies on PPS films, focusing on the morphology and emission characteristics. The results and discussions presented were devoted to the better understanding of the properties of this important polymer material.

Raman studies

Raman spectra of biaxial crystalline and amorphous poly(p-phenylene sulfide) (PPS) films have been recorded using the micro-Raman technique. The Raman spectra of its corresponding trimer and tetramer from KBr pellets and the infrared spectrum from the PPS film were also recorded for understanding the normal vibrational modes in PPS. The difference of the Raman spectra between biaxial and amorphous films is presented. It was observed that the intensity of the Raman peak at 1076 cm^{-1}, which results from phenylene-sulfur stretching vibration, was related to the chain length and alignment of PPS molecules. A model was proposed to describe this vibration and to calculate the effective force constant of the phenylene-sulfur stretching. New modes at 840 and 919 cm^{-1} were observed in the polymer films which were missing in previous studies.

Absorption and Photoluminescence

UV and visible absorption and Photoluminescence (PL) studies have been carried out on various poly (p-phenylene sulfide) (PPS) films. A frequency-tripled pulsed Nd:YAG laser at 355 nm wavelength was used as the exciting source in PL measurements. The main luminescence of PPS is attributed to the intrachain singlet $\pi^* \rightarrow \pi$ transition (possibly an exciton transition) [2,21] in the PPS molecule. We found that the PL intensity and shape are dependent on the duration of the thermal-aging treatment. We used a deconvolution method to determine the luminescence decay which is approximately exponential with a lifetime independent of the crystallinity and thermal treatments of the sample. We also discussed the temperature dependence of PL from PPS films. In addition, the well resolved vibronic structure was observed in the PL spectra at low temperatures, which provided the evidence that the transition of the π-electron was coupled to the intrachain stretching in the PPS backbone. A lattice-relaxation model with a two-level system was then developed to interpret the experimental data. Our results show that the electron-lattice coupling strength in PPS is slightly reduced after the thermal-aging treatment.

CHAPTER II

RAMAN STUDIES OF PPS FILMS

Introduction

In this chapter the basic vibrational characteristics of PPS and how these change with chain length and crystalline content are addressed. IR and Raman spectra from PPS films as well as from low molecular weight oligomers in the form of KBr pellets are presented. In particular, measurements have been performed on two biaxial (crystalline) films, one amorphous film of pristine PPS, and one sample each of its corresponding trimer and tetramer oligomers. The IR and Raman spectra of PPS films are consistent with the results previously reported by P. Piaggio et al on polycrystalline powders of PPS [35]. However, two new Raman peaks at 840 cm^{-1} and 919 cm^{-1} were observed from the polymer films in this study. It has been found that most of the Raman frequencies also appear in the IR spectra. We discuss the assignment of Raman bands as the localized vibrational modes of the phenylene-sulfide unit. The influence of polymer crystallization on the Raman spectra is discussed and a model describing the phenylene-sulfur stretching vibration is proposed. Finally, we report on the fluorescence spectra which indicate that different Stokes shifts result from the biaxial film than from the amorphous

film.

Experimental

The two crystalline PPS samples used were biaxially oriented films with thicknesses of 1.8 μm and 28 μm. The amorphous PPS film used was 65 μm thick. The trimer and tetramer samples were studied as crystalline powders in KBr pellets. The formulas of trimer and tetramer are (C_6H_5-S-C_6H_4-S-C_6H_5) and (C_6H_5-S-C_6H_4-S-C_6H_4-S-C_6H_5), respectively. All samples were obtained from Phillips Petroleum Company [36].

The synthesis of the trimer and tetramer is well documented [37]. The fabrication of the amorphous and biaxial oriented films is conducted by a heat compression molding technique whereby the material is pressed between two steel plates at 500-600 psi at a temperature of 320° C. After molding, the amorphous films are quickly transferred to a cold press, thus rapidly quenching the material. These films were not allowed to crystallize, although some small amount of crystallinity remains. The biaxial films were prepared by extrusion having been drawn in two directions, the machine direction and a direction transverse to it. The draw is on the order of 200 to 300%. This produces highly-oriented material with greater crystallinity (≈60%) than the amorphous films. The average molecular weight of these polymer films is between 40,000 to 50,000 atomic units [32].

Figure 4 shows the experimental setup used in Raman measurements. The Raman spectra were taken using the 514.5 nm

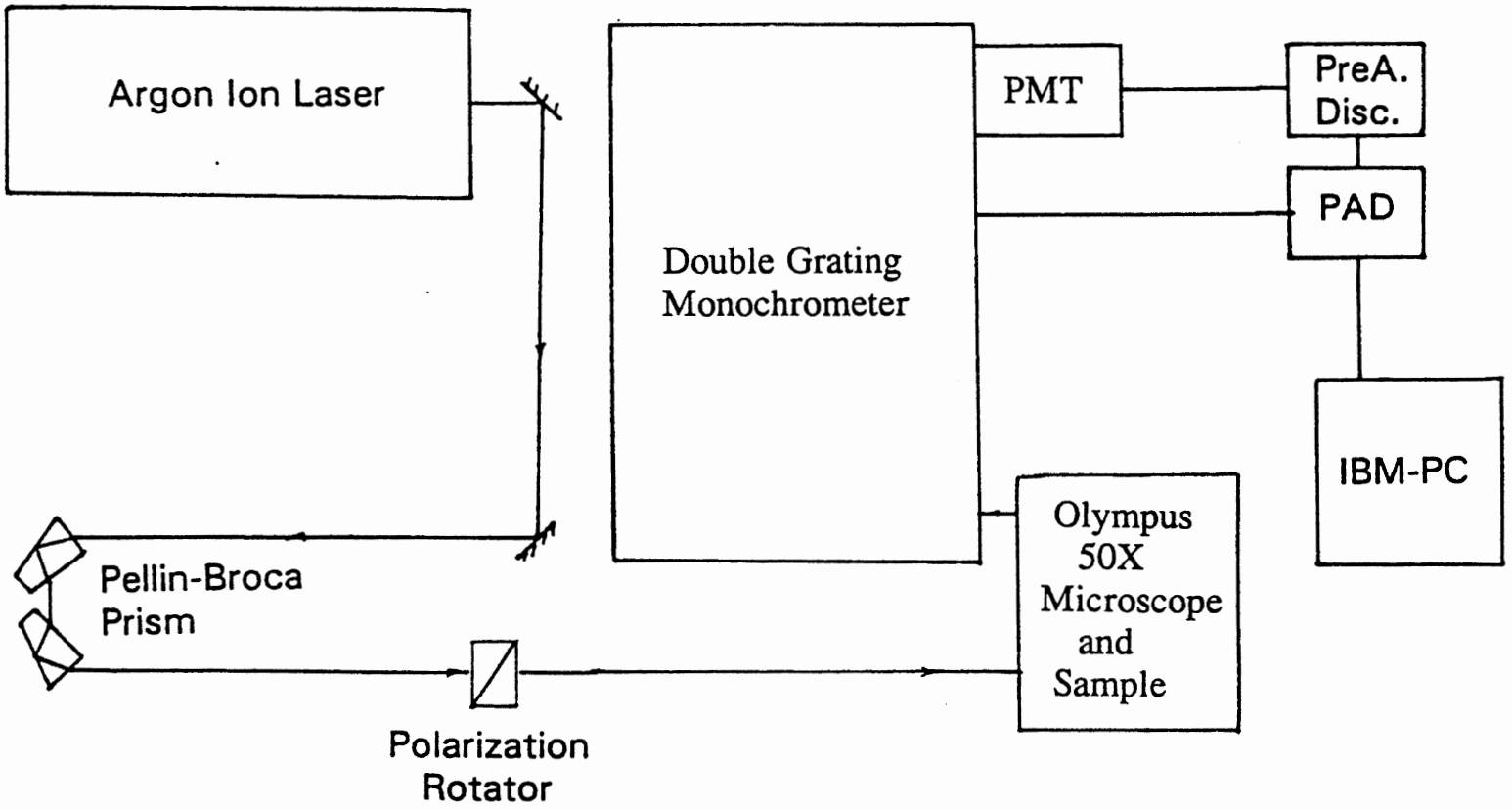

Figure 4. The Micro-Raman Scattering Apparatus.

line from a Spectra-Physics model 2020 argon-ion laser as the excitation source. The micro-Raman probe, which has fine adjustments to both focus the laser beam on the sample and collect the scattered Raman signal, allows us to use lower laser power. Therefore, most of the Raman lines from the PPS film were recorded with high quality. The laser beam entered the Olympus BHSM-L microscope chamber and was focused on the sample by an adjustable lens. The backscattered light was collected using a 50X objective. The scattered light was then analyzed by a Ramanor U-1000 double grating monochromator and detected by a RCA-C3134A photomultiplier tube cooled to -25° C. Both the monochromator and photomultiplier tube were monitored and controlled by an IBM computer. The spectrometer was scanned from 450 cm^{-1} to 1650 cm^{-1}.

To avoid overheating and to minimize the fluorescence, the laser beam was focused slightly below the film while keeping the objective focused inside the film. In addition, the PPS sample was rested on a copper plate to aid the dissipation of local heating caused by the laser.

Results and Discussion

Raman, IR Spectra, and Raman Mode Assignments

Figure 5 shows Raman spectra of the PPS film and its trimer and tetramer. The Raman frequencies and the proposed Raman mode assignments for PPS film are listed in Table I. These results reveal several significant features:

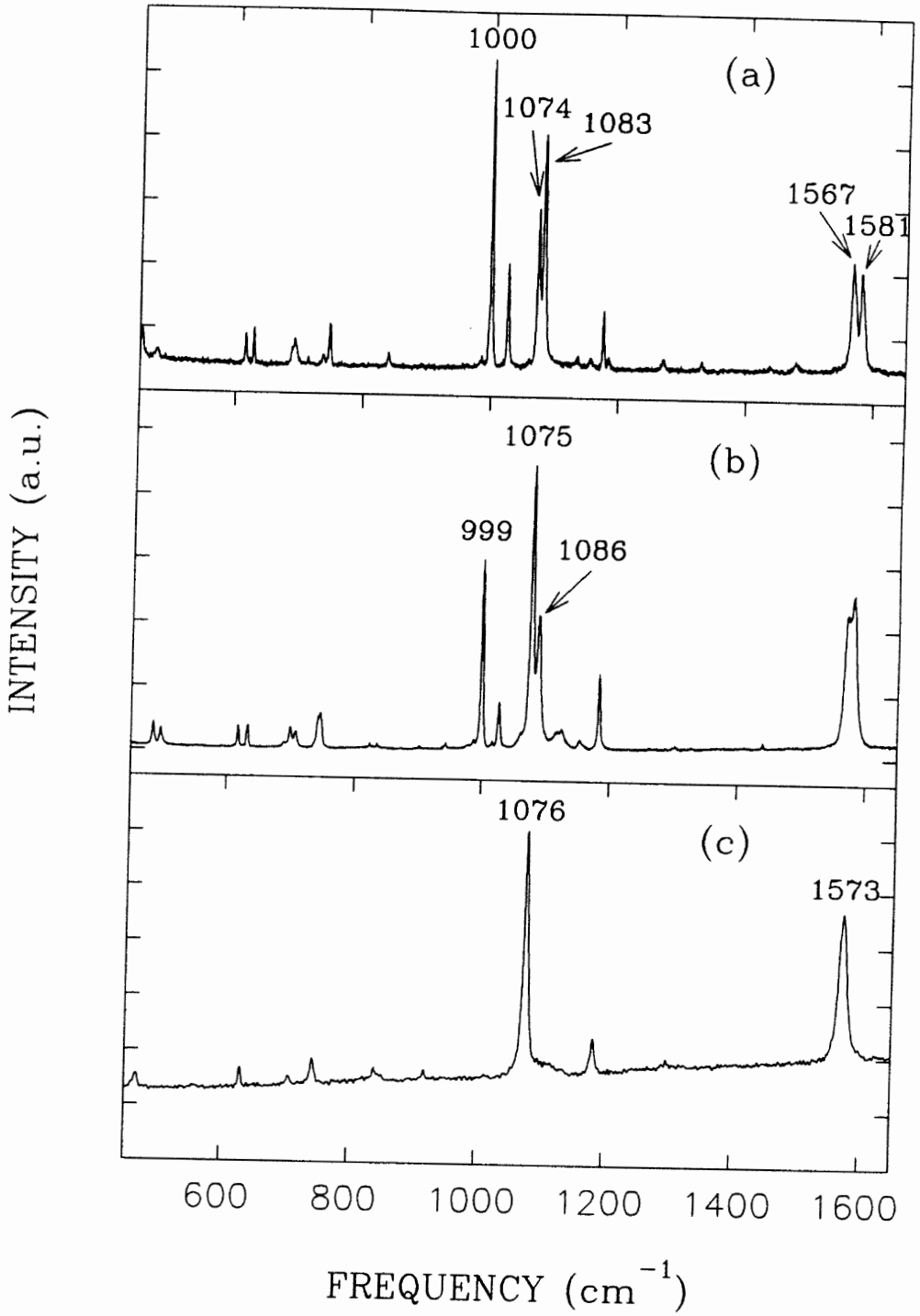

Figure 5. Raman Spectra of the (a) Trimer, (b) Tetramer, and (c) 1.8 μm Thick Biaxial PPS Film.

TABLE I

THE RAMAN FREQUENCIES FOR TRIMER AND TETRAMER, THE IR AND RAMAN FREQUENCIES FOR PPS FILM, AND THE PROPOSED RAMAN MODE ASSIGNMENTS FOR PPS

Trimer Raman	Tetramer Raman	PPS IR	PPS Raman	Assignment
1581^{s}	1579^{vs}			
1567^{s}	1568^{s}	1573^{S}	1573^{vs}	ring C-C str. S-ϕ-S
1478^{w}		1472^{vs}		
	1439^{vw}	1440^{m}		
		1391^{s}		
		1349^{m}		
1331^{w}				
	1301^{vw}	1296^{vw}		
1271^{w}				
		1260^{vw}		
		1236^{vw}		
1185^{s}	1182^{s}	1182^{w}	1183^{m}	C-H i.p.bend. S-ϕ-S
1176^{s}				
1156^{w}	1152^{w}			
	1123^{m}	1119^{w}		
		1108^{m}		
1083^{vs}	1086^{s}	1094^{vs}		
1074^{s}	1075^{vs}	1075^{m}	1076^{vs}	ϕ-S i.p.str. S-ϕ-S
1027^{s}	1026^{s}			
		1010^{vs}		
1000^{vs}	999^{vs}			
		963^{w}		
	942^{vw}			
			*919^{w}	C-H o.p.bend. S-ϕ-S
	901^{vw}			
		875^{w}		
840^{m}	835^{vw}		*840^{w}	C-H o.p.bend. S-ϕ-S
	823^{vw}	824^{s}		
		821^{s}		
		811^{s}		
748^{m}	744^{s}	742^{m}	743^{m}	C-H o.p.bend. S-ϕ-S
	706^{m}	705^{w}	706^{w}	ring o.p.def.S-ϕ-S
693^{m}	698^{m}			
629^{m}	631^{m}	630^{w}	630^{w}	ring i.p.def. S-ϕ-S
616^{m}	616^{m}			

TABLE I (Continued)

Trimer Raman	Tetramer Raman	PPS IR	PPS Raman	Assignment
		590^{w}		
		568^{m}		
		545^{m}		
	495^{m}			
	484^{m}			
477^{w}		480^{s}		
454^{m}			468^{m}	ϕ-S o.p.def. ϕ-S

*: these were observed from the 1.8 μm biaxial film.
^{vs}=very strong; ^{s}=strong; ^{m}=medium; ^{w}=weak; ^{vw}=very weak.
str., stretching; i.p., in plane; o.p., out of plane;
def., deformation; bend, bending.

(1) all Raman lines from the PPS film have corresponding peaks from the trimer and/or tetramer except for the new peak observed at 919 cm^{-1}; (2) the 1076 cm^{-1} and 1083 cm^{-1} lines are sensitive to the chain length. The intensity of the 1076 cm^{-1} line, which is characteristic of the phenylene-sulfur stretching mode in the S-ϕ-S unit, increases with the chain length (especially from trimer to tetramer) while the 1083 cm^{-1} line which probably comes from the phenylene-sulfur stretching in the ϕ-S unit, decreases with the chain length; (3) the 999 cm^{-1} line decreases from trimer to tetramer and is absent in the PPS polymer. The 999 cm^{-1} Raman line in the trimer and tetramer results from the ring stretching of the mono-substituted benzene (ϕ-S) which possess a C_{2v} symmetry [38]. As the chain length increases, most of the rings in the PPS polymer become para-substituted benzene (S-ϕ-S). The symmetry of the ring increases to D_{2h} where the 999 cm^{-1} line is no longer allowed [39]. (4) The 1573 cm^{-1} line is also sensitive to the chain length. There are two distinct peaks at 1567 and 1581 cm^{-1} in the trimer. These two peaks move closer together in the tetramer until only one peak at 1573 cm^{-1} remains in the PPS film. It is not entirely clear whether these two peaks merge together as the oligomers increase from trimer to polymer or the peak at 1581 cm^{-1} in the trimer decreases [35] while the mode at 1567 cm^{-1} intensifies and moves to higher energies.

A unit cell in the single PPS chain is shown in Figure 6.

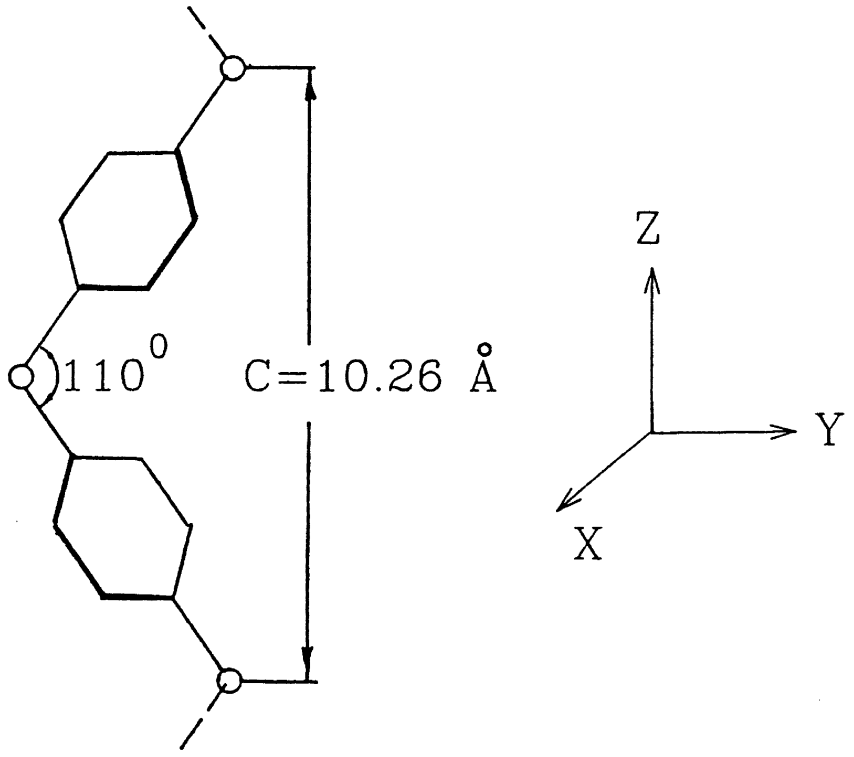

Figure 6. Repeating Unit of the PPS Chain.

As indicated by P. Piaggio et al [35], the line group has the glide reflection symmetry $\sigma(xy)$, the two-fold rotation symmetry $C_2(y)$ and the inversion symmetry (i), relative to the center point of one phenylene ring. Therefore the IR and Raman bands are expected to be mutually exclusive by using the C_{2h} group [35,39]. However, the experimental data, whether reported previously [35,40] or from this study, have shown that most Raman frequencies of PPS were also observed in the IR spectra. These experimental results suggest that these modes are both Raman and IR active. This may result for several reasons: First, the glide reflection $\sigma(xy)$ and the inversion symmetry of a single chain are held on two conditions: (1) The chain has infinite length; (2) All sulfide atoms are aligned in two parallel straight lines. However, these ideal conditions are only partially satisfied in real PPS. It has been reported that the fully crystallized PPS has a crystallinity index of about 65 % and a linear structure contains approximately 150 - 200 repeating units [41,42].

In addition, if we consider a molecule in PPS, there are 175 repeated units on average and 22 atoms in each unit, giving 175 X 22 X 3 - 6 = 11544 internal vibrational modes. This situation is extremely complicated. In general, we can approximately solve this problem in two steps. First, consider the sulfur-phenylene-sulfur unit, S-ϕ-S, as a single unit because most of the vibrational modes of PPS are internal within this unit and the corresponding atoms in each ring are

moving in phase at the wavevector $\mathbf{q} \rightarrow 0$. Second, consider the coupling along the chain. The movements of the sulfur atoms, which are covalently bonded by two phenylene rings at an angle of 110^0, are restricted by the structure of the PPS chain.

T.C. Clarke et al [43] had reported that Raman bands in the PPS spectra can be identified as "localized" vibrations of the phenylene groups. The spectral activity of these modes can then be analyzed by the local symmetry of the ring. This is reasonable because both Raman and IR spectra reflect the internal vibration among atoms.

Table I lists the observed Raman frequencies from the biaxial PPS film, as well as from the trimer and tetramer pellets. The infrared absorption frequencies of the PPS film are also listed for comparison. Most of the proposed vibrational assignments result from using the localized phenylene ring symmetry group following the discussion given by D.H. Whiffen and R.R. Randle [38,39]. As listed in this table, the Raman lines at 1573, 1183, 1076, 743, 706, 630 cm^{-1} also appear in the IR spectrum while the Raman modes corresponding to 919, 840, 468 cm^{-1} lines are Raman active only.

According to Ref. 38, we assign the new Raman peaks at 840 cm^{-1} and 919 cm^{-1} to the out of plane C-H bending modes in the S-ϕ-S unit. To our knowledge, these two Raman bands have not been reported previously. We should point out that these peaks were only observed in the thin 1.8 μm biaxial film. The

thickness of these films is important in Raman scattering measurements since more laser power can be applied without melting the sample. Such new peaks have not been observed on polymer samples in pellet form [35].

The approximate modes of vibration assigned to the Raman lines of PPS film are illustrated in Figure 7 [38,39].

Figure 8 shows the infrared spectra of trimer, tetramer, and 1.8 μm biaxial PPS film. The observed IR frequencies are listed in table II. The IR frequencies reported by P. Piaggio et al from similar samples are also listed for comparison. The IR frequencies from our trimer sample and PPS film are in agreement with the results previously reported by P. Piaggio et al from his sample A and from his polycrystalline PPS sample, while several different IR frequencies between our tetramer sample and Piaggio's sample C were observed. The reason is that the chemical formula of our trimer is the same as Piaggio et al's sample A, while our tetramer is not quite the same as their sample C which is terminated by bromine instead of hydrogen.

Phenylene-Sulfur Stretching Vibrations

The intensity of the strong Raman line at 1076 cm^{-1} is sensitive to the chain length and chain alignment, while the frequency does not change much with the chain length. It has been reported that the 1076 cm^{-1} Raman band results from the phenylene-sulfur stretching vibration [35,43,44]. In a PPS

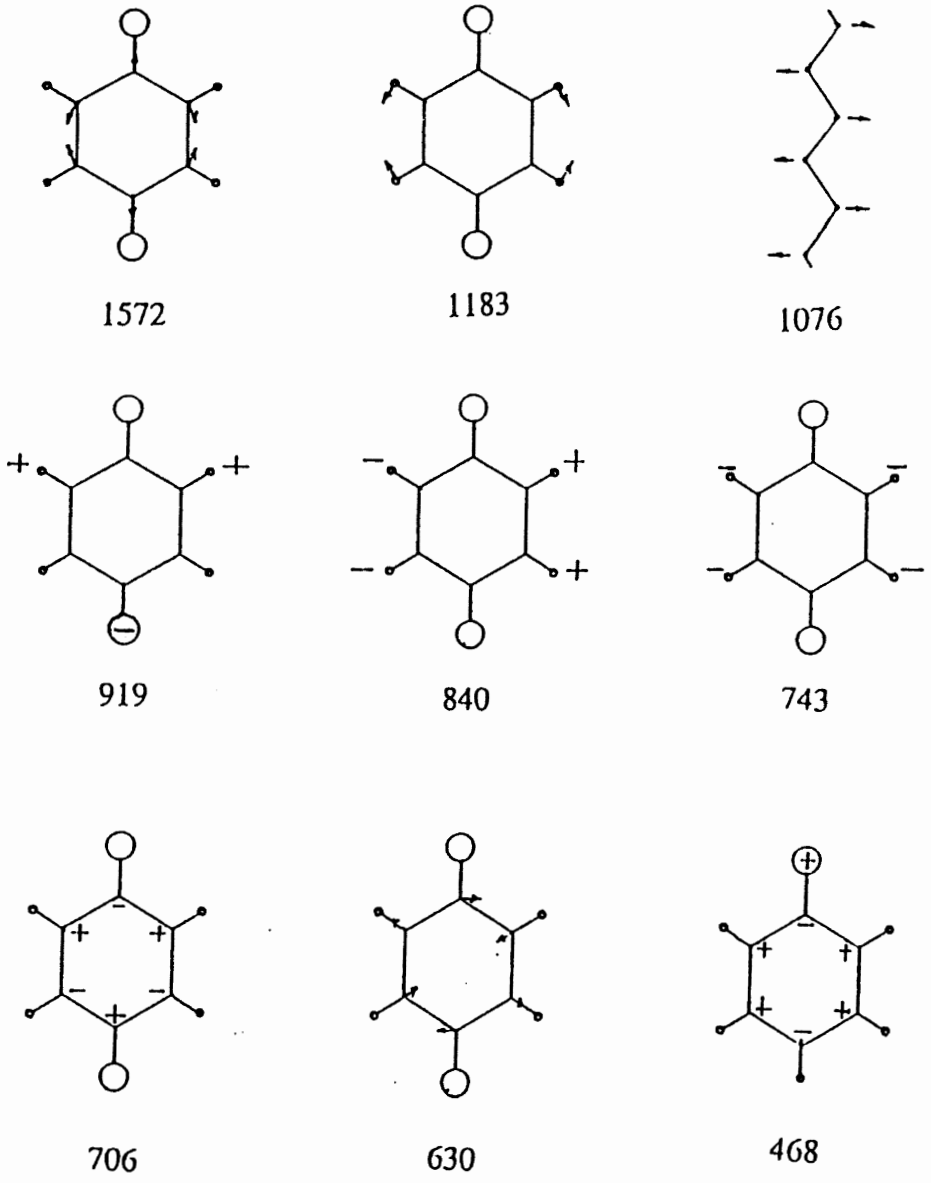

Figure 7. The Approximate Modes of Vibration Assigned to Raman Lines of the PPS Film.

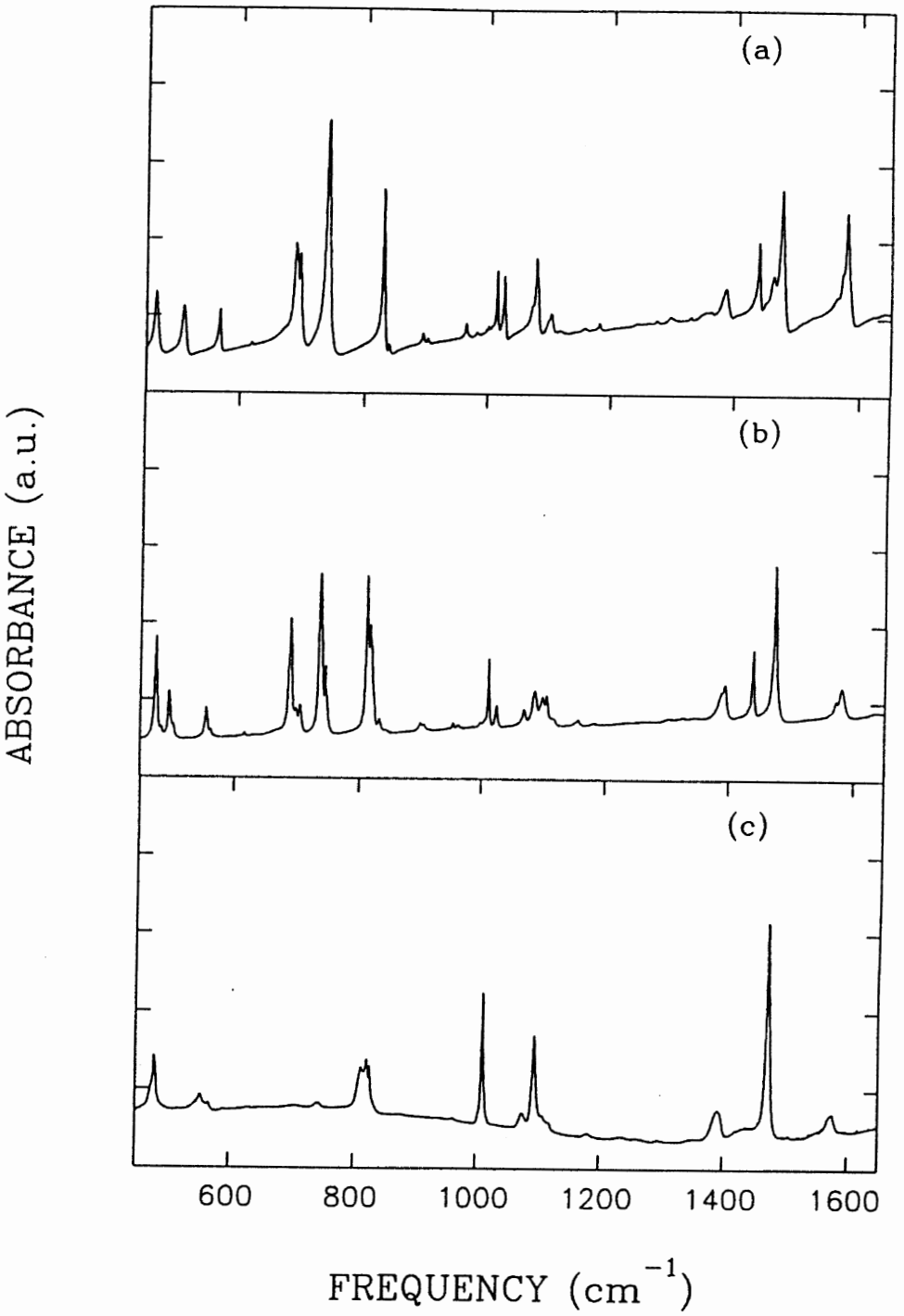

Figure 8. Infrared Absorption Spectra of the (a) Trimer, (b) Tetramer, and (c) 1.8 μm Thick Biaxial PPS Film.

TABLE II

THE INFRARED ABSORPTION LINES FOR TRIMER, TETRAMER, AND PPS FILM

Trimer	A	Tetramer	C	PPS	PPS*
1579^{s}	1580^{s}	1581^{s}	1581^{mw}		
1571^{m}		1572^{m}		1573^{S}	1572*
1563^{w}					
1475^{vs}	1475^{s}	1474^{vs}	1472^{s}	1472^{vs}	1471^{s}
1461^{m}	1462^{w}		1462^{sh}		1390^{ms}
1438^{s}	1438^{vw}	1439^{s}	1438^{mw}	1440^{m}	
		1393^{s}	1390^{m}		
1385^{m}	1385^{mw}	1386^{m}		1391^{s}	
1361^{w}	1361^{vw}				
			1348^{vw}	1349^{m}	1348^{w}
1329^{w}	1330^{vw}	1327^{w}	1330^{vw}		1330^{vw}
1295^{w}	1297^{w}	1304^{w}	1298^{vw}	1296^{vw}	1298*
1263^{w}	1274^{vw}			1260^{vw}	1260*
	1243^{vw}			1236^{vw}	1236^{w}
1180^{w}	1181^{vw}	1183^{w}	1180^{vw}	1182^{w}	1181*
1157^{w}	1157^{vw}	1157^{w}	1156^{vw}		
1117^{w}		1118^{w}		1119^{w}	
1102^{m}	1102^{mw}	1106^{m}	1107^{w}	1108^{m}	1109^{w}
		1099^{m}	1097^{w}	1094^{vs}	1096^{s}
1078^{s}	1079^{ms}	1087^{s}	1089^{ms}	1075^{m}	1075*
1071^{w}		1059^{m}	1070^{m}		
1026^{s}	1026^{m}	1024^{m}	1025^{w}		
1014^{s}	1014^{m}	1012^{s}	1009^{ms}	1010^{vs}	1010^{s}
1000^{w}	982^{vw}				
964^{w}	964^{w}	954^{w}	964^{vw}	963^{w}	963^{w}
902^{w}	902^{sh}	906^{w}	904^{w}		948*
893^{w}	894^{w}	900^{w}			
				875^{w}	
838^{w}	838^{ms}	832^{m}			
829^{vs}	828^{ms}		824^{sh}	824^{s}	
		817^{s}	816^{vs}	821^{s}	818^{vs}
		811^{vs}		811^{s}	812*
739^{vs}	739^{vs}	745^{s}	746^{w}	742^{s}	743*
		736^{vs}	739^{m}		

TABLE II (Continued)

Trimer	A	Tetramer	C	PPS	PPS*
695^{s}	694^{ms}	704^{m}	704^{sh}	705^{w}	706*
688^{s}		696^{s}			
		689^{vs}	689^{m}		
	618^{vw}	616^{w}		630^{w}	630*
				590^{w}	
567^{m}	568^{mw}	563^{w}			
		555^{m}	557^{mw}	568^{m}	566*
			524^{vw}	545^{m}	556^{mw}
510^{m}	511^{w}	504^{w}	503^{w}		
		496^{s}			
		483^{w}		480^{s}	483^{ms}
465^{m}	467^{m}	475^{s}	478^{ms}		

Notes:

Data of sample A, C, and PPS* are from ref. 35; the formula of sample A is $\phi(S\text{-}\phi)_2H$ while the formula of sample C is $\phi(S\text{-}\phi)_3Br$.

^{vs}= very strong, ^{s}= strong, ^{m}= medium, ^{w}= weak, ^{vw}= very weak.

chain, two neighboring S-ϕ-S are connected with an angle of 110^0. The ϕ-S stretching has to be combined with a rotation about each phenylene center (about the x-axis in Figure 6).

There are two possible Raman active phenylene-sulfur stretching modes in the PPS chain which are illustrated in Figure 9. In mode 1, the stretching vibration for the neighboring S-ϕ-S are in-phase; in mode 2, an alternating stretching vibration of the neighboring S-ϕ-S groups is taking place. In both modes, the S-ϕ-S shape is different at the vibrational extremes so that the polarizability ellipsoid changes. Therefore they are Raman active [45]. In the following, small vibrations are assumed. Let M_1 denote the mass of the phenylene ring, M_2 denote the mass of the sulfur atom, and C_{eff} denote the effective force constant between M_1 and M_2. For the alternating stretch mode, the resultant force component directed along either bond axis of the ϕ-S group is equal to $C_{eff}\ \Delta x\ (1-\cos\alpha)$, where Δx is the displacement between the center of phenylene ring and the sulfur atom, α is the angle between two neighboring S-ϕ-S units. For Raman active modes with wavevector $q \rightarrow 0$, the center of mass of the phenylene group does not move. Therefore, the vibrational frequency, ν, is given by

$$\nu = \frac{1}{2\pi}\sqrt{\frac{C_{eff}(1-\cos\alpha)}{M_2}} \qquad (2.1)$$

If the mass is expressed in atomic mass units and the force constant is expressed in millidynes/angstrom, then the

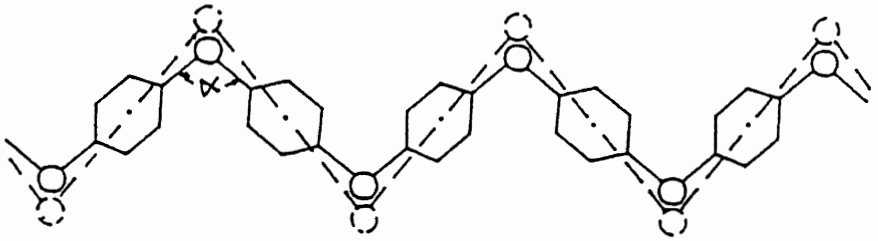

(a)

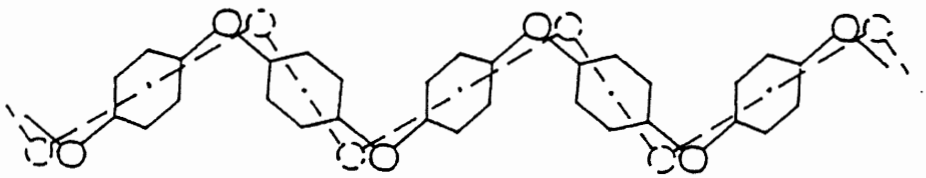

(b)

Figure 9. The Two Possible Phenylene-Sulfur Raman Stretching Modes in PPS; (a) In-phase Chain Stretching, (b) Alternating Chain Stretch.

frequency ν, in cm^{-1}, is given by

$$\nu = 1303\sqrt{\frac{C_{eff}(1-\cos\alpha)}{M_2}} \qquad (2.2)$$

As indicated in Ref. 46, the alternating chain stretch mode does not involve angle bending in the first order approximation (α is constant), but the in-phase stretch mode does. The expression for the in-phase chain stretching frequency to first order is (Appendix A)

$$\nu = 1303\sqrt{[C_{eff}(1+\cos\alpha) + \frac{2\zeta}{L^2}(1-\cos\alpha)](\frac{1}{M_2})} \qquad (2.3)$$

where ζ is the bending force constant, L is the length between sulfur atom and the center of phenylene ring, and ζ/L^2 has the same units as C_{eff}. If we assume that the two modes represented by Eqs.(2.2) and (2.3) have the same frequency, we then obtain $\zeta/2L^2 \approx 0.127\ C_{eff}$ for $\alpha = 110^0$. We note from Ref. 46, that for single bonds, $\zeta/2L^2$ is roughly an order of magnitude smaller than C_{eff}. This is consistent with the above result. Therefore, the assumption that both the alternating stretch mode and in-phase mode have the same frequency is possible. This may be the reason why only one Raman peak at 1076 cm^{-1} was observed.

Using the fact that the atomic mass of sulfur is 32, and continuing our assumption of small vibrations, we can solve for the effective force constant, C_{eff}, of the phenylene sulfur stretching mode from Eq. (2.2). A value of about 16 (millidynes/angstrom) is obtained. Using the length L = 2.1

(angstrom) from Fig. 9, we obtained the value of the bending force constant which is 8.96 (mdyn. angstrom). We note that the real situation will be more complicated because the molecular chain is embedded in a solid environment.

We can then explain the effects on the Raman intensity by utilizing both intrachain and interchain coupling: (1) The effect of intrachain coupling is stronger if the chain is longer. This is what we observe for the intensity of 1076 cm^{-1} line as it increases from trimer, tetramer to the PPS polymer; (2) The effect of interchain coupling is stronger if the chains are aligned in the same direction. This explains why the intensity of this line is larger in the biaxial crystalline film than in the amorphous film.

Figure 10 shows the Raman spectra from a biaxial crystalline film and from an amorphous film. Two differences can be noticed: (1) On the higher frequency side of the 1076 cm^{-1} line a more pronounced shoulder appears from the amorphous film than from the biaxial film. This shoulder possibly corresponds to the lines of 1086 and 1123 cm^{-1} in its tetramer spectrum, (2) The 1076 cm^{-1} line is more intense than the 1573 cm^{-1} line in the biaxial film while the relative intensity of these two lines is reversed in the amorphous film. The intensity of 1076 cm^{-1} line is also related to the interchain coupling and is sensitive to the chain alignment which can easily be understood by inspecting the vibrational mode shown in the Figure 9. Therefore, we may use this feature to

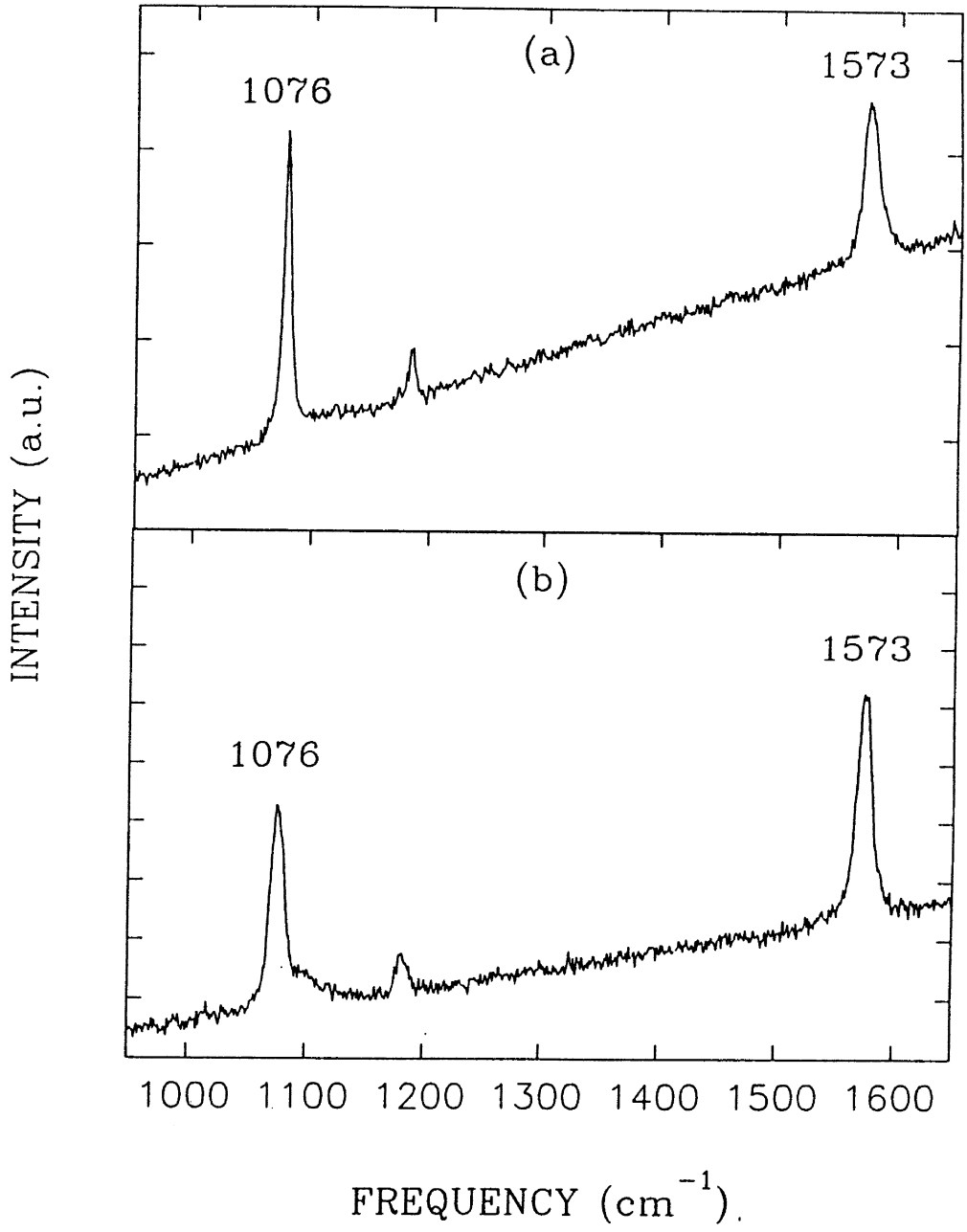

Figure 10. Raman Spectra of the (a) Biaxial and (b) Amorphous PPS Films.

characterize the crystallinity of PPS films.

Fluorescence Background

The fluorescence backgrounds of the spectra from the biaxial and amorphous PPS films, when excited at 514.5 nm, are shown in Fig. 11. The maximum fluorescence intensity is at about 598 nm for the biaxial film and at about 616 nm for the amorphous film. These fluorescence emissions result from impurity states inside the gap and have a broad band feature. A possible interpretation is that the luminescent centers in the PPS film are coupled to the lattice. The normal vibrational coordinates are shifted in an electronic transition resulting in the vibronic transitions of molecules and impurity centers [47,48]. The difference in Stokes shifts from the biaxial PPS film and from the amorphous PPS film possibly imply, according to the Franck-Condon principle [46], that amorphous PPS has a larger temporary lattice distortion during an electronic transition. This result is consistent with our recent fluorescence studies of PPS films using a pulsed Nd:YAG laser [49]. These latter studies will be presented in chapter III which will also discuss how these electronic transitions are coupled to the phenylene-sulfur stretching modes.

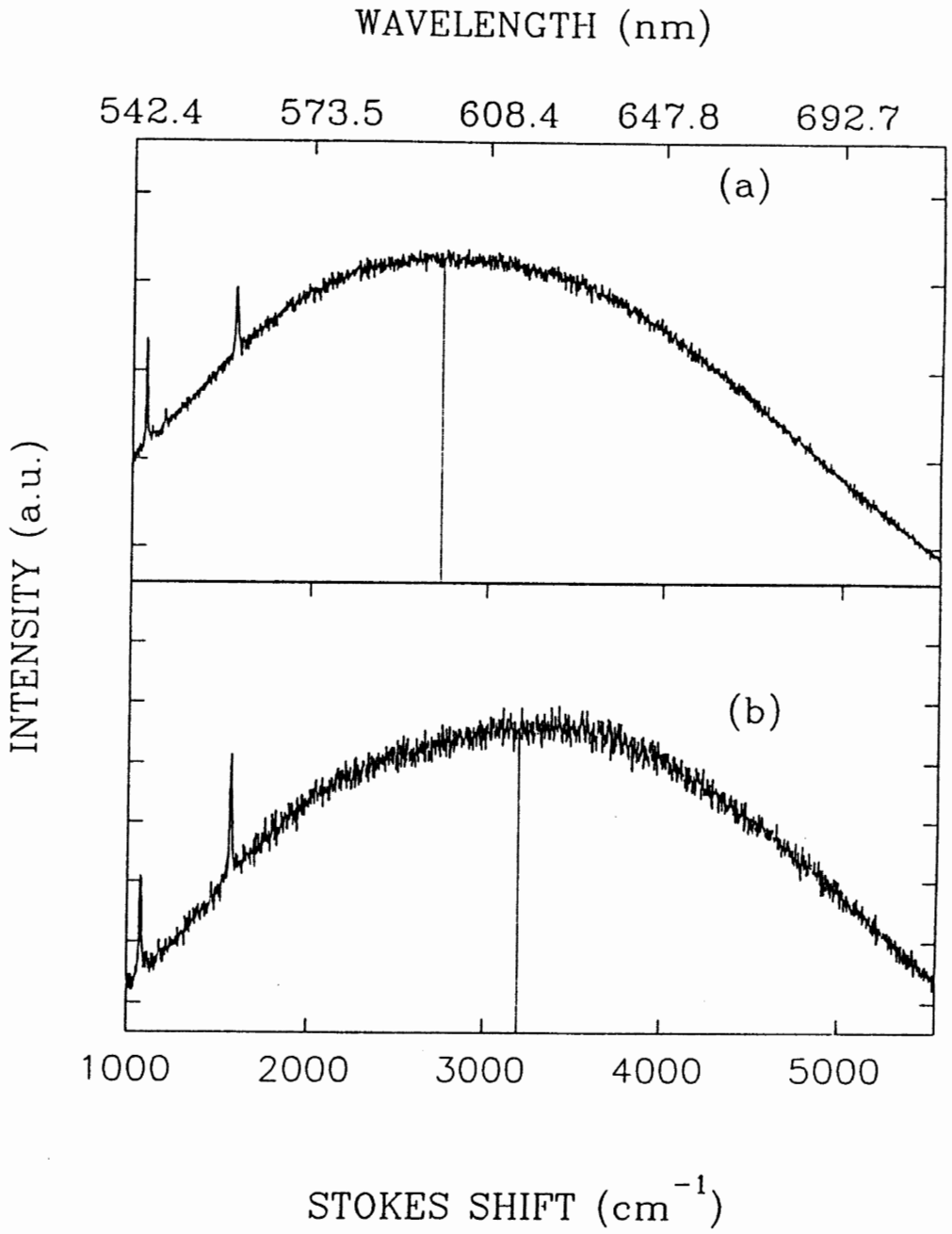

Figure 11. Fluorescence Background from the (a) Biaxial and (b) Amorphous PPS Films Resulting from Excitation at 514.5 nm.

CHAPTER III

ABSORPTION AND PHOTOLUMINESCENCE (PL) OF PPS FILMS

Theory

The Origins of Luminescence

Organic materials are held together by van der Waals forces between molecules and are therefore molecular solids [50]. The consequence of this molecular nature is that the luminescence processes in organic materials are associated with the excited states of molecules. Those hydrocarbons which contain double or triple bonds between the carbon atoms, the unsaturated hydrocarbons, commonly give rise to strong luminescence emission. This luminescence originates from the excited state of the delocalized π-electrons in these molecules. These π-electrons exist as a consequence of the particular configuration of the carbon atom in the hydrocarbon molecule. The electronic configuration of the six electrons of the carbon atom in its ground state is denoted by $1s^2 2s^2 2p^2$. In sp^2 hybridization, one of the original p-orbital is left unchanged and the sp^2 hybridization gives rise to three hybrid orbitals lying in the same plane and at 120^0 to each other. These hybrid orbitals form the σ-bonds between carbon-carbon and carbon-hydrogen atoms and account for the ring-structure

of molecules such as benzene. The remaining p-orbital extends above and below the molecular plane in a direction perpendicular to it, with a node (zero electron density) in this plane. This p-orbital overlaps with the p-orbital of a neighboring carbon atom to produce a π-bond (Fig. 12). The degree of overlap of the π-bond is much less than that of σ-bonds and this is reflected in the binding energy of the bonds.

In benzene, the p_z-orbital for each atom is in close contact with both its neighbors; thus the π-orbital extends completely around the benzene ring, producing a delocalized orbital with a node along the σ-bonded molecular skeleton. As might be expected, these π-electrons are less tightly bound to their parent carbon nuclei than the localized σ-electrons and thus require less energy to excite them. Absorption in the ultraviolet and visible regions of the spectrum, therefore, readily occurs for these molecules [50]. The system loses most of its excitation energy by the luminescence emission of light. Significant shifts of the absorption spectra to longer wavelengths occur when a phenyl group having its own π-electronic system is connected to the neighboring benzene ring. Further extension of phenyl groups shift these spectra to even longer wavelengths. Gillam and Hey [51] have measured optical absorption in systems up to sexiphenyl and observe an energy shift of the absorption maximum from 6.1 eV in benzene to 3.9 eV in sexiphenyl, which they take as an indication of

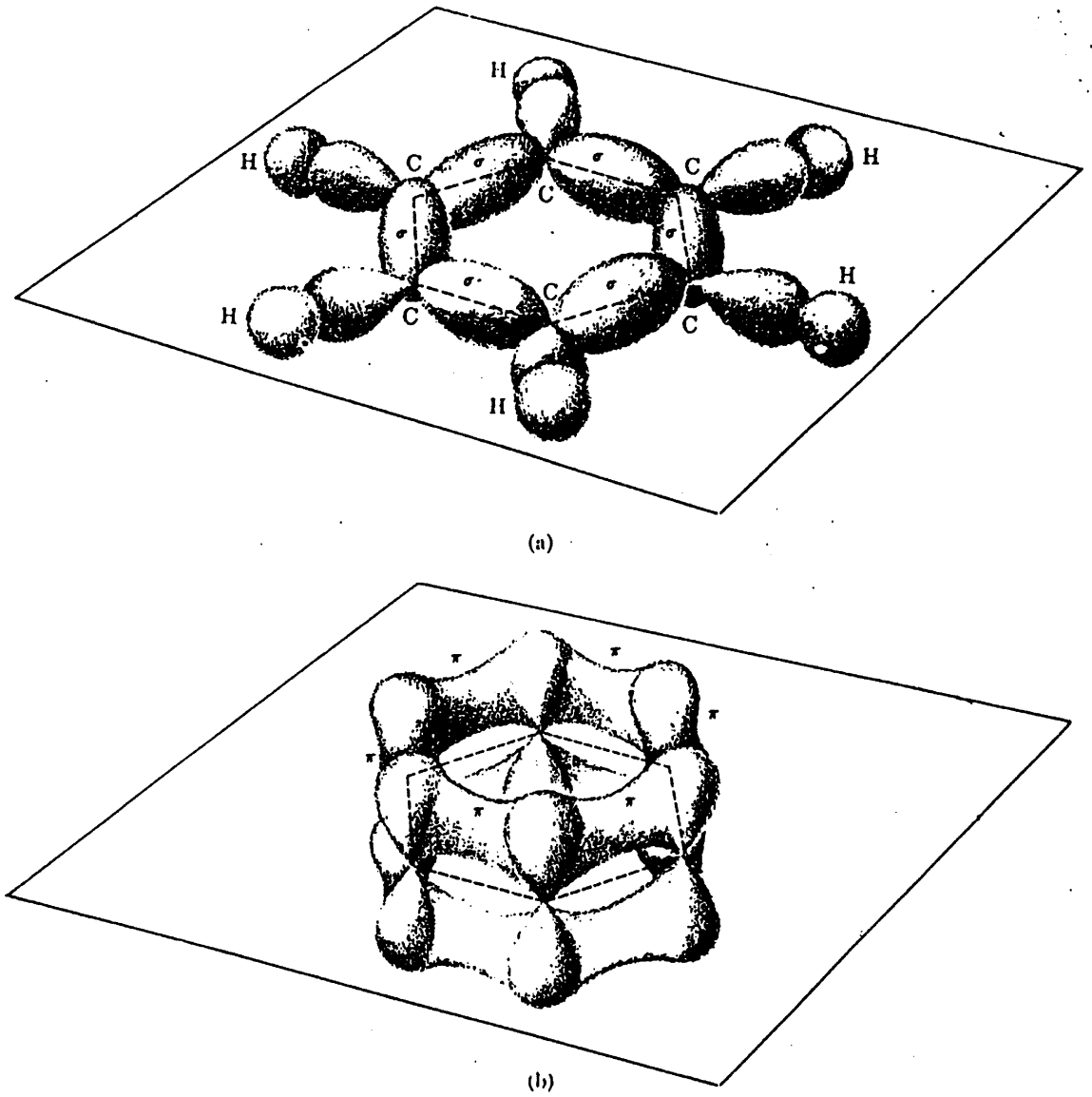

Figuire 12. Benzene Molecular Orbitals. (a) Localized σ-bonds and (b) Unlocalized π-bonds.

appreciable delocalization of the π electrons. The band structure of a poly (p-phenylene) (PPP) chain has been calculated by Whangbo et al.,[52] Grant and Batra,[53] and Bredas et al [54]. The width of the highest occupied π band according to their results is about 3 eV, which is taken as an indication of large π overlap and delocalization along the chain. By inserting heteroatoms S between the phenyl groups, the degree of delocalization of the π electrons is supposed to be reduced. Bredas's band-structure calculations [54] gave a width of the highest occupied π band in PPS of 1.2 eV, which indicates that the delocalization of the π electrons along the PPS chain still exists. Calculations on both the oligomers and the polymer show that substantial orbital overlap occurs along the chain via participation of the lone pairs on the sulfur atoms [55]. The width of the π^* - π energy gap for PPS is well defined as 3.4 ev by the energy-loss spectra [56] and absorption spectra [34].

In our PL experiment, the excited source used is at 355 nm (~3.5 ev). The singlet $\pi \rightarrow \pi^*$ transition creates the electron-hole pair which is mainly confined in a phenylene ring and may be described as the localized exciton state. The main fluorescence of the PPS films comes from these intrachain exciton states [21]. The partially delocalized π-electron system plays an important role in the electronic properties of PPS. The excited states of the π-electron system are therefore of considerable interest in this study.

The Lattice Relaxation Model and The Vibronic Transitions

1. The Lattice Relaxation Model

In general, there are interactions between the π-electrons of the phenylene rings and their neighboring atoms in a PPS molecule. The electronic transition of the localized π-electron changes the equilibrium atomic configuration surrounding this state. To simplify the concerned question we take the phenylene ring with its π-electron system as a single unit. The center of each ring represents the average nuclear position of the six carbon atoms in the chain. The π-electron in a phenylene ring interacts with its surrounding, behaving as the electron-lattice interaction. The total Hamiltonian of the electron-lattice interaction system can be written as

$$H = H_e + H_{eL} + H_L \qquad (3.1)$$

where H_e, H_{eL}, H_L represent the electronic, electron-phonon and lattice vibration Hamiltonians, respectively. An exact solution for such problems is lacking both in classical and quantum mechanics. The substantial difference between the electron mass and the nuclear mass suggests that the heavy nuclei move much slower than the electrons. Therefore we use the adiabatic approximation as a basis for the quantum-mechanical theory of molecules and crystals. In the adiabatic approximation, the total wave function of the system can be written as a product of two functions

$$\Psi(r,q) = \phi(r,q)\,\chi(q) \qquad (3.2)$$

Here r represents the electronic coordinates and q represents the nuclear coordinates, the function $\phi(r,q)$ is an electronic wave function which depends parametrically on the nuclear coordinates, and $\chi(q)$ is a vibrational wavefunction which describes the nuclear motion, The electronic and vibrational wave functions are solutions of the following eigenvalue equations [57]:

$$(H_e + H_{eL})\,\phi_i(r,q) = E_i(q)\,\phi_i(r,q) \qquad (3.3)$$

$$(H_L + E_i(q))\,\chi_{i,n}(q) = E_{i,n}\chi_{i,n}(q) \qquad (3.4)$$

The first equation of the system describes the stationary states of the electrons in the adiabatic approximation, which can be regarded as a set of Schrödinger equations for the electrons with nuclei fixed at positions q. The energy eigenvalue E(q) of the electronic state depends on the nuclear positions. We say that the electronic Schrödinger equation depends parametrically on the nuclear coordinates.

The second equation of the system is a Schrödinger equation which governs the motion of nuclei in the molecule. The function E(q), the eigenvalue of the electronic equation which depends parametrically on the nuclear coordinate, plays a large role in this equation. We will also call this equation the vibrational equation, since it plays the role of the potential energy for nuclear motion. Each eigenvalue of this equation is also an eigenvalue of the total energy of the molecule in the adiabatic approximation. Here, i and n

enumerate the eigenfunctions and eigenvalues of the electronic (3.3) and vibrational (3.4) Schrödinger equations. This means that the vibrational functions $\chi_{i,n}(q)$ depend on the electronic level i and $\psi_{in} = \phi_i \chi_{i,n}$ are referred to as vibronic states. The index i in (3.4) does not have all the usual properties of a quantum number. Thus the functions $\chi_{i,n}$ and $\chi_{i',n}$ are not mutually orthogonal. This is of fundamental significance in the theory of vibronic transitions.

In describing the small vibrations, the harmonic approximation is used and the lattice Hamiltonians may be written explicitly

$$H_L = \sum_k \frac{1}{2} \left[-\hbar^2 \frac{\partial^2}{\partial q_k^2} + \omega_k^2 q_k^2 \right] \qquad (3.5)$$

where q_k represent the normal coordinates of vibrational modes. In a simplified model, the electron-phonon interaction Hamiltonian H_{eL} and the electronic eigenvalue $E_i(q)$ is taken as the linear function of the lattice coordinates q_k. The influence of the localized electronic states on lattice vibrations is through the displacement of the lattice equilibrium position [58]. In practice, this simplified lattice relaxation model is most useful and widely applied to the study of specific problems.

2. Vibronic Transitions with a Single Vibrational Mode

By the term "vibronic transition", we refer specifically to the optical emission or absorption accompanied with

multiphonon transitions in molecular or crystal systems. In the following, two levels i and j of the system are assumed. For an optical transition (emission or absorption), the transition probability is proportional to the square of the transition matrix element. For localized centers showing lattice relaxation, the atomic configuration changes with the transition, so in forming the transition matrix element, the atomic vibrational wave functions $\chi_{i,n}(q)$, $\chi_{j,n'}(q)$, as well as the electronic wave functions $\phi_i(r)$ and $\phi_j(r)$, have to be taken into account. So one should write the transition probability

$$W_{rad} \propto \left| \int \chi_{j,n'}(q) \left[\int \phi_j \, er \, \phi_i \, dr \right] \chi_{i,n}(q) \, dq \right|^2 \qquad (3.6)$$

where the electric dipole moment er is assumed. As the integral over the electronic coordinates can be considered as approximately independent of the vibrational coordinates (the 'Condon approximation'), one has approximately

$$\int \phi_i(r,q) \, er \, \phi_j(r,q) \, dr = M_{ij} \qquad (3.7)$$

which is independent of lattice coordinates q. The optical transition probability then is approximately

$$W_{ij} \propto M_{ij}^2 \left| \int \chi_{j,n'}(q) \, \chi_{i,n}(q) \, dq \right|^2 \qquad (3.8)$$

In this formula, the vibronic transition probability is determined by the overlap integral between the initial and final state vibrational wave functions.

Based on the formula (3.8) we can predict that if a single phonon mode of frequency ω_0 is involved the emission

spectrum will include a series of lines with frequencies

$$E = E_{j-i} - p\hbar\omega_0 \qquad (3.9)$$

This kind of spectral structure is known as the vibronic structure and p is a integer.

Many times, the cause for multi-phonon vibronic structure in a spectrum is dominated by a single lattice vibration mode with frequency ω, a single mode approximation is used. For a polymer system, a two level configuration coordinate model is a good approximation [59] to account for the lattice-relaxation (Fig. 13). The main peak in the absorption spectrum is corresponding to a vertical transition from the vibronic ground state of the level i to the vibronic state of the level f (A→B). The main peak in the emission spectrum is corresponding to a vertical transition from the vibronic state of the level f to the vibronic state of i (C→D). The Stokes loss which is the energy spacing between the main peak and the zero-phonon line is

$$L = \frac{1}{2}\omega^2\Delta_{if}^2 \qquad (3.10)$$

where Δ_{if} is the displacement of the two adiabatic potential curves in a normalized configurational coordinate. We can write the Stokes loss in terms of the number of vibrational quanta which is

$$S = \frac{L}{\hbar\omega} = \frac{\omega}{2\hbar}\Delta_{if}^2 \qquad (3.11)$$

Here, S is known as the Huang-Rhy's parameter [60] describing

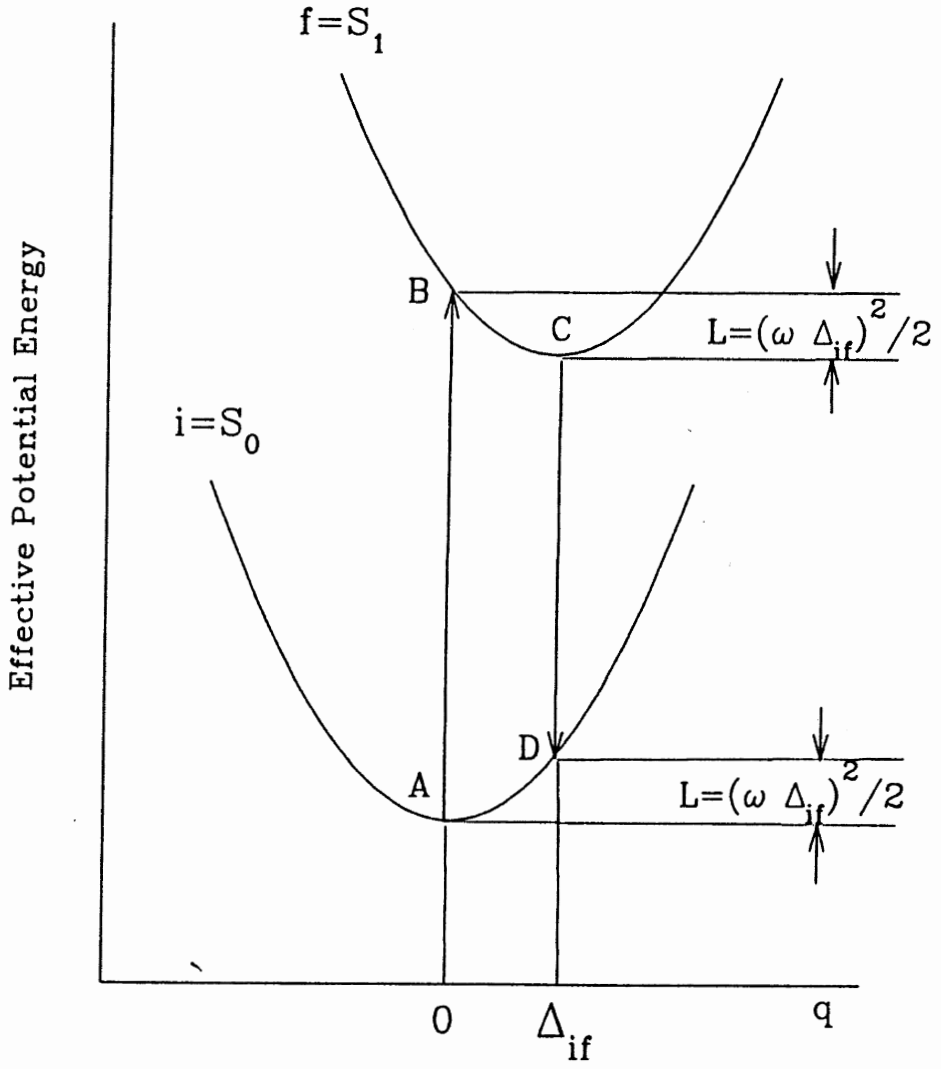

Figure 13. Configurational Coordinate Diagram for Two Levels i and f. The Lower Parabola Represents the Potential Curve of the Ground Electronic State of the PPS Molecule while the Upper Parabola Represents the Potential Curve of the Excited State. The Abscissa q Represents the Configurational Coordinate.

the strength of the electron-phonon coupling. The Huang-Rhy's parameter S can also be used in a general situation with multiple vibrational modes and is written as [58]

$$S=\sum_k \left(\frac{\omega_k}{2\hbar}\right) \Delta_{if,k}^2 \qquad (3.12)$$

The Stokes loss then becomes

$$L=S\overline{\hbar\omega}=S\hbar\omega_{eff} \qquad (3.13)$$

The overbar represents the weighted average over all phonon modes and the ω_{eff} is the effective phonon frequency.

Now consider the vibronic transition from the zero vibronic state of the upper level $\psi_{1,0}$ to the vibronic state of low level $\psi_{0,n}$, corresponding to the transition at the low temperature limit. Using harmonic oscillator eigenfunctions [61]:

$$\chi_{10}(q)=\chi_0(q)=\frac{1}{\sqrt{q_0}}\frac{1}{\sqrt[4]{\pi}}\exp\left(-\frac{1}{2}(y-y_0)^2\right) \qquad (3.14)$$

$$\chi_{0n}(q)=\chi_n(q)=\frac{1}{\sqrt{q_0}}\frac{(-1)^n}{\sqrt{2^n n!\sqrt{\pi}}}\exp\left(\frac{y^2}{2}\right)\frac{d^n}{dy^n}\exp(-y^2) \qquad (3.15)$$

where

$$y=\frac{q}{\sqrt{\hbar/\omega}}\ ;\quad q_0=\sqrt{\hbar/\omega}\ ;\quad y_0=\frac{\Delta_{01}}{\sqrt{\hbar/\omega}} \qquad (3.16)$$

The overlap integral between the initial and final state vibrational wave functions can be solved [61]:

$$\left|\int \chi_{10}(q)\,\chi_{0n}(q)\,dq\right|^2=e^{-S}\frac{S^n}{n!} \qquad (3.17)$$

The distribution of the emission intensity versus energy (different phonon orders) then can be written as

$$I = M_{fi} e^{-S} \left(\frac{S^n}{n!}\right) \qquad (3.18)$$

This formula exhibits the "Pekarian Profile" [61] which follows a Poisson distribution. M_{fi} is the matrix element of the transition between the excited and ground states, S is the Huang-Rhy's parameter describing the strength of the electron-phonon coupling, the values e^{-S} equals the Condon factor, giving the relative size of the transition which occurs without the creation or annihilation of phonons ($0 \rightarrow 0$ line), and n = 0,1,2... represents the number of phonons involved in a transition. Figure 14 illustrates the relative vibronic transition rates with creation of vibrational quanta for different S values.

In our PL measurements, the excited source used is at a wavelength of 355 nm which excites only the first singlet π^* state of the PPS molecule. Therefore we can approximately use a two-level system to analyze the localized π-electronic system of the poly (p-phenylene sulfide) film: a ground level and an excited level. The dominant vibrational mode which couples to the $\pi^* \rightarrow \pi$ transition will be shown to be the phenylene-sulfur stretching mode.

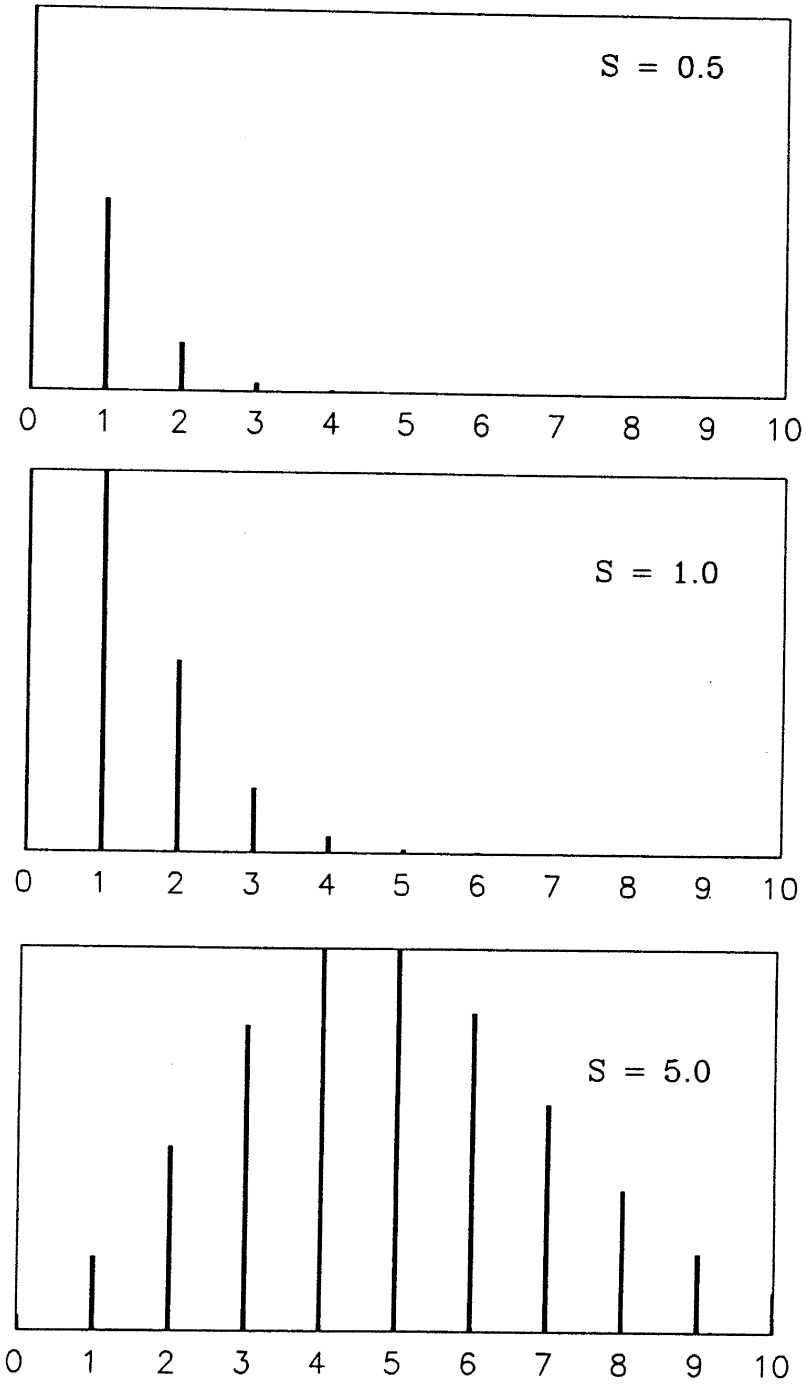

Figure 14. The Relative Vibronic Transition Rates with Creation of Vibrational Quanta for Different S Values

Experimental

The samples used for the absorption and photoluminescence studies were two biaxially-oriented films and a set of amorphous films with or without thermal treatments. The thicknesses of two biaxially oriented films were 1.8 μm and 28 μm while all amorphous films were about 65 μm thick. Enhancement of the properties of PPS could be obtained through a thermal treatment for a variety of products and applications [11]. In thermal-aging process the polymer powder is heated to 260 ^{0}C in air for a specified number of hours succeeded by a fast cooling (2-3 minutes) while in the heat set process it is heated to 210 ^{0}C in air for 20-30 minutes followed by a slow cooling. The trimer and tetramer samples used in absorption measurements were in the CCl_4 solution. The formulas of trimer and tetramer are (C_6H_5-S-C_6H_4-S-C_6H_5) and (C_6H_5-S-C_6H_4-S-C_6H_4-S-C_6H_5), respectively.

The experimental system used for PL measurements is shown in Figure 15. The exciting light source was a Spectra Physics GCR-4 Nd:YAG, using its third harmonic wavelength of 355 nm with a pulse width of 6 ns, operating at 10 Hz. The exciting power was reduced to about 50 μJ per pulse by passing through two attenuators. A 10 cm focal length cylindric lens was used to focus the beam onto the sample surface at a angle of 50 degrees. The sample was mounted inside a Janis He-Dewar model 8DT. A Lake Shore temperature controller model DRC-91C was used to control the temperature. The light emitted from the

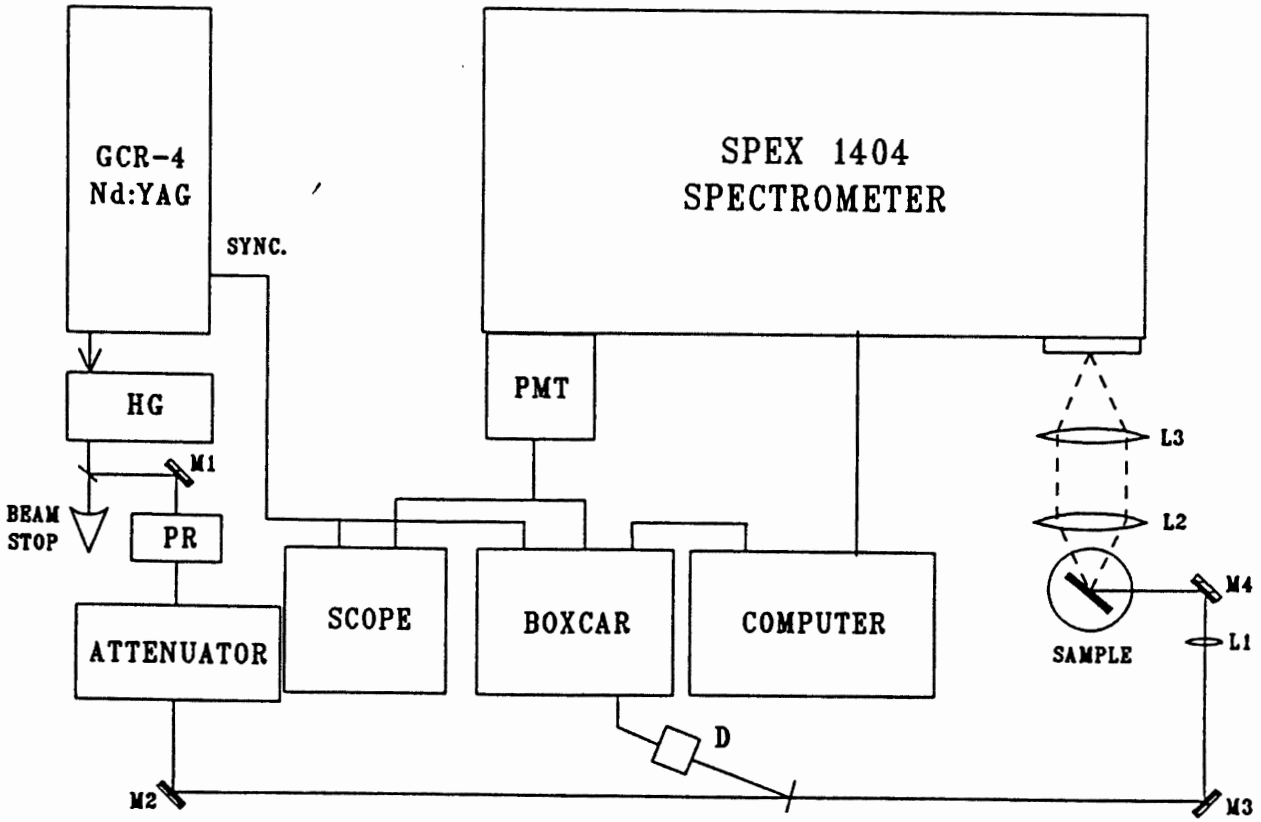

Figure 15. Experimental Setup for Photoluminescence Measurements.

PPS sample was collected at the right angles to the incident beam, focused onto the entrance slits of a SPEX 1404 double grating spectrometer, and detected by a HAMAMATSU R943-02 photomultiplier tube(PMT). This PMT has a GaAs(Cs) cathode with a wide spectral response ranging from 160 nm to 930 nm. The PMT is thermoelectrically cooled to -25^{0}C. The signal from PMT was directly input to an EG&G 4422 gated sampler with impedance of 50 Ω and averaged by the 4420 Boxcar Averager. The spectral response of our spectrometer from 360 nm to 660 nm has been calibrated by using a standard quartz tungsten halogen (QTH) lamp from The Eppley Laboratory. All our photoluminescence spectra were corrected (see Appendix B).

The absorption spectra of PPS samples were measured using a Cary 2400 spectrophotometer.

Results and Discussion

In the following sub-sections we present the absorption and fluorescence spectra from two biaxially oriented crystalline PPS films and from a set of amorphous PPS films with different thermal treatments. The main luminescence of PPS is attributed to the $\pi^* \rightarrow \pi$ transition [50] while the peak intensity and shape are related to the sample morphology and thermal process. We use a deconvolution method to determine the luminescence decay which is approximately exponential with a lifetime independent of the sample morphology and thermal process. We present and discuss the PL change upon photodegradation (UV exposure). We also present the low temperature PL spectra which show the well resolved vibronic structure. We then use the lattice-relaxation model developed in the previous section (see "Theory") to interpret these experimental data. Our results indicate that the electron-lattice coupling strength is slightly reduced after the thermal-aging treatment.

Absorption Spectra

The absorption spectra of the PPS film and its trimer, tetramer oligomers in the CCl_4 solution were measured at room temperature in the region from 300 to 400 nm. As shown in Figure 16, the absorption edge significantly shifts to longer wavelengths when the phenylene-sulfide chain extends from trimer (3-phenyl rings), tetramer (4-phenyl rings), to polymer

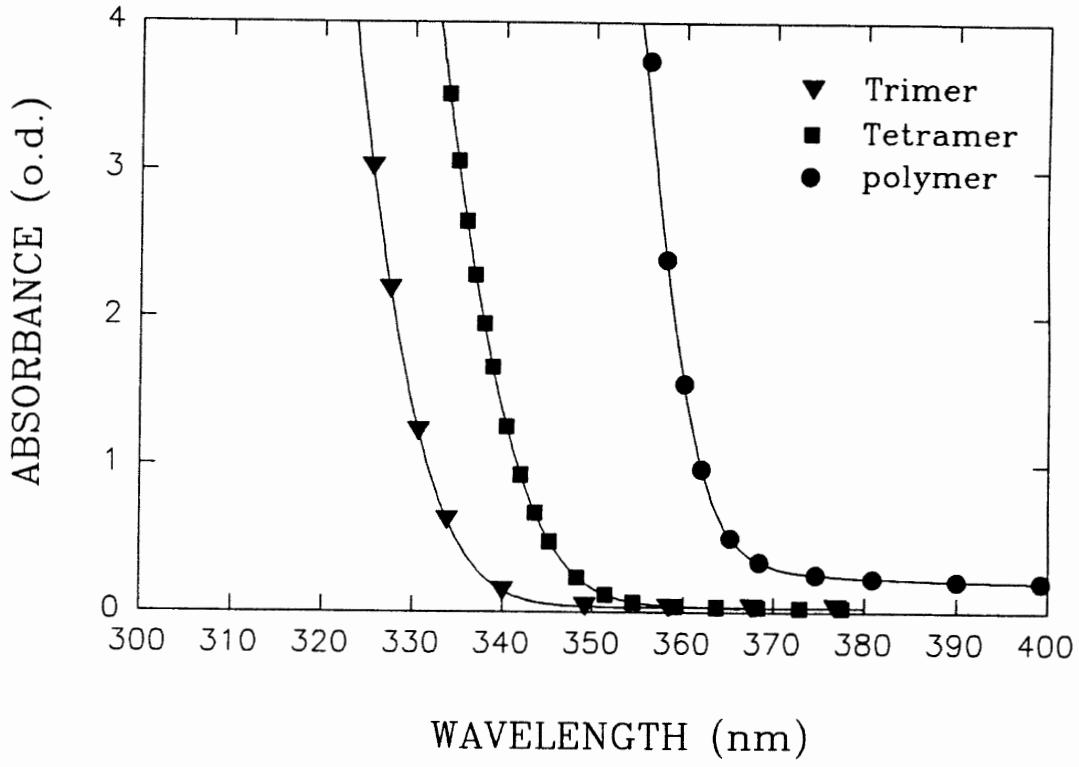

Figure 16. Room Temperature Absorption Spectra From a 1.8 μm PPS Film and From the Trimer and Tetramer Oligomers in the CCl_4 Solution.

(~ 400-phenyl rings). The absorption edges (at an absorbance value of 0.5) are at 334, 344, and 365 nm, corresponding to trimer, tetramer, and a biaxially oriented PPS film, respectively. The energy gap decreases when the π-obital overlap extends over more phenylene rings. This property indicates that even though the phenyl rings are orthogonal to one another, the appreciable delocalization of the π-electrons along the PPS chain still exists. This result is in agreement with the previous study by J.L. Bredas et al [55].

Figure 17 shows the absorption spectra from a set of amorphous PPS films with different durations of the thermal-aging treatments. The spectrum of aged sample has a higher absorption tail and shows higher broad-band absorption in the visible region compared with that of the un-aged sample. The absorption edges represent the $\pi \rightarrow \pi^*$ transitions in PPS [50]. The sharp absorption edge shifts from 364 nm for the un-aged film to 365.5 nm for the two-hour aged sample and shifts slightly further for samples with longer aging times. The absorption peak was taken at 326 nm for un-aged PPS film from the absorption spectrum (Fig. 18) of a PPS thin film reported by R.H. Fried and J.M. Giles [34]. It was reported that cross-linking, chain-extension and oxidization occurred when PPS was thermal-aged at 260^{0}C in air [62]. Therefore, the higher absorption tail most possibly reflects the collective absorption behavior from thermal degraded PPS molecules. The broad-band absorption in the visible region are from these

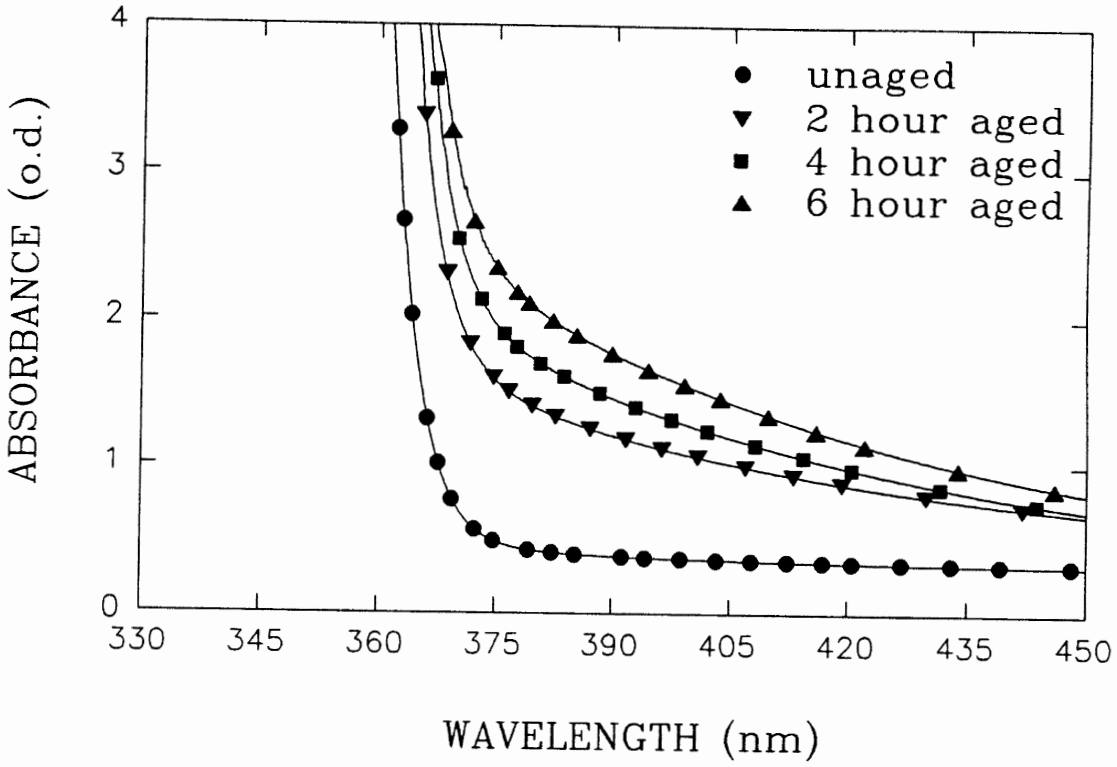

Figure 17. Room Temperature Absorption Spectra From a Set of Amorphous PPS Films with Different Thermal-aging Times.

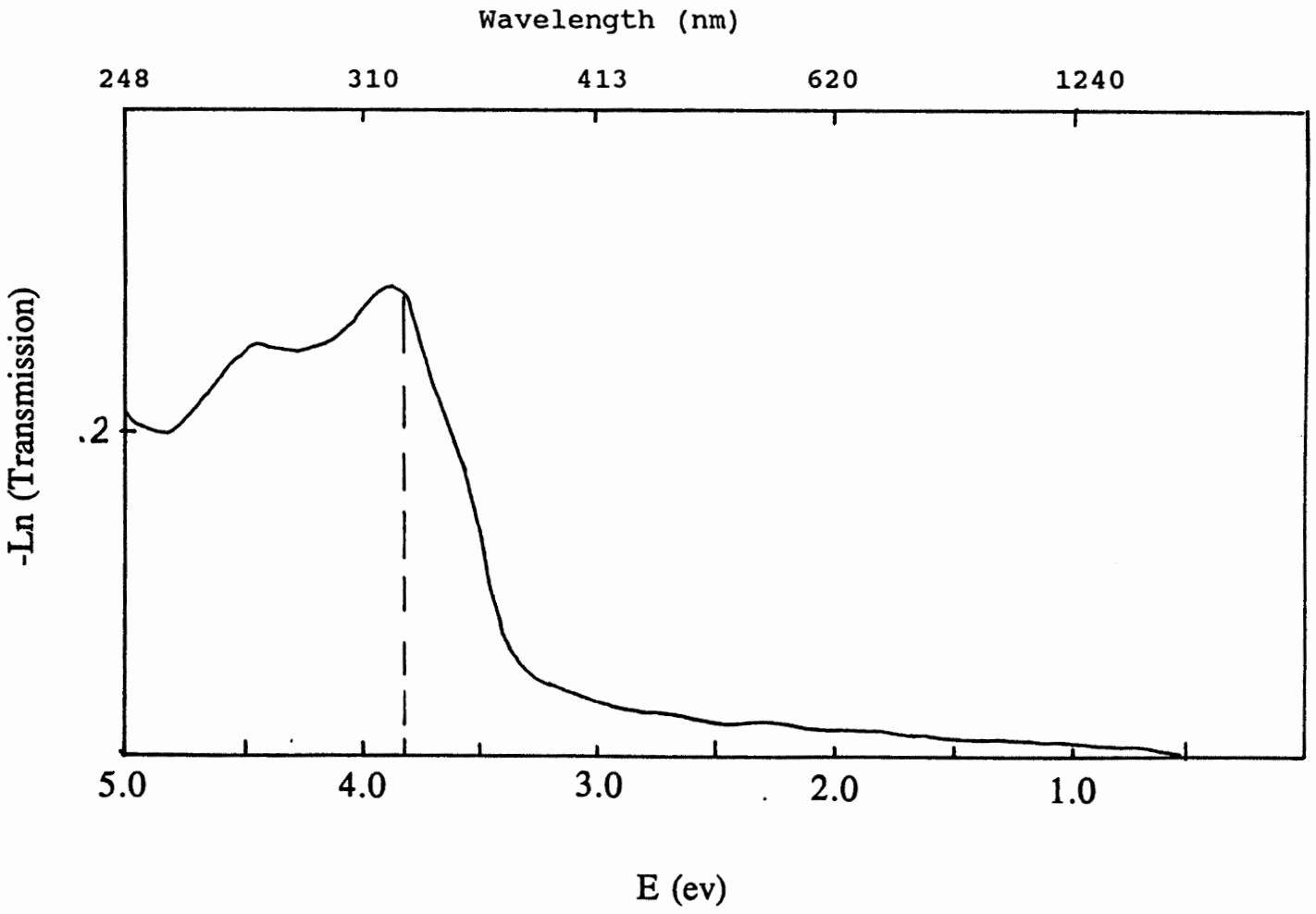

Figure 18. The Absorption Spectrum of a PPS Thin Film (< 0.1 μm). (From R.H. Friend and J.R.M. Giles, J. Chem. Soc., Chem. Commun., 1101(1984).)

chemical species which have smaller energy gaps. These species with smaller gaps were formed during heating of the polymer in air [63].

Figure 19 shows the temperature dependence of the absorption from a biaxially oriented PPS film. These spectra were taken at T = 10k, 77k, 300k, respectively. The results show that the absorption edge in PPS has a small temperature dependence with an energy change of -8.3×10^{-5} ev/K. We found that the absorption edge of the amorphous and thermal-aged films have the same temperature dependence.

Room Temperature Photoluminescence

PL measurements were carried out on PPS films. The PL spectra from a biaxially oriented crystalline film, an amorphous film, and a heat-treated film are shown in (a), (b), (c) of Figure 20, respectively. All these PL spectra show a broad band emission peaked between 375 nm to 390 nm. The FWHM (full width at half maximum) for each sample is between 2200 and 2800 cm^{-1}. This broad band feature is due to the amorphous nature and the multiphonon assisted transitions [64]. The main peak of luminescence is attributed to the $\pi^* \rightarrow \pi$ singlet transition. The π-electron in PPS is partially delocalized along the chain [65]. As a result, the dominant "electronic" excitations are inherently coupled to chain distortions. The π-electron also plays a key role in conductivity upon doping [66]. Comparing the emission profile of the biaxial film with

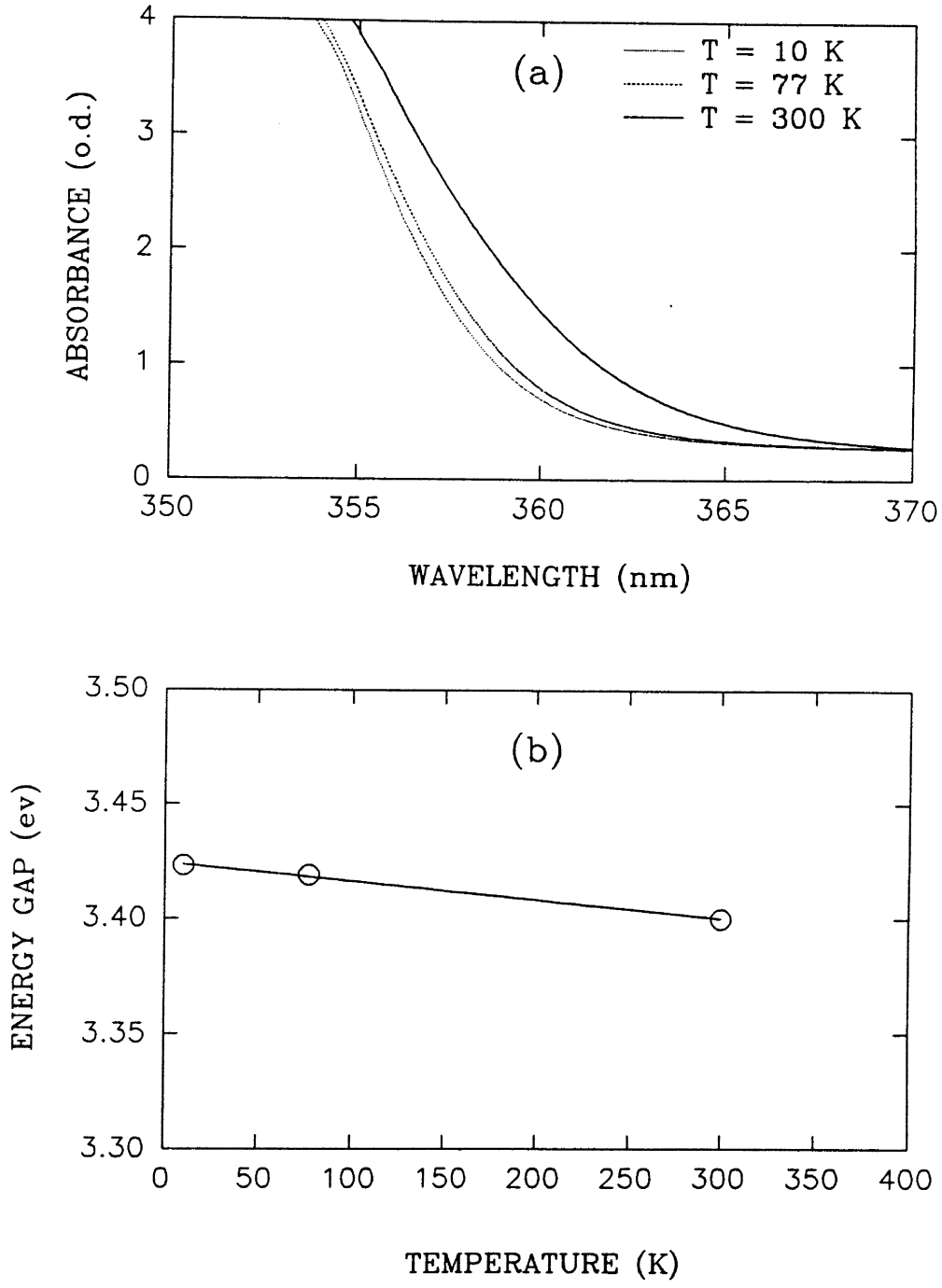

Figure 19. The Temperature Dependence of the Absorption Edge of the PPS Film. (From a 1.8 μm PPS Film)

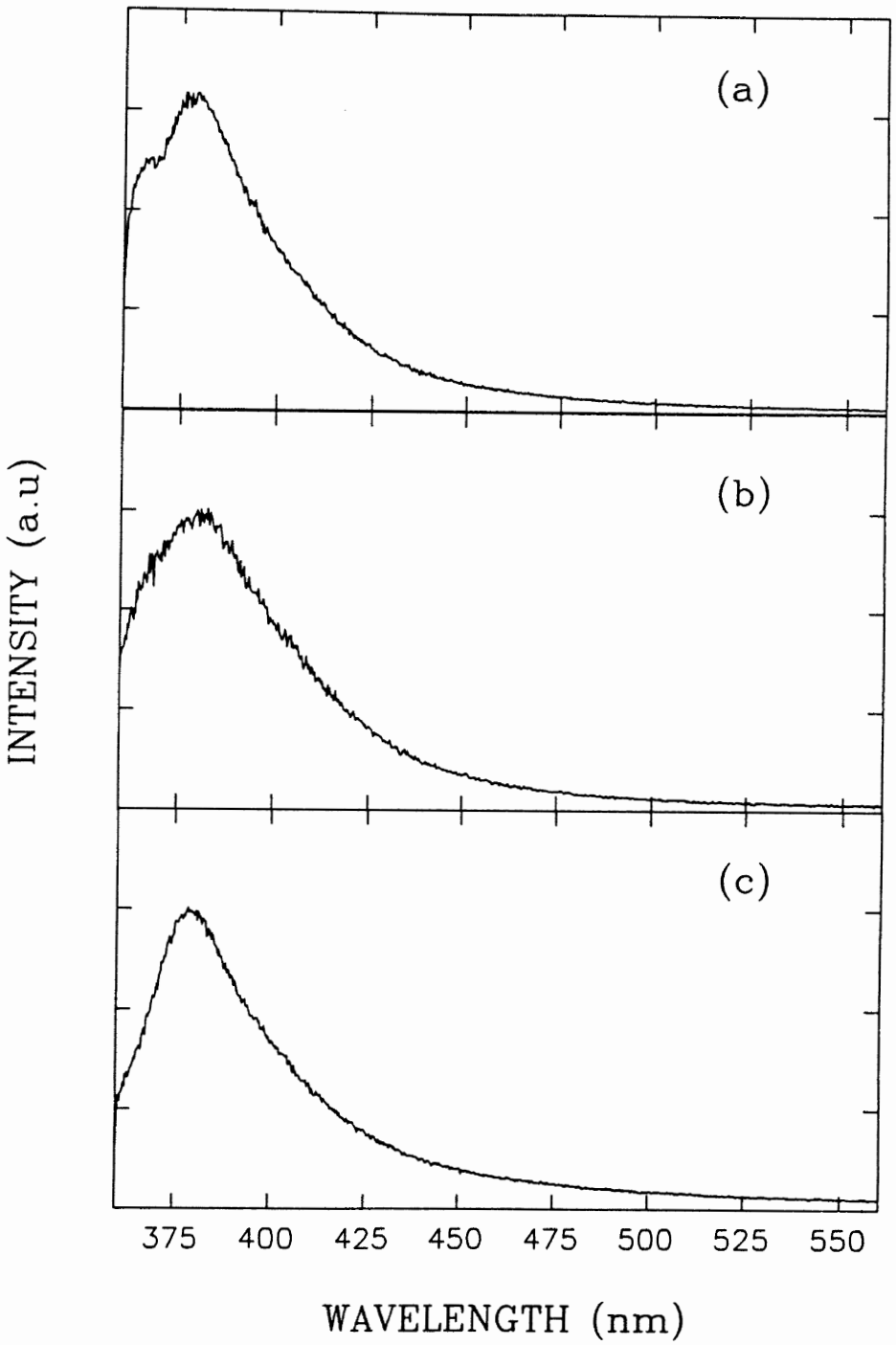

Figure 20. Room Temperature PL Spectra of PPS Films. (a) Biaxial Film, (b) Amorphous Film, (c) Heat Treated Film.

that of the amorphous film, we found that the emission of the biaxial film had a sharper peak and a shoulder at shorter wavelength, and shifted about 6 nm towards shorter wavelengths. The PL spectrum of the heat-treated film shows some characteristics of recrystallization, which has a sharper peak and slightly shifts to a shorter wavelength compared to the un-heated amorphous film.

The spectra shown in Fig. 21 were from a set of amorphous PPS films with different time durations of the thermal-age treatment. The intensity of the fluorescence from aged films is reduced while the broad band emission at longer wavelengths is relatively enhanced. The peak intensity from aged films is probably reduced due to the presence of quenching impurities which were unintentionally introduced during the heating of the PPS in air. This process of impurity quenching is commonly due to an increase in the rate of both intersystem and intra-system crossing from the first excited singlet state to the first triplet state and to the ground state in the presence of the quencher [67]. The process can be represented as

$$ {}^1M^* \xrightarrow{Q} {}^3M^*; \qquad {}^1M^* \xrightarrow{Q} M; \qquad {}^3M^* \xrightarrow{Q} M. \tag{3.19} $$

where $^1M^*$, $^3M^*$, M represent the first singlet excited state, the first triplet state, and the ground state of the PPS molecule while Q is the quencher. Such quenching behavior is typical of impurities such as oxygen. Previous investigations [62,68] confirmed that the oxygen atoms entered the polymer when PPS

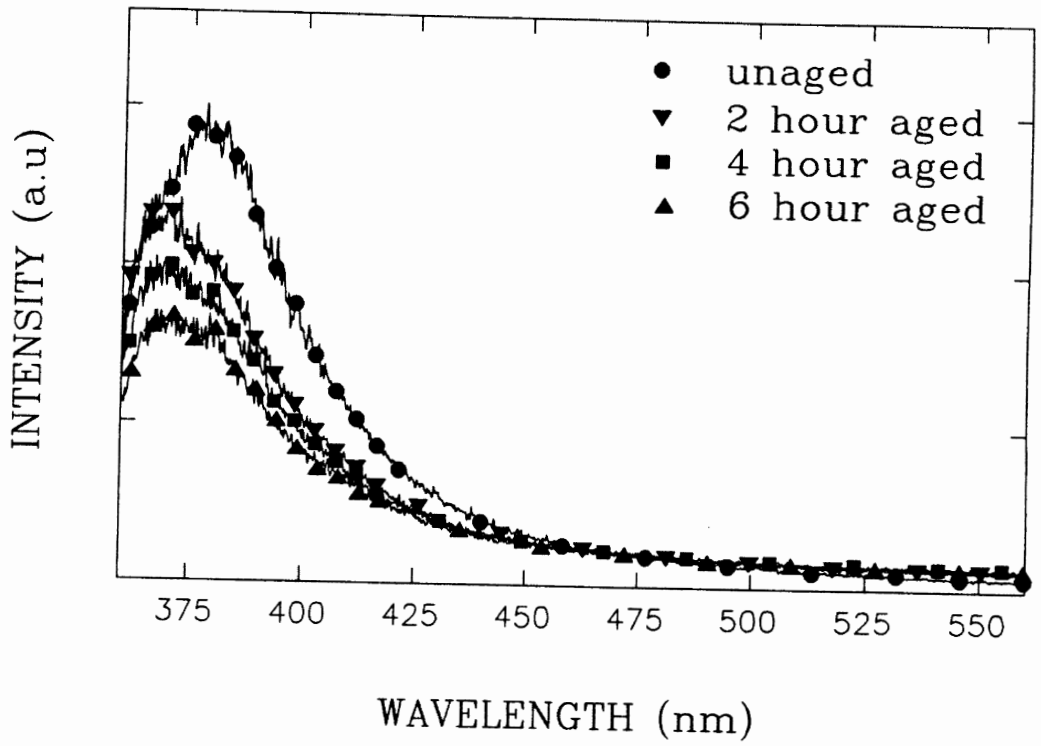

Figure 21. Room Temperature PL Spectra From a Set of Amorphous PPS Films with Different Aging Times.

was heated close to its melting point in air. The relation between the fluorescence quantum yield Φ_{QM} in the presence of a concentration [Q] of Q and the yield Φ_M in the absence of Q is given by

$$\frac{\Phi_M}{\Phi_{QM}} = 1 + K_{QM}[Q] \qquad (3.20)$$

where $K_{QM} = k_{QM}\,\tau_M$ is the Stern-Volmer coefficient of impurity quenching, k_{QM} is the impurity quenching rate parameter, and τ_M is the fluorescence lifetime of $^1M^*$ in the absence of Q. In addition, the energy of the excited state of PPS molecules may also be transferred to secondary radiating centers which in turn emit their own luminescence in the region of longer wavelengths; these emissions at longer wavelengths is increased for aged samples.

We also noticed that the peak position of the aged PPS films was slightly shifted to shorter wavelengths, while their absorption edge was shifted to longer wavelengths. Presumably, this is due to the change of the electron-vibration coupling strength after the aging processing. We will discuss the electronic-vibration coupling in the PPS later.

Emission Decay of PPS

The fluorescence lifetime measurements were carried out using a deconvolution technique owing to the comparable events in the time range between the PL decay and the light source duration of 6 ns. In addition, the PMT rise time is also of

concern. At room temperature, we measured the temporal emission profiles of all PPS films at their peak positions (380 to 385 nm). We found that different samples have the same decay profiles. The lifetimes were found to be 2.6 ± 0.5 ns. We also recorded the emission decay profile from the photodegraded sample at 500 nm and found the lifetime at 500 nm was about twice as long as at 380 nm. The longer lifetime at 500 nm probably indicates that the emissions around 500 nm may come from degraded species in PPS. At low temperature of T = 6 K, we measured the emission decay profiles at both the main peak (365 to 370 nm) and the second peak (380 to 385 nm). We found that the luminescence at these two peaks has the same decay profiles. The fluorescence life time is 3.2 ± 0.5 ns. Although the lifetime data obtained have significant errors, they are still valuable because no fluorescence lifetime data of PPS have been available in the literature. We describe the deconvolution method in the following:

Denote the measured emission signal at the fluorescence peak as S(t). Suppose our detection system has a response function h(t) and the true emission temporal profile of PPS, when excited by a impulse laser source (δ(t)), is E(t). Denote the temporal profile of laser as l(t) and the observed laser pulse by the same PMT as L(t), Using linear system approximation [69], we have

$$L(t) = l(t) \otimes h(t) \tag{3.21}$$

$$S(t) = l(t) \otimes h(t) \otimes E(t) = L(t) \otimes E(t) \tag{3.22}$$

where $\otimes$ denotes the convolution and is defined as

$$S(t) = L(t) \otimes E(t) = \int_0^t L(\tau) \cdot E(t-\tau) \cdot d\tau \qquad (3.23)$$

or

$$S(n) = L(n) \otimes E(n) = \sum_{k=0}^{n} L(k) \cdot E(n-k) \qquad (3.24)$$

Obviously, we can obtain the true emission decay E(t) by deconvoluting the measured pulse profile of the laser signal and the measured pulse profile of the emission signal. We record the observed emission pulse S(t) and the laser pulse L(t), then convolute the laser pulse and an exponential decay function E(t) with time constant τ, search for a value of τ with which the convolution result has a best fit to the measured signal S(t). The situation at room temperature is illustrated in Figure 22 where τ = 2.6 ns gives the best fit and the situation at T = 6 K is illustrated in Figure 23 where τ = 3.2 ns. In both situations the exponential decay fitting is consistent with the measured results. This indicates that the actual emission decay is approximately exponential. Figure 24 compares the emission profiles of a biaxial film at the wavelength of 382 nm and at 500 nm after an additional 1.5 hour UV exposure, both were recorded at room temperature.

The room temperature PL of different PPS films are summarized in Table III.

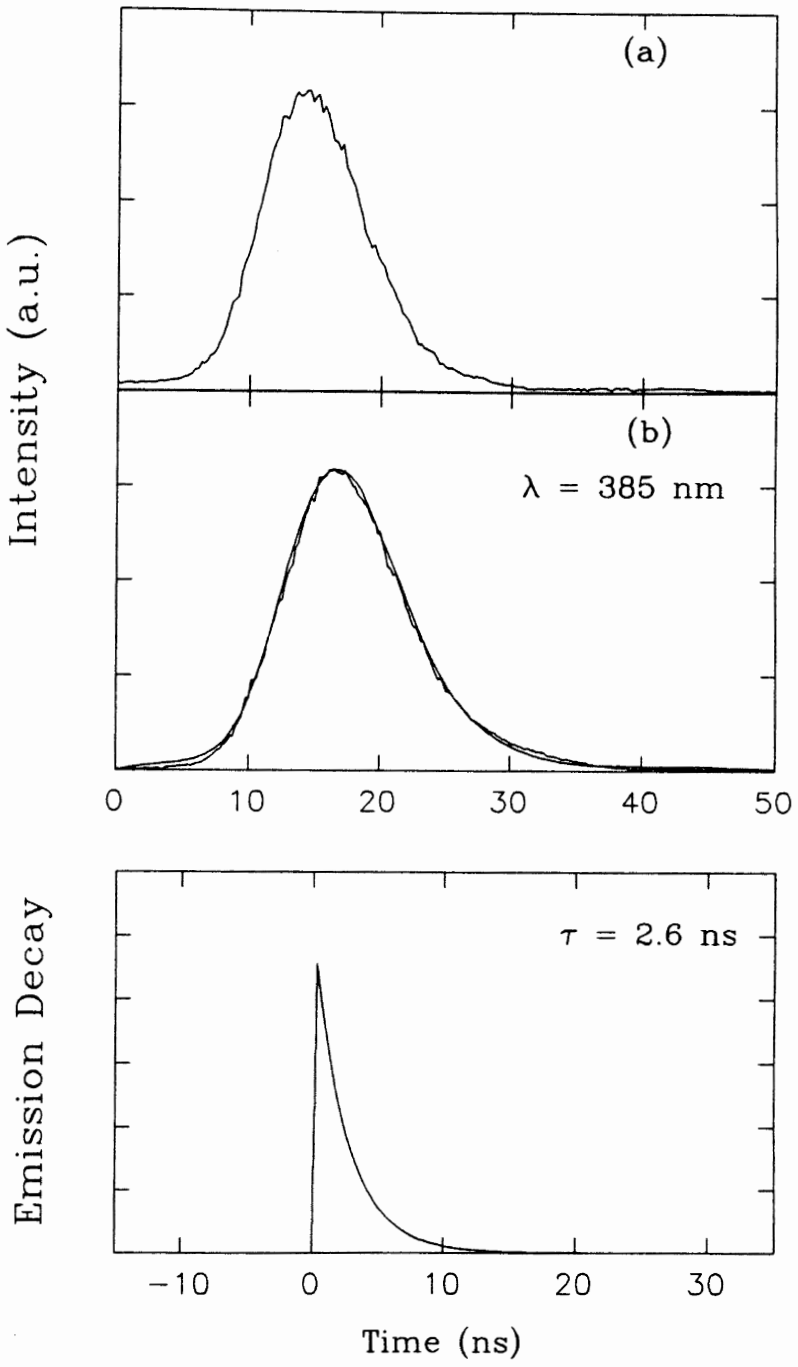

Figure 22. Emission Decay of an Amorphous Film at Room Temperature. Deconvolution of the Laser Pulse and the Emission Pulse, (a) the Measured Laser Pulse, (b) the Measured Emission Pulse, (c) the Deconvoluted Result.

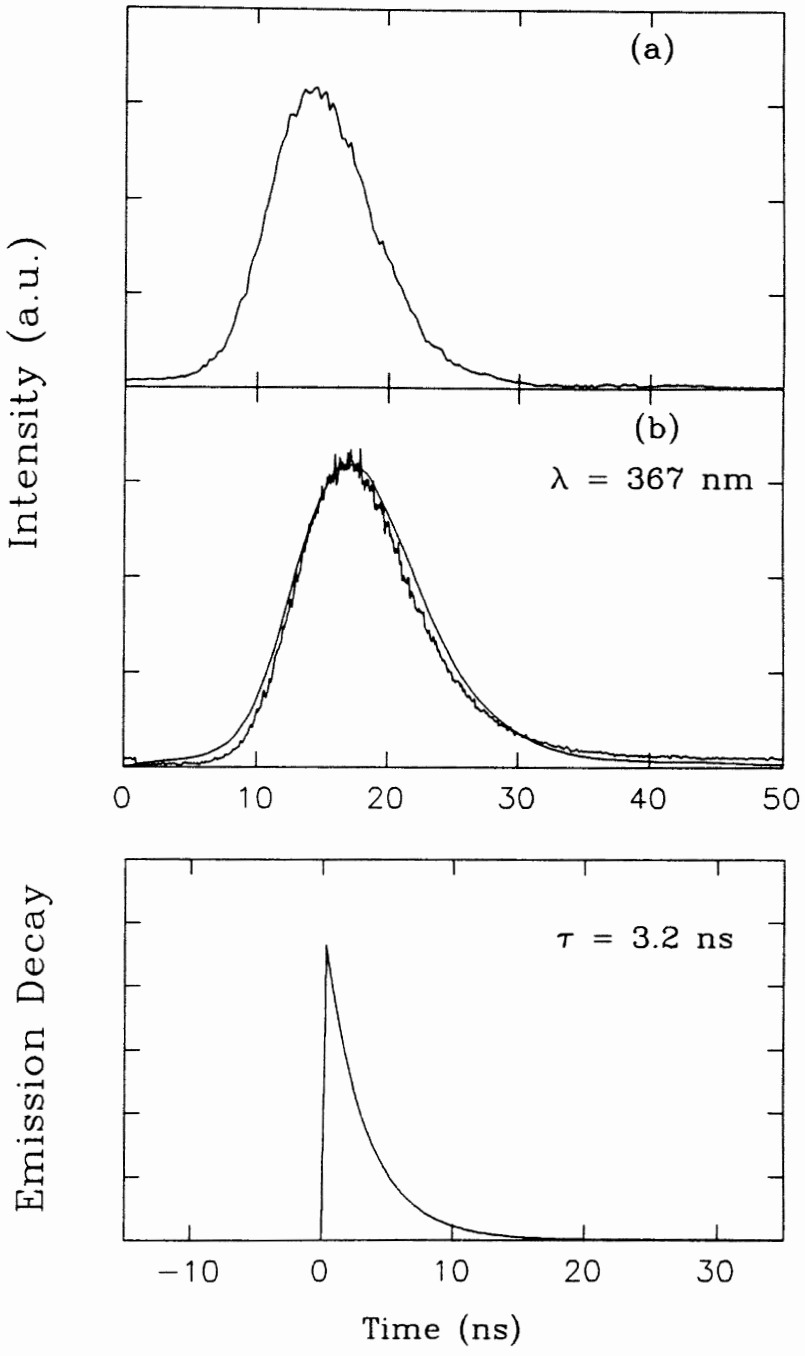

Figure 23. Emission Decay of an Amorphous Film at T = 6 K. Temperature. Deconvolution of the Laser Pulse and the Emission Pulse, (a) the Measured Laser Pulse, (b) the Measured Emission Pulse, (c) the Deconvoluted Result.

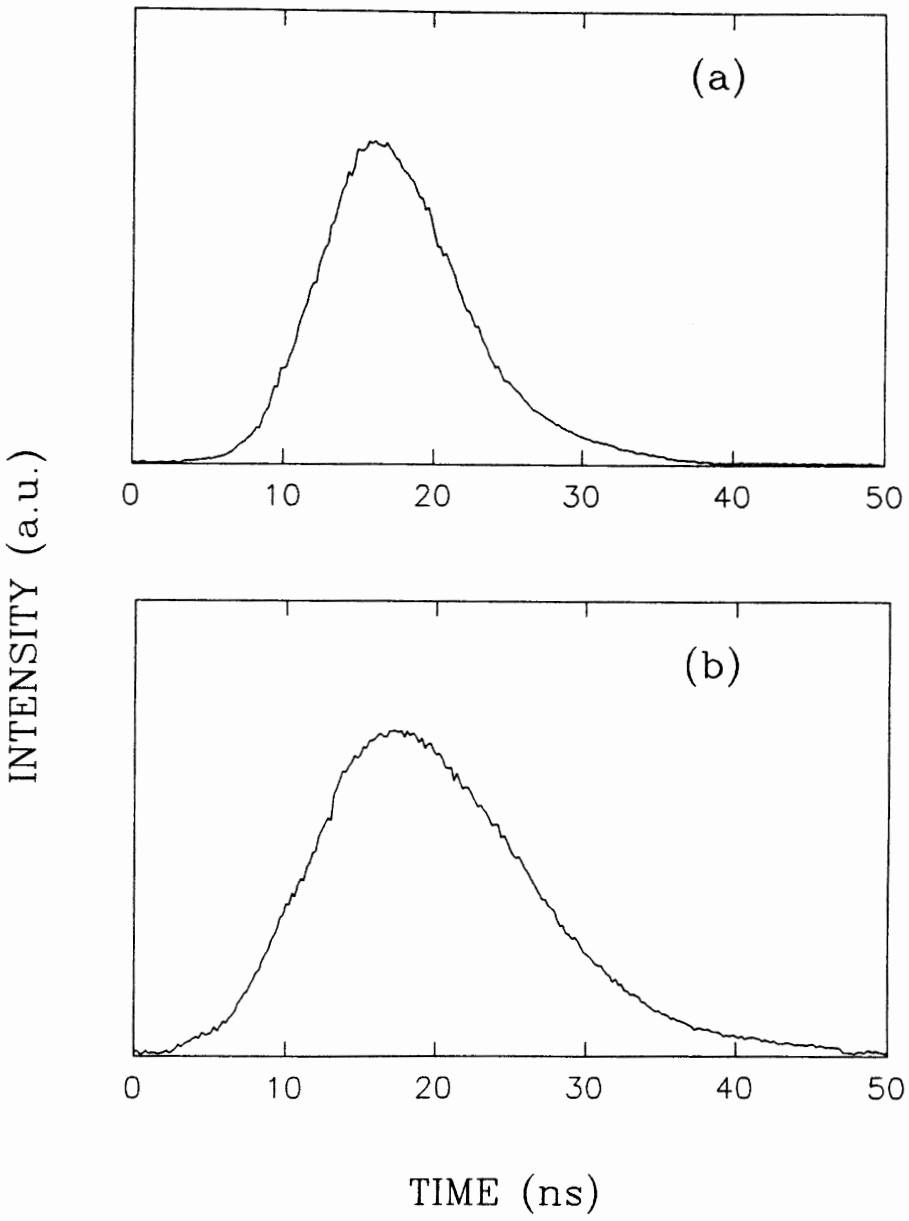

Figure 24. Room Temperature Emission Decay Profile of a Photodegraded Biaxial Film at (a) λ = 382 nm, (b) λ = 500 nm after an additional 1.5 hr. UV exposure.

TABLE III

ROOM TEMPERATURE PL SUMMARY

	λ_p (nm)	FWHM (cm^{-1})	I_p	τ_p (ns)
#1	~ 381	~ 2500	1.0	2.6 ± 0.5
#2	~ 387	~ 2800	~ 0.7	2.6 ± 0.5
#3	~ 383	~ 2400	~ 0.9	2.6 ± 0.5
#4	~ 382	~ 2800	~ 0.4	2.6 ± 0.5

where samples #1, #2, #3, and #4 represent biaxial, amorphous, heat set, and two-hour aged PPS films, respectively; λ_p, FWHM, I_p, and τ_p are peak position, full width at half maximum, relative peak intensity, and luminescence life-time, respectively.

Spectral Change Upon Photolysis

PPS degrades upon exposure to radiation [70] and, like most commercial organic polymers, undergoes chemical reactions upon irradiation with ultraviolet (UV) light because it possesses chromophoric groups (as regular constituents and as impurities) capable of absorbing UV light. During our fluorescence measurements, we found that the fluorescence intensity at the main peak from the PPS film decreases with the exposure time (Fig. 25). This reduced intensity cannot be recovered. In the meantime, however, we found that the broad band emissions at the longer wavelength region of 420 to 500 nm is relatively enhanced after the longer time of UV exposure. This enhancement is even more significant if the sample was under a nitrogen gas atmosphere. Figure 26 shows the spectral change from an amorphous heat set film before and after an additional 1.5 hr. UV exposure. These spectral changes are permanent. As reported by C.E. Hoyle and K-J Kim [71], the photo-Fries rearrangement and cleavage-type products were found in aromatic polyurethanes upon UV exposure. We believe that the similar photolysis can also happen in the PPS film [72]. The Photolysis may begin with the photo-decomposition of the PPS molecule under the UV exposure, followed by the formation of photo-Fries products. The more colored species could be formed through further photochemical reactions. The possible photo-Fries rearrangement of PPS and further reactions are illustrated in Figure 27 [72]. The broad

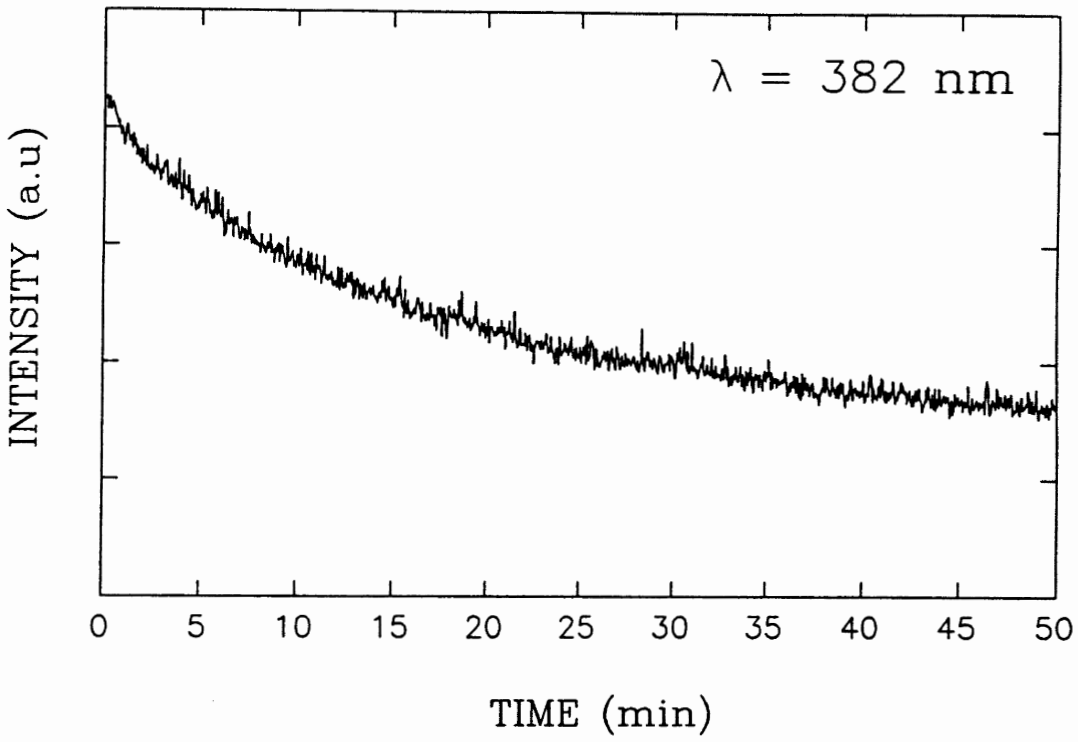

Figure 25. PL Peak Intensity Versus Time. (From a Heat Set PPS Film)

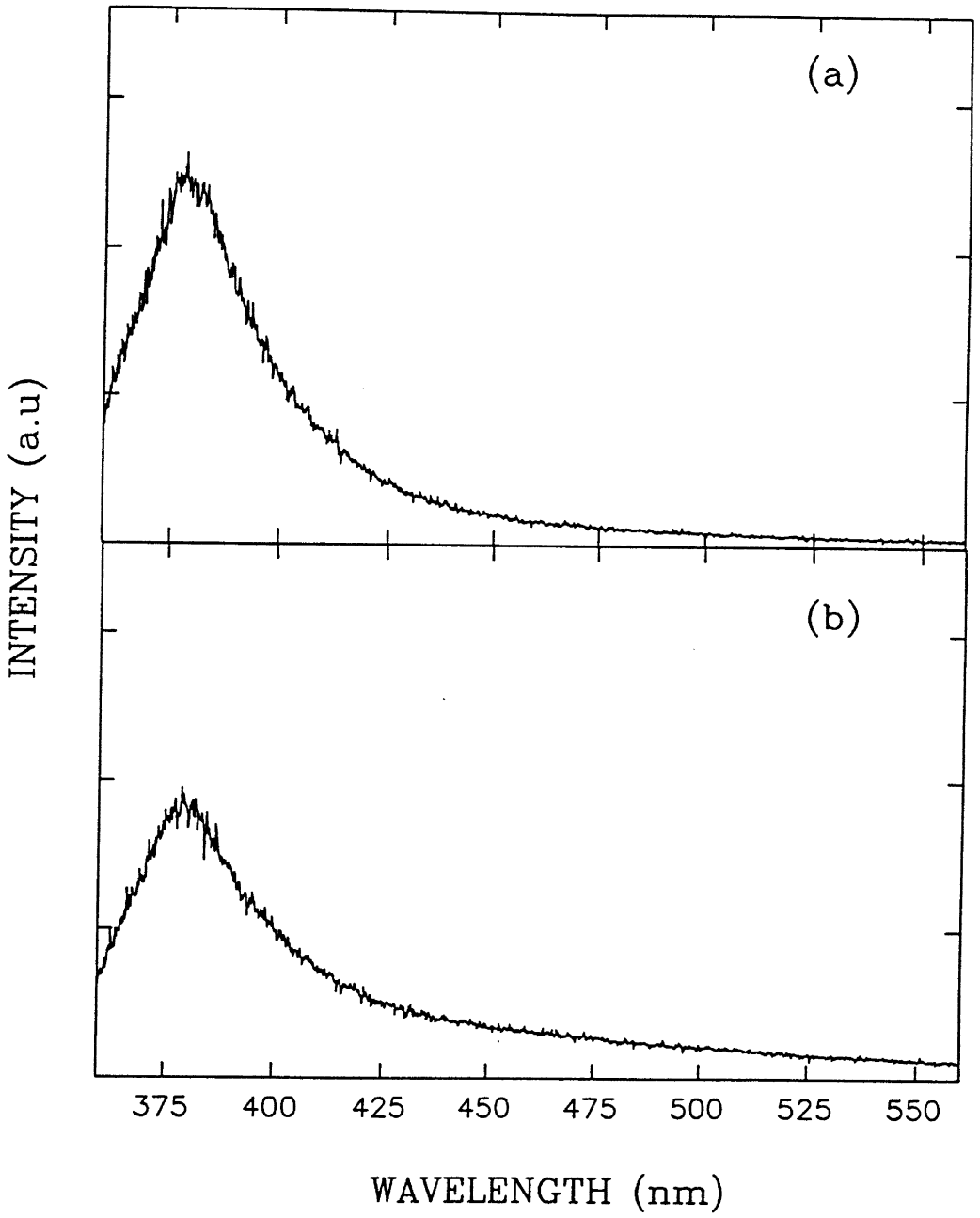

Figure 26. PL Spectra of a Heat Treated PPS Film (Sample is Under N_2 Gas Atmosphere), (a) Before Additional UV Exposure, (b) After Additional 1.5 hr. UV Exposure.

(1) Possible photo-Fries rearrangement:

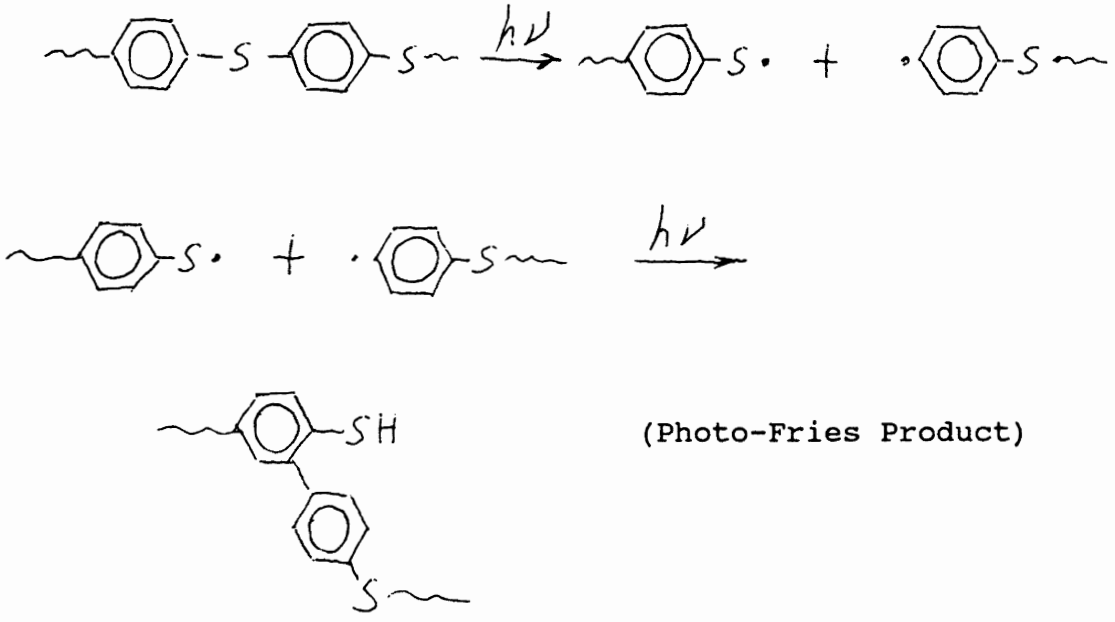

(2) Further reaction may be:

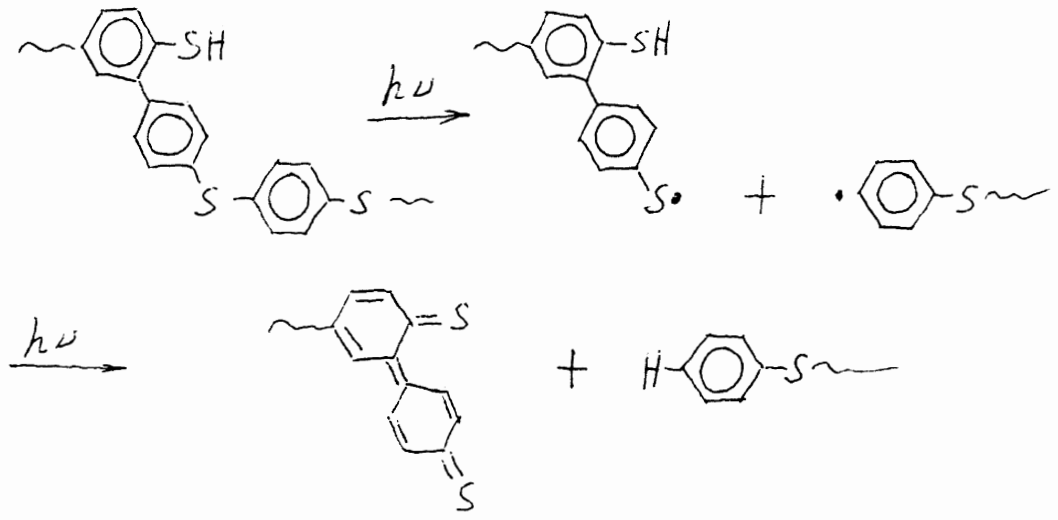

(more colored species)

Figure 27. Possible Photo-Fries Rearrangement and Further Reactions in PPS.

band emissions are related to the new formed chromophores. These new formed colored species may be different depending upon whether oxygen is present. As indicated by Roger Clough [73], photochemical reactions in a polymer material were different in the presence of oxygen than under an inert condition. Oxygen favors chain scission, while irradiation under inert conditions frequently results in crosslinking.

Low Temperature PL - Vibronic Structure

The PL spectra of an amorphous PPS film at T = 293 K, 150 K, 80 K, and 6 K are shown in Figure 28. The PL intensity increases when temperature decreases. At low temperatures the emission spectrum shows two well-resolved peaks at 367 nm and 382 nm. Apparently this emission profile is broadened due to the amorphous nature of the PPS film. The accompanied low energy emission with a long tail expanding to about 450 nm can be recognized as phonon sideband associated with the vibrational states of the polymer chain. The energy spacing between the two peaks is about 1080 cm^{-1}, which is consistence with the intrachain phenylene-sulfur stretching vibration. The latter has an energy of 1076 cm^{-1} from our Raman measurements [74].

Figure 29 shows PL spectra of a two-hour aged amorphous PPS film at temperature of 293, 150, 80, and 6 K. The fabrication of this sample is the same as the amorphous film except for the thermal-aging treatment. The main peak and the

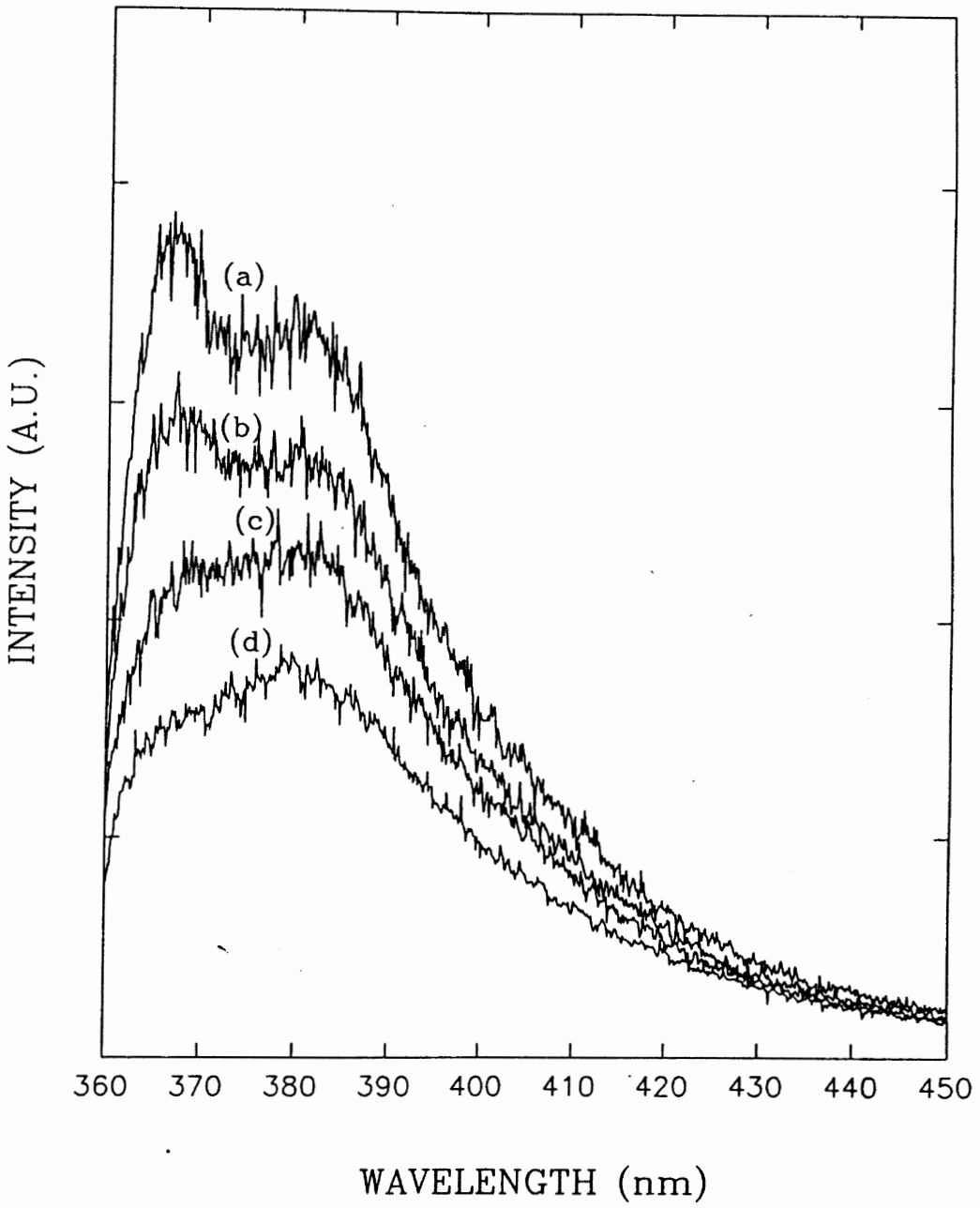

Figure 28. PL Spectra of an Amorphous PPS Film at Four Different Temperatures: (a) T = 6 K, (b) T = 80 K, (c) T = 150 K, (c) T = 150 K, and (d) T = 293 K.

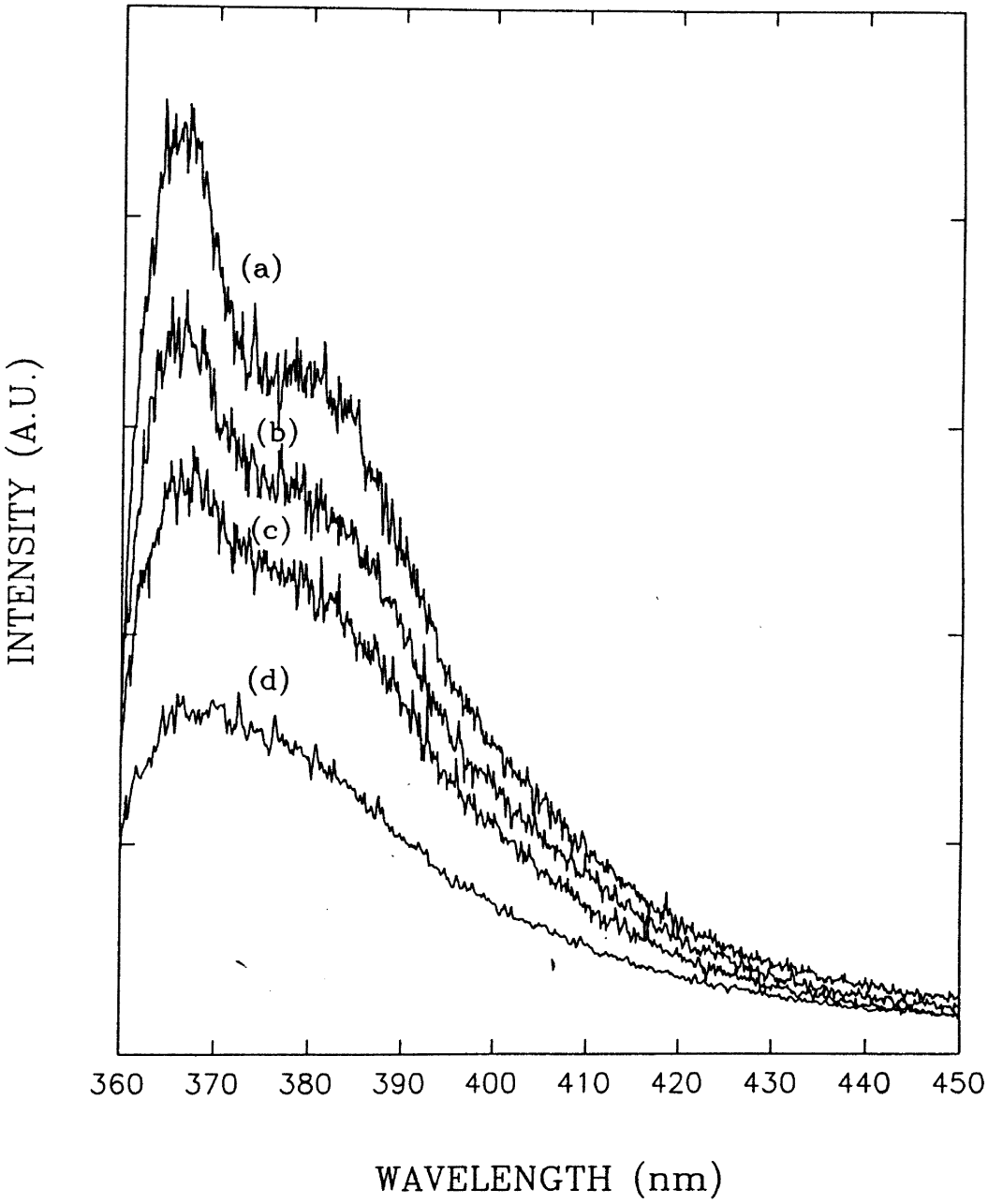

Figure 29. PL Spectra of a 2 hr. Aged Amorphous PPS Film at Four Different Temperatures: (a) T = 6 K, (b) T = 80 K, (c) T = 150 K, and (d) T = 293 K.

sideband of the low temperature spectrum are at 366 nm and 381 nm, respectively. Comparing the spectra of the aged film with that of the un-aged film, it is found that the relative intensity between the main peak and sideband is changed significantly. The main peak of PL is much more intense than the sideband from the aged film. The peak position in the PL spectrum is shifted towards higher energy by about 80 cm^{-1} ($\Delta\lambda \approx 1.1$ nm), while the absorption is shifted towards lower energy by about 120 cm^{-1} ($\Delta\lambda \approx 1.5$ nm) (see Fig. 17) relative to that of the un-aged amorphous film.

The PL spectra of a biaxial-oriented film and a heat-set film at these four different temperatures are shown in Figure 30 and Figure 31, respectively. All these PL spectra from PPS films revealed that: (i) the vibronic structure with an energy spacing of 1080 cm^{-1}, which is nearly identical to the energy of the intrachain phenylene-sulfur stretching vibration; (ii) the PL intensity decreases when temperature increases. This decrease is reasonable for polymer material because at high temperature the quenching rate is increased [75]. Figure 32 shows the PL peak intensity versus temperature from an amorphous film and a two-hour aged amorphous film. The PL intensities from the biaxial and heat set films have similar temperature dependences.

Based on the lattice relaxation model described in the theory section, the main PL peak is associated with the vertical transition from the zero vibronic state of the upper

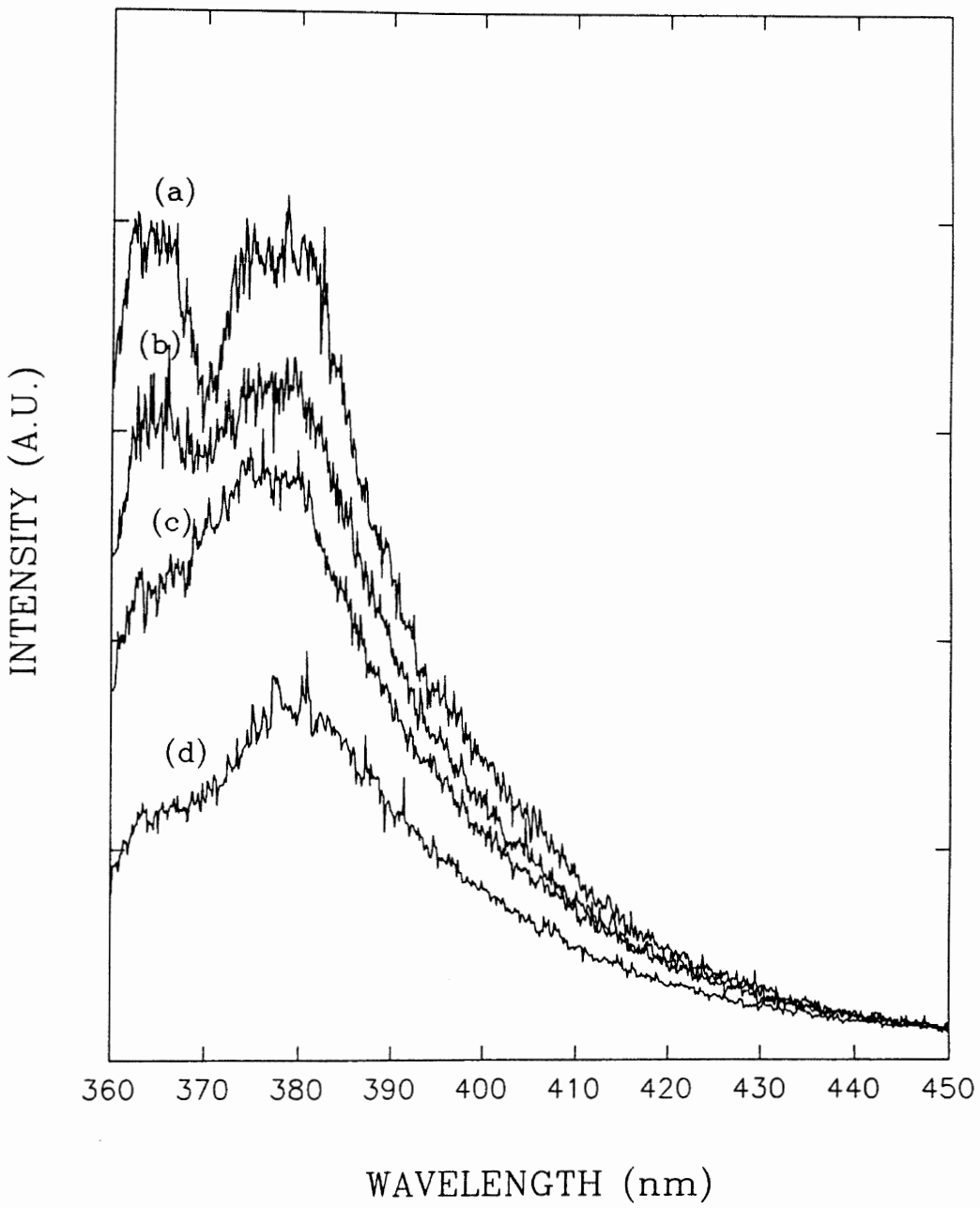

Figure 30. PL Spectra of a Biaxially oriented PPS Film at Four Different Temperatures: (a) T = 6 K, (b) T = 80 K, (c) T = 150 K, and (d) T = 293 K.

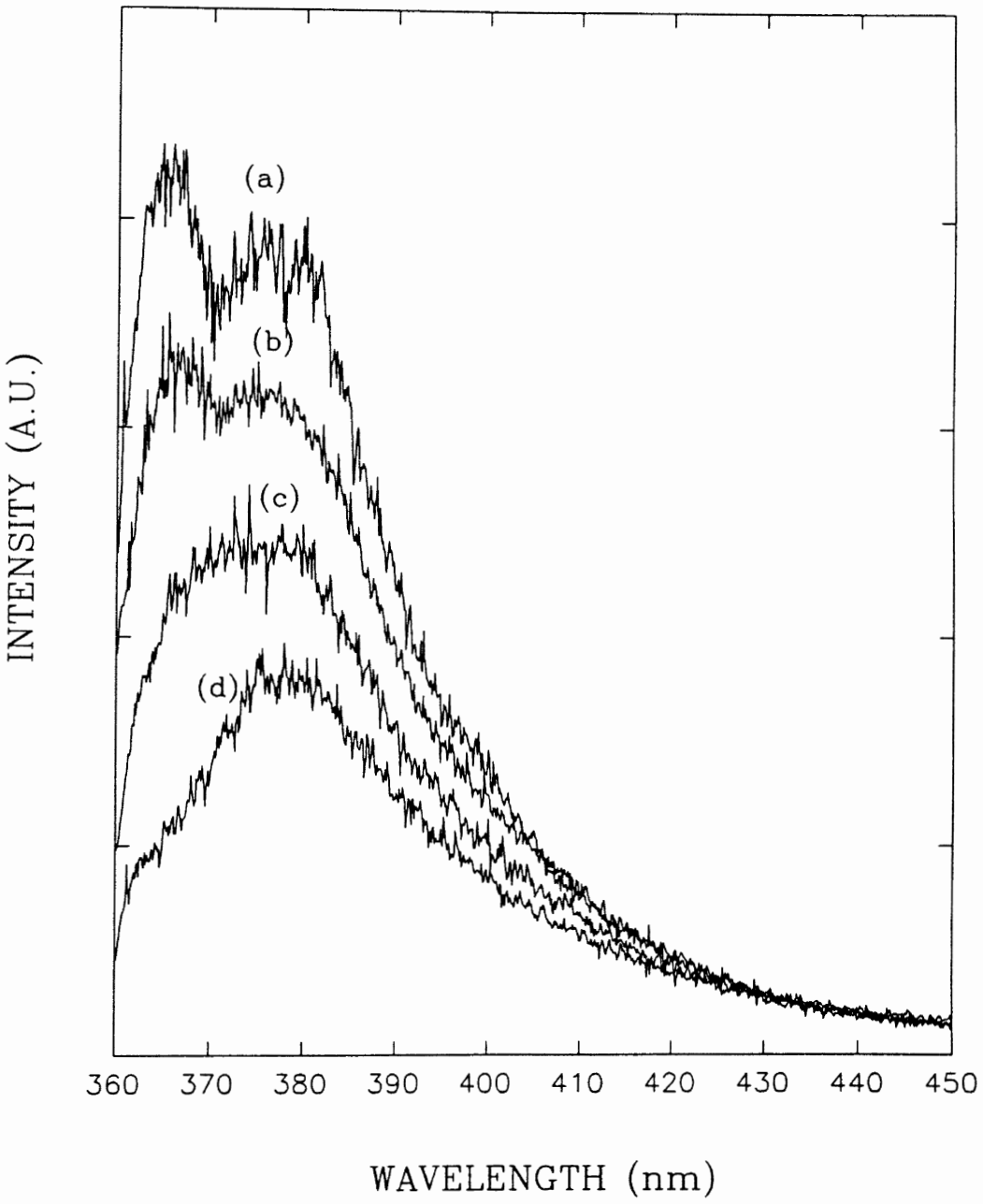

Figure 31. PL Spectra of a Heat-Set PPS Film at Four Different Temperatures: (a) T = 6 K, (b) T = 80 K, (c) T = 150 K, and (d) T = 293 K.

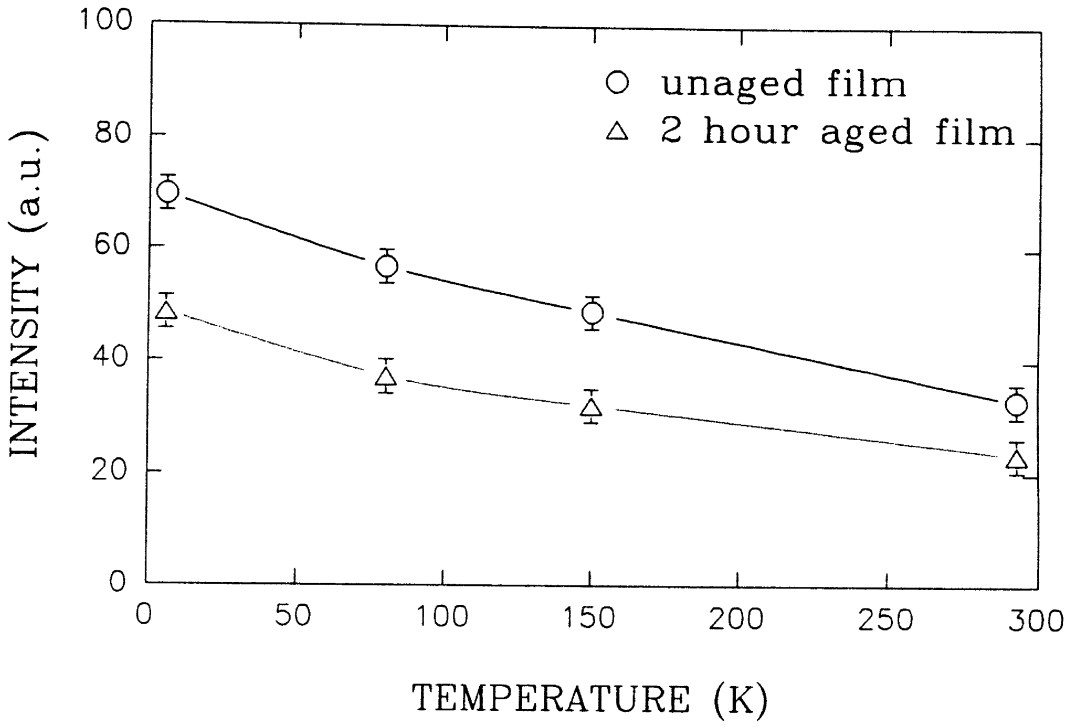

Figure 32. Temperature Dependence of the PL Peak Intensity of an Amorphous Film and a 2 hour Aged Film.

level to the vibronic state of the lower level (C→D in Fig. 13); the main PL peak of the un-aged amorphous PPS film is at about 27250 cm^{-1} (367 nm). The absorption peak is associated with the vertical transition from the zero vibronic state of the lower level to the vibronic state of the upper level (A→B in Fig. 13). The absorption peak was taken at 30680 cm^{-1} (326 nm) (Fig.18 from Ref. 34). The Stokes shift is then about 1700 cm^{-1}. According to our Raman results, the highest Raman frequency is 1573 cm^{-1} while the lowest one is 468 cm^{-1}. We then took the Raman mode of 1076 cm^{-1} as the effective frequency and obtained the Huang-Rhy's parameter $S \approx 1.6$ (Eq. 3.13) for the amorphous PPS film. This value is larger than the S value of 1.1 in poly (3-methylthiophene) reported by J. Poplawski and E. Ehrenfreund [76]. This result indicates that the electron-lattice coupling in PPS is greater than that in poly (3-methylthiophene). It indicates that the π-electron in PPS is less extended than the π-electron in a conjugated polymer.

Fig. 33 shows the analysis for the PL spectrum of an un-aged amorphous PPS film at 6 K. Based on the "Pekarian Formula" Eq. (3.18), the PL spectrum is composed of a main peak and the accompanied sidebands with a neighboring energy spacing of 1076 cm^{-1}. We used a curve fitting program to fit the PL spectrum by adding a series of gaussian-shape lines with spacing of 1076 cm^{-1}. Each subsequent band corresponds to different phonon orders. The relative intensities of these bands approximately follow the Poisson distribution with S =

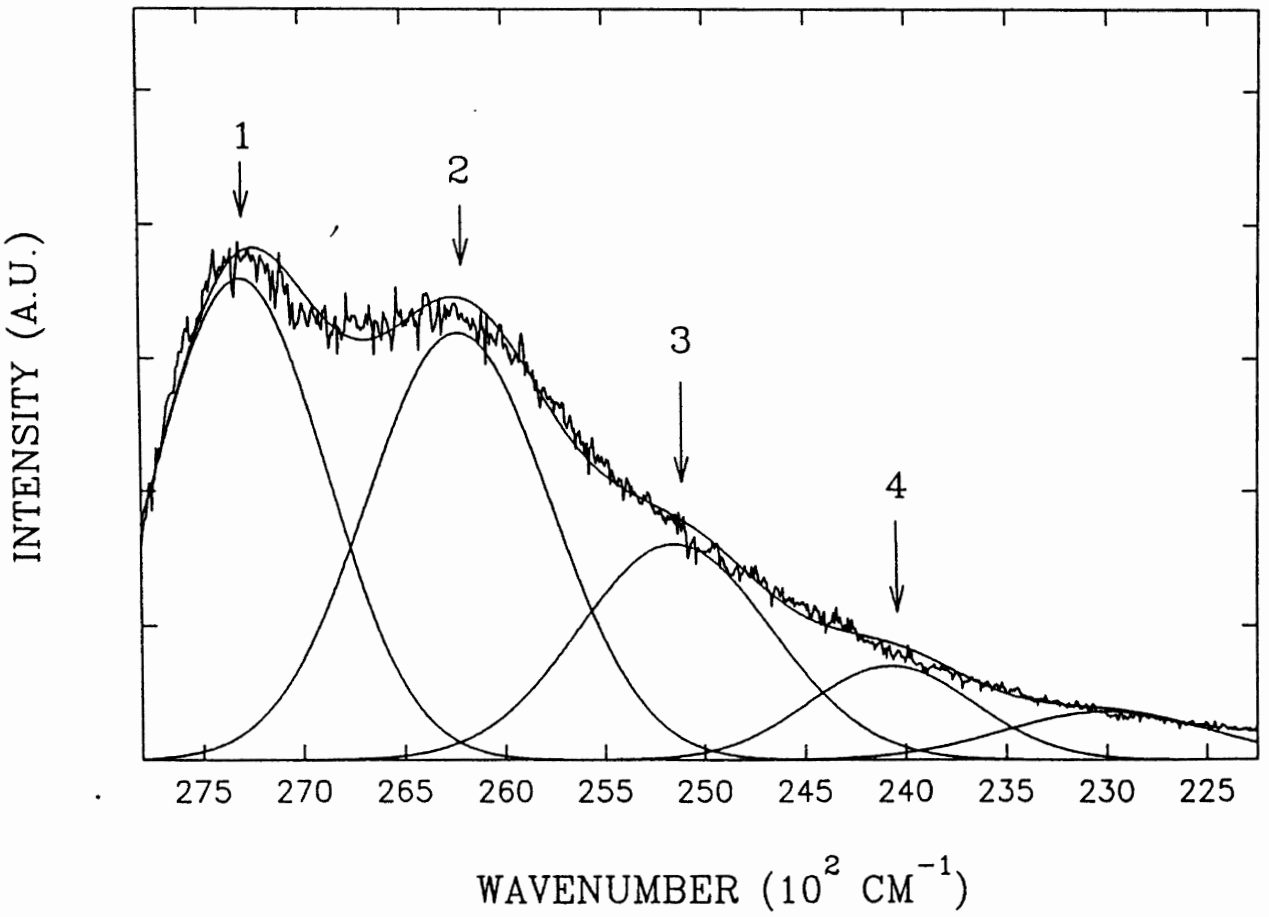

Figure 33. Curve Fitting for PL Spectrum of an Amorphous PPS Film at T = 6 K. The Decomposed Vibronic Structure Shows Different Phonon Orders with Gaussian-shape Lines.

1.6. The intensity ratio between first and second peaks is about 1.2. The mechanism of the large band width is mainly attributed to the inhomogeneous broadening. The polymer sample is a complicated molecular ensemble and has amorphous nature. The molecules in a polymer sample have different molecular weights which are widely distributed between 40,000 to 55,000 [32]. There are derivants, faults, unintentional impurities, etc inside the sample. The frequency of a transition is influenced by the molecular change as well as environmental change. Hence, the profile, being a composite of the transitions from different sites, shows a gaussian line shape.

Figure 34 illustrates the analysis for the PL spectrum of a two-hour aged PPS film at 6 K. The spectrum is composed of a main peak and its sidebands with the same energy spacing of 1076 cm^{-1} as in the spectrum of the un-aged sample. The Stokes shift for the aged PPS sample is reduced because its absorption spectrum is shifted to a longer wavelength while its emission spectrum is shifted to a shorter wavelength. The Stokes shift for the two-hour aged PPS film is reduced to about 1600 cm^{-1} and a value of $S \approx 1.5$ was obtained. The change of the S value indicates that the strength of electron-phonon coupling in PPS is modified after the aging process. According to the Poisson distribution, the change of the S value will modify the relative intensity among the main peak and sidebands in a PL spectrum (Fig. 14). This has been seen in Fig. 34 where the spectrum shows a distinct intensity ratio of

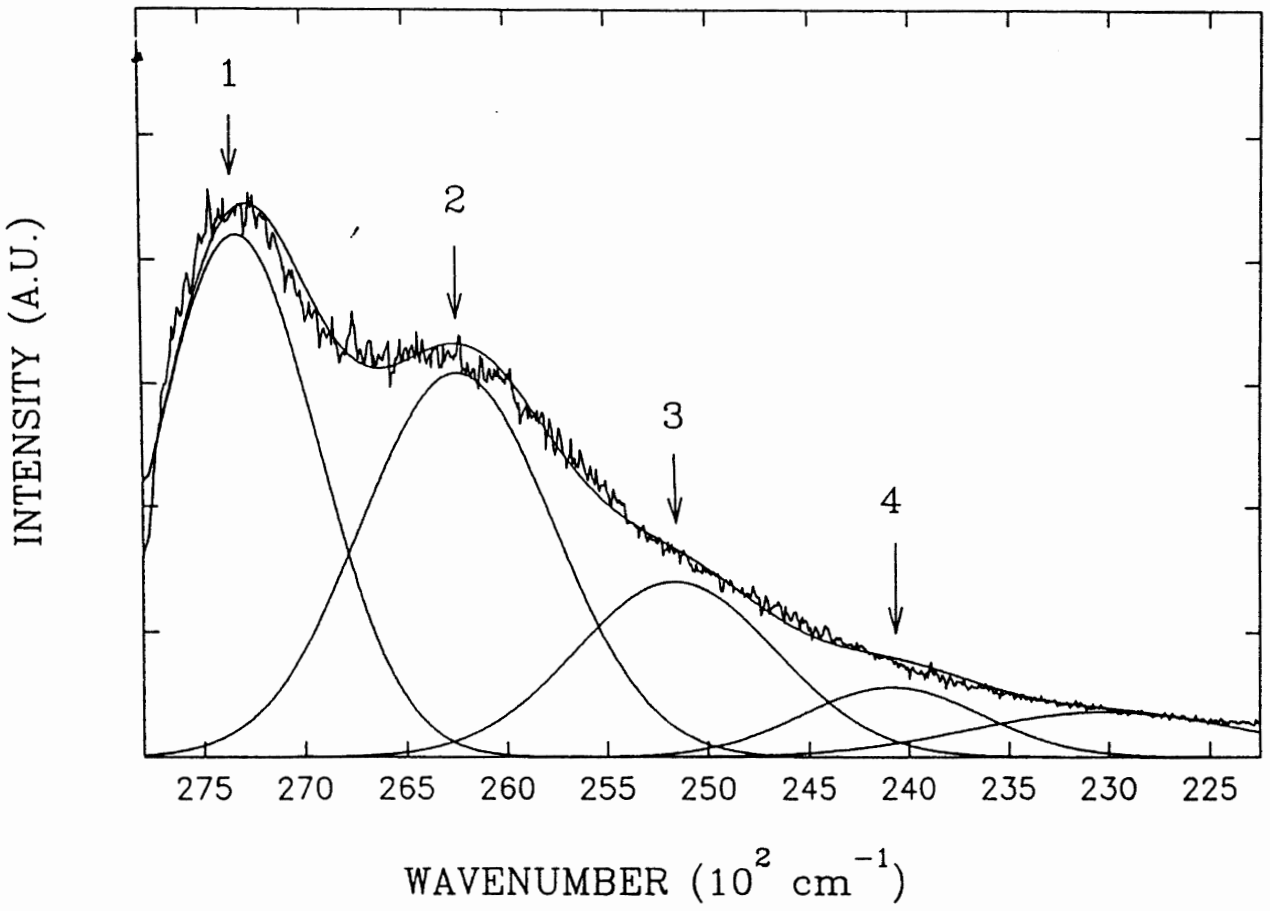

Figure 34. Curve Fitting for PL Spectrum of a Two-hour Aged PPS Film at T = 6 K. The Decomposed Vibronic Structure Shows Different Phonon Orders with Gaussian-shape Lines.

the main peak emission to the sideband. The intensity ratio between first and second peaks for aged sample is 1.36, which approximately follows the Poisson distribution. The reduced Stokes shift for an aged PPS film also implies that the displacement Δ_{if} of the configurational coordinate between two electronic levels in the aged sample is a little smaller than that in the un-aged PPS film. The results of the curve fitting for PL spectra (Fig. 33 and Fig.34) from an unaged and a two-hour aged PPS films, the peak positions and standard deviations for different phonon orders, are listed in Table IV and Table V.

We can relate the Stokes shift $S\hbar\omega$ to the lattice distortion energy and solve the lattice distortion Δ_{if} upon knowing the effective lattice force constant. Using the data obtained in the previous chapter [74], the effective force constant for the phenylene-sulfur displacement is $C_{eff} \approx 16$ (millidynes/angstrom). We can estimate the lattice distortion Δ'_{if} in terms of

$$\Delta'_{if} = \sqrt{\mu}\,\Delta_{if} \qquad (3.25)$$

where μ is the effective mass and Δ'_{if} has the unit of length. The lattice distortion energy, $1/2\ C_{eff}\ (\Delta'_{if})^2$, is equal to the Stokes shift in our model (3.10). We then solved the lattice distortion $\Delta'_{if} \approx 0.065$ Å for the un-aged amorphous PPS film and $\Delta'_{if} \approx 0.062$ Å for the two-hour aged film. The distance between the center of phenylene ring and sulfur atom is 3.13 Å which was obtained from the lattice size of PPS given by B.J. Tabor,

TABLE IV

THE CURVE FITTING RESULTS OF THE PL SPECTRUM FROM AN UNAGED PPS FILM (SEE FIG. 33)

Phonon orders	1	2	3	4
P (cm^{-1})	27,250	26,170	25,094	24,018
σ (cm^{-1})	418	455	483	412

TABLE V

THE CURVE FITTING RESULTS OF THE PL SPECTRUM FROM A TWO-HOUR AGED PPS FILM (SEE FIG. 34)

Phonon orders	1	2	3	4
P (cm^{-1})	27,330	26,250	25,174	24,098
σ (cm^{-1})	397	474	499	447

Note:

In Table IV and V, P represents the peak positions while σ represents the standard deviations for different phonon orders.

et al [77]. The distortion therefore is about 2.1 %. These values are much smaller than the lattice displacement of the ion impurity center in crystal [78,79]. This is reasonable because a π-electron in PPS is shared by six carbon atoms in a phenyl ring rather than confined in a single atomic site. This distortion is larger than the soliton distortion in a trans-polyacetylene, which has a distortion of 0.03 Å along the chain projection [80]. The lattice relaxation parameters for an un-aged amorphous PPS film and a two-hour aged PPS film are listed in Table VI.

It is not surprising of the small Δ_{if}' value compared to that of impurity center in a crystal because in our simplified model the temporary lattice distortion represents the displacement relative to the center of the phenylene ring rather than a single ion site. In general, the strength of the electron-lattice coupling of an electronic state depends strongly upon the spatial extent of that state [81]. If an electronic state were to be confined to a single atomic site, the strength of that state coupling to the lattice would be substantial, that is, very much greater than unity. However, for states of larger spatial extent, the electron-lattice interaction is generally very much smaller. This is because an electronic state only interacts effectively with atomic vibrations of wavelengths greater than its characteristic length. As a result, with a short range electron-lattice interaction (e.g., the deformation potential), the electron-

TABLE VI

THE ELECTRON-PHONON COUPLING PARAMETERS

	$L(cm^{-1})$	$E_1(cm^{-1})$	$E_2(cm^{-1})$	E_1-E_2	S	$\Delta'_{if}(\AA)$
#1	1700	27250	26170	1080	1.6	0.065
#2	1600	27330	26250	1080	1.5	0.062

#1: an unaged amorphous film; #2: a two-hour aged film.
L: Stokes shift; E_1: main peak position; E_2: sideband peak position.

lattice coupling strength varies inversely as the volume of the electronic state. Thus, for example, an electronic state that is confined to a single atomic state has a large electron-lattice coupling strength S. However, if the electronic state were to extend over a large monomer, the coupling to those lattice vibrations would be very weak. These differences are of crucial importance in discussing the magnitude and temperature dependence of the hopping conductivity among such states [81]. As indicated by our absorption results as well as previous studies [13,65], the π-electron in PPS is partially delocalized along the chain, therefore we expect to have a smaller S value. Previous investigations also indicated that both interchain and intrachain crosslinking in PPS occurred during the aging process [82] and the photoconductivity near the absorption edge was significantly enhanced after PPS was annealed in oxygen at temperatures ranging from 250 to 295^{0}C [83]. The intrachain crosslinking will increase the π-orbital overlap along the PPS chain. The increased photoconductivity is the evidence of this behavior. Therefore, the electron-lattice coupling strength could be reduced for aged sample, which is consistent with our PL results.

CHAPTER IV

SUMMARY

This dissertation has reported the results of Raman, absorption, and photoluminescence (PL) experiments performed on various poly (p-phenylene sulfide) films. A phenylene-sulfur stretching vibration model was proposed to interpret the Raman data and the lattice relaxation model was used to explain the PL results.

In chapter I, the recent developments of conducting polymers were addressed. The poly (p-phenylene sulfide) (PPS), referred to as one of the "engineering thermoplastics", has a variety of applications owing to its excellent mechanical, electrical, thermal and chemical resistance properties. PPS was also the first not fully carbon-backbone-linked polymer made highly conducting upon doping. Some extensive studies have been carried out in the last decade. However, because of its chemical complexity and the lack of an attractive physical model such as the soliton in conjugated polymers, the research on the electronic properties of the PPS has lagged behind that on conjugated polymers. Many electronic and lattice dynamical properties of PPS remain to be studied.

In Chapter II the basic vibrational characteristics of PPS and how these change with the chain length and crystalline

content are discussed. A Raman active phenylene-sulfur stretching vibrational model was proposed to describe the main Raman band at 1076 cm^{-1}. The intensity and line profile of this Raman peak were used to characterize the chain length and crystallinity of the PPS film. Based on this model and the observed frequency, the effective stretching force constant and the bending force constant of this Raman mode were determined. In addition, new Raman lines at 840 and 919 cm^{-1} were observed and assigned to the out of plane C-H bending modes. These two Raman lines had been missing in previous studies.

In Chapter III the absorption and PL spectra from two biaxially oriented PPS films and from various amorphous PPS films with different thermal treatment were reported. The exciting source used was at 355 nm with pulse width of 6 ns by a Nd:YAG laser. The singlet $\pi \rightarrow \pi^*$ excitation creates the partially delocalized electron-hole pair which may be described as the localized exciton. The main luminescence of PPS then presumably comes from these intrachain excitons. The π-electron system plays a key role in determining the electronic properties of PPS, such as the conductivity upon doping. Our study indicated that the π-electron in PPS is partially delocalized along the chain and the dominant "electronic" excitations are coupled to chain distortions. Our low temperature measurements show that the PL of PPS films is accompanied by strong phonon sidebands whose frequency is

similar to the phenylene-sulfur stretching vibrations in the polymer backbone. The lattice relaxation model with a two-level system was then developed to analyze the PL data. The low level represents the ground electronic state and the upper level represents the excited electronic state (π^*) of the PPS molecule. Our low temperature PL data were well interpreted by using this model. The electron-phonon coupling strength, the Huang-Rhy's parameter S, as well as the temporary lattice distortion $\Delta_{i,f}'$ were determined for both the unaged amorphous PPS film and the two-hour aged PPS film. The results indicated that the strength of the electron-lattice coupling was slightly reduced after the aging process. This change is expected because the π-orbital overlap along the PPS chain was increased by the crosslinking which resulted from the thermal-aging process. In addition, the luminescence decay lifetime was determined by using a deconvolution method. The room temperature PL intensity and peak shape, which we found to be related to the sample morphology and the thermal process, were also discussed.

BIBLIOGRAPHY

1. C.K. Chiang, C.R. Fincher, Y.W. Park, A.J. Heeger, H. Shirakwa, E.J. Louis, S.C. Gau, and A.G. MacDiarmid, Phys. Rev. Lett., **39**, 1098(1977).

2. S. Roth, in: Electronic Properties of Polymers and Related Compounds, Springer-Verlag, New York, 2(1985).

3. D.M. Ivory, G.G. Miller, J.M. Sowa, L.W. Shacklette, R.R. Chance, and R.H. Banghman, J. Chem. Phys., **71**, 1506(1979).

4. R.H. Baughman, J.L. Bredas, R.R. Chance, R.L. Elsenbaumer, and L.W. Shacklette, Chem. Rev., 209 (1982).

5. N. Basescu, Z.-X. Liu, D. Moses, A.J. Heeger, H. Naarmann, and N. Theophilou, Nature (London), **327**, 403(1987).

6. H. Naarmann and N. Theophilou, Synth. Met., **22**, 1(1987).

7. A.J. Heeger, S. Kivelson, J.R. Schrieffer, and W.-P. Su, Rev. Mod. Phys., Vol. 60, No. 3, 781(1988).

8. D. Moses, A. Denenstein, J. Chen, P. McAndrew, T. Woerner, A.J. Heeger, A.G. MacDiarmid, and Y.W. Park, Phys. Rev. B, **25**, 7652(1982).

9. J.R. Ellis, in: Handbook of Conducting Polymers, ed. by T.A. Skotheim, Vol. 1, Marcel Dekker, Inc., New York and Basel, 489(1986).

10. L.W. Shacklette, R.L. Elsenbaumer, R.R. Chance, H. Eckhardt, J.E. Frommer, and R.H. Baughman, J. Chem. Phys. **75**, 1919(1981).

11. J.F. Geibel and R.W. Campbell, in: Comprehensive Polymer Science, 543(1989).

12. J.N. Short and H.W. Hill, Chem. Technol., 1972, **2**, 481.

13. J.L. Bredas, R.L. Elsenbaumer, R.R. Chance, and R. Silbey, J. Chem. Phys., 78:5656 (1983).

14. J.F. Rabolt, T.C. Clarke, K.K. Kanazawa, J.R. Reynolds, and G.B. Street, J. Chem. Soc. Chem. Commun., **1980**, 347(1980).

15. R.R. Chance, L.W. Shacklette, G.G. Miller, D.M. Ivory, R.L. Elsenbaumer, and R.H. Baughman, J. Chem. Soc. Chem. Commun., **1980**, 348(1980).

16. J.E. Frommer, R.L. Elsenbaumer and R.R. Chance: ACS Symposium Ser. **242**, 447(1984).

17. R.L. Elsenbaumer and L.W. Shacklette, in: Handbook of Conducting Polymer, ed. by T.A. Skotheim, Vol. 1, Marcel Dekker, New York, 214(1986).

18. A.J. Lovinger, F.J. Padden Jr, and D.D. Davis, Polymer **29**, 229(1988).

19. B.J. Tabor, E.P. Magre, and J. Boon, Eur. Polym. J. **7**, 1127(1971).

20. J. Riga, J.P. Boutique, J.J. Pireaux, and J.J. Verbist, Proceedings of the ACS International Symposium on Physico-Chemical Aspects of Polymer Surfaces, New York, 45(1981).

21. Satoshi ASADA, Kazuhiko SEKI, and Hiroo INOKUCHI, Chem. Phys. Lett. **130**, 155(1986).

22. Y. Takai, T. Mizutani, M. Ieda, K. Seki, and H. Inokuchi, Polymer Photochem. **2**, 33(1982).

23. J.L. Bredas, R.R. Chance, R. Silbey, G. Nicolas, and Ph. Durand, J. Chem. Phys. **77**, 371(1982).

24. Hideki Ueno and Katsumi Yoshino, Jan. J. Phys. Soc. **55**, 4382(1986).

25. Yoshikazu Tanabe, Hiroshi Shimizu, and Nobutsugu Minami, Jan. J. Appl. Phys., **27**, 1748(1988).

26. Akio Takimoto, Eiichro Tanaka, and Masanori Watanabe, Jan. J. Appl. Phys., **28**, 1252(1989).

27. K.C. Cole, D. Noel, and J.J. Hechler, J. Appl. Polym. Sci., **39**, 1887(1990).

28. P. Piaggio, C. Cuniberti, G. Dellepiane, and G. Capannelli, Synth. Met., **29**, E61(1989).

29. H. Sakai, T. Matsuyama, H. Yamaoka, and Y. Yutaka, Chem. Phys. Lett., **101**, 490(1983).

30. P. Piaggio, C. Cuniberti, G. Dellepiane, E. Campani, G. Gorini, G. Masetti, M. Novi, and G. Petrillo, Spectrochim. Acta, **45A**, 347(1989).

31. J.P. Buisson, J.Y. Mevellec, S. Zeraoui, and S. Lefrant, Synth. Met. **41-43**, 287(1991).

32. C.-H. M. Ma and L.-T. Hsiue, J. Appl. Poly. Sci. **39**, 1399(1990).

33. S.K. Brauman, J. Poly. Sci. **A27**, 3285(1989).

34. R.H. Friend and J.R.M. Giles, J. Chem. Soc., Chem. Commun., 1101(1984).

35. P. Piaggio, C. Cuniberti, G. Dellepiane, E. Campani, G. Gorini, G. Masetti, M. Novi and G. Petrillo, Spectrochim. Acta **45A**, 347 (1989).

36. It should be noted that the biaxially oriented samples were initially provided by the Toray Corporation.

37. W. Koch and W. Heitz, Macromol. Chem. **184**, 779 (1983).

38. D.H. Whiffen, J. Chem. Soc. 1350 (1956).

39. R.R. Randle and D.H. Whiffen, Molecular Spectroscopy, p. 111. Institute of Petroleum, London (1955).

40. J.P. Buisson, J.Y. Mevellec, S. Zeraoui and S. Lefrant, Synth. Met. **41-43**, 287 (1991).

41. J.F. Geibel and R.W. Campell, in: Comprehensive Polymer Science: The Synthesis, Characterization, Reactions, and Applications of Polymers, ed. by G.C. Eastmond, Vol. 5, p. 545. Pergamon, New York (1989).

42. D.G. Brady, J. Appl. Polym. Sci. **20**, 2541 (1976).

43. T.C.Clarke, E.K. Kanazawa, V.Y. Lee, J.F. Rabolt, J.R. Reynolds and G.B. Street, J. Polym. Sci: Polym. Phys. Edn. **20**, 117 (1982).

44. D.A. Long, Raman Spectroscopy, McGraw-Hill, New York, (1977).

45. N.B. Colthup, L.H. Daly and S.E. Wiberley, Introduction to Infrared and Raman Spectroscopy, p. 64. Academic Press, New York (1975).

46. Ibid, p. 203.

47. K. Huang and A. Rhys, Proc. Roy. Soc. Lond. **A 204**, 406 (1950).

48. K.K. Rebane, Impurity Spectra of Solids, p. 13. Plenum Press, New York (1970).

49. Z. Pan and J.P. Wicksted, Bull. Am. Phys. Soc. **37**, 506 (1992).

50. M.D. Lumb, Luminescence Spectroscopy, Academic Press, New York, 94(1978).

51. A.E. Gillam and P.H. Hey, J. Chem. Soc., 1170(1939).

52. M.H. Whangbo, R.Hoffmann, and B.B. Woodward, Proc. R. Soc. London, Ser. A **366**, 23(1979).

53. D.M. Grant and I.P. Batra, Synth. Met. **1**, 193(1980).

54. J.L. Bredas, R.R. Chance, R. Silbey, G. Nicolas, and P. Durand, J. Chem. Phys. **77**, 371(1982).

55. J.L. Bredas, R.L. Elsenbaumer, R.R. Chance, and R. Silbey, J. Chem. Phys., **78**, 5656(1983).

56. G. Crecelius et al, Physical Review B, **28,** 1802(1983).

57. Kun Huang, Scientia Sinica, China, **116**, 27(1981).

58. Kun Huang, Progress in Physics, **1**, 31(1981).

59. W.A. Phillips, J. Low Temperature Phys., **7**, 351(1972).

60. K. Huang and A. Rhys, Proc. R. Soc. London, Ser. A **204**, 406(1950).

61. B. Di Bartolo, Radiationless Processes, Plenum, New York, 39(1979).

62. Chen-Chi M.Ma, Lin-Tee Hsiue, Wen-Guey Wu, and Wen-Liang Liu, J. Appl Polym. Sci., **39**, 1399(1990).

63. W.T. Ford, Private Communication, Chemistry Department, OSU, (1992).

64. Kun Huang, Contemp. Phys., **22**, No.6, 599(1981).

65. G. Grecelius, J. Fink, J.J. Ritsko, M. Stamm, H.-J. Freund, and H. Gonska, Phys. Rev. B, **28**, 1802(1983).

66. S. Roth, in: Electronic Properties of Polymers and Related Compounds, Springer, New York, 2 (1985).

67. A.H. Alwattar, M.D. Lumb and J.B.Birks, in: Organic Molecular Photophysics, J.B. Birks ed., John Wiley & Sons, New York, 414(1973).

68. A. Takimoto, E. Tanaka, and M. Watanabe, Jan. J. Appl. Phys., **7**, 1252(1989).

69. Kendall L. Su, Time-domain Synthesis of Linear Networks, Prentice-Hall, Inc., Englewood Cliffs, New Jersey, 40(1971).

70. J.P. Wicksted, F.K. Wood-Black, Development of Polyphenylene Sulfide, Proposal, (unpublished, 1990).

71. C.E. Hoyle and K-J Kim, J. Polym. Sci. A, **24**, 1879(1986).

72. W.T. Ford, Private Communication, Chemistry Department, OSU, (1992).

73. Roger Clough, in: Encyclopedia of Polymer Science and Engineering, Vol. 13, ed. by J.I. Kroschwitz, John Wiley & Sons, New York, 687(1988).

74. Z. Pan, T. Savard, and J. P. Wicksted, J. Raman Spectrosc., (to be published), (1992).

75. A.H. Alwattar, M.D. Lumb, and J.B. Birks, in: Organic Molecular Photophysics, Vol. 1, ed. by J.B. Birks, John Wiley & Sons, 421(1973).

76. J. Poplawski and E. Ehrenfreund, in: Electronic Properties of Conjugated Polymers III, H. Kuzmany, M. Mehring, and S. Roth ed., Springer, New York, 86 (1989).

77. B.J. Tabor, E.P. Magre, and J. Boon, Eur. Polym. J., **7**, 1127(1971).

78. M.D. Sturge and H.J. Guggenheim, Physcal Review. B, **2**, 2459(1970).

79. C.D. Struck and W.H. Fonger, J. Luminescence, **10**, 1(1975).

80. A.J. Heeger, in: Handbook of Conducting Polymers, **2**, ed. by T.A. Skotheim, Marcel Dekker, Inc., New York and Basel, 738(1986).

81. D. Emin, in: Handbook of Conducting Polymers, **2**, ed. by T.A. Skotheim, Marcel Dekker, Inc., New York and Basel, 992(1986).

82. A.B. Port and R.H. Still, Polymer Degradation and Stability, **2**, 1(1980).

83. Eiichiro Tanaka, Akio Takimoto, and Masanori Watanabe, J. Appl. Phys. **67**, 842(1990).

84. in: Handbook of Mathematics, High Education Publishing House, Beijing, China, 41(1977).

84. Operation & Maintenance Instructions, SPEX Industries, Inc., New Jewcy, (1990).

85. Certificate of Calibration of a Standard of Spectral Irradiance, Lamp Serial No. EN-23, The Eppley Laboratory, Inc., (1989).

APPENDIX A

THE FREQUENCY FORMULAS FOR PHENYLENE-SULFUR STRETCHING VIBRATION MODES

1. For Alternating Stretching Mode:

In Fig. 35(a) we illustrate the alternating stretching mode in PPS chain. Let M_1 denote the mass of the phenylene ring, M_2 denote the mass of the sulfur atom, η is the displacement between the center of phenylene ring and the sulfur atom, and C_{eff} denote the effective force constant between M_1 and M_2. As illustrated in Fig. 35(a), this alternating chain stretch mode does not involve angle bending in the first order approximation (α is constant). Therefore we only need consider the stretching force directed along the S-ϕ-S line. The resultant force component directed along either bond axis of the ϕ-S group is equal to $C_{eff}\ \eta\ (1 + \cos(180-\alpha)) = C_{eff}\ \eta(1 - \cos\ \alpha)$, where α is the angle between two neighboring S-ϕ-S units. For Raman active modes with wavevector $q \rightarrow 0$, the center of mass of the phenylene group does not move, the equation of motion for M_2 is

$$M_2 \frac{d^2(\eta)}{dt^2} = -C_{eff}(1-\cos\alpha)\,\eta \qquad (A1)$$

Therefore, the vibrational frequency, ν, is given by

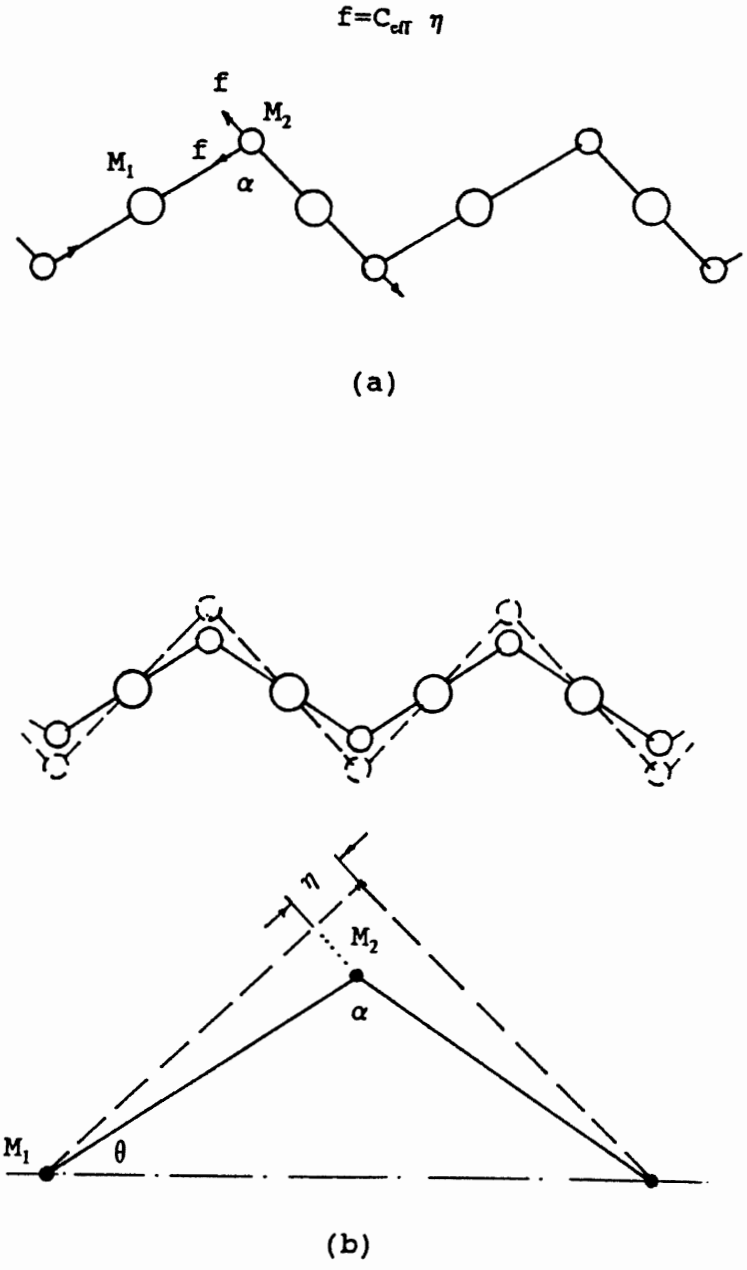

Figure 35. The Alternating and In-Phase Stretching Modes of an Infinite Chain. (a) Alternating Stretching, (b) In-Phase Stretching.

$$\nu = \frac{1}{2\pi}\sqrt{\frac{C_{eff}(1-\cos\alpha)}{M_2}} \qquad (A2)$$

2. For In-Phase Stretching Mode:

In Fig. 35(b) we illustrate the in-phase stretching mode in PPS chain. Because this in-phase vibration involves angle bending, we have to consider the stretching force as well as the bending force. Let L denote the distance between M_1 and M_2. Define the bending force constant ζ as the torque per radian of the angle α deformation. Under the condition that the center of mass M_1 does not move (Raman active mode), we can solve the motion of the sulfur atom with two neighboring springs (Fig. 35(b). The position of M_2 is determined by (r,θ) in a polar coordinates. Let η denote Δr, the kinetic energy T is

$$T = \frac{1}{2}M_2\left(\frac{d\eta}{dt}\right)^2 + \frac{1}{2}M_2L^2\left(\frac{d\theta}{dt}\right)^2 \qquad (A3)$$

the potential energy V is

$$V = \frac{1}{2}C_{eff}(\eta)^2 + \frac{1}{2}C_{eff}(\eta)^2 + \frac{1}{2}\zeta(\Delta\alpha)^2 \qquad (A4)$$

The constrained conditions are

$$\because \frac{1}{2}(\alpha+\Delta\alpha) + (\theta+\Delta\theta) = \frac{1}{2}\alpha + \theta$$

$$\therefore \Delta\theta = -\frac{1}{2}\Delta\alpha \qquad (A5)$$

and

$$\because\ (\Delta\theta)\,L = (\eta)\tan\left(\frac{\alpha}{2}\right)$$

$$\therefore\ \left(\frac{d\theta}{dt}\right)^2 = \frac{\tan^2\left(\frac{\alpha}{2}\right)}{L^2}\left(\frac{d\eta}{dt}\right)^2 \qquad (A6)$$

Using above relations we rewrite T and V as:

$$T = \frac{1}{2}M_2\left(\frac{d\eta}{dt}\right)^2 + \frac{1}{2}M_2\tan^2\left(\frac{\alpha}{2}\right)\left(\frac{d\eta}{dt}\right)^2 \qquad (A7)$$

$$V = C_{eff}\eta^2 + \frac{1}{2}\zeta\,(2\Delta\theta)^2 = C_{eff}\eta^2 + 2\zeta\frac{\tan^2\left(\frac{\alpha}{2}\right)}{L^2}\eta^2 \qquad (A8)$$

The Lagrange is defined as L = T - V, then

$$\frac{\partial L}{\partial \eta} = \frac{\partial V}{\partial \eta} = -2C_{eff}\eta - 4\zeta\frac{\tan^2\left(\frac{\alpha}{2}\right)}{L^2}\eta \qquad (A9)$$

$$\frac{d}{dt}\left(\frac{\partial L}{\partial \dot{\eta}}\right) = M_2\ddot{\eta} + M_2\tan^2\left(\frac{\alpha}{2}\right)\ddot{\eta} \qquad (A10)$$

The equation of motion becomes

$$M_2\ddot{\eta} + M_2\tan^2\left(\frac{\alpha}{2}\right)\ddot{\eta} = -\left(2C_{eff}\eta + 4\zeta\frac{\tan^2\left(\frac{\alpha}{2}\right)}{L^2}\eta\right) \qquad (A11)$$

Using trigonometric relations [84]:

$$1 + \tan^2\left(\frac{\alpha}{2}\right) = \frac{2}{1+\cos\alpha} \qquad (A12)$$

$$\tan^2\left(\frac{\alpha}{2}\right) = \frac{1-\cos\alpha}{1+\cos\alpha} \qquad (A13)$$

we obtained the expression for the in-phase chain stretching frequency

$$\nu = \frac{1}{2\pi}\sqrt{\left[C_{eff}(1+\cos\alpha) + \frac{2\zeta}{L^2}(1-\cos\alpha)\right]\left(\frac{1}{M_2}\right)} \qquad (A14)$$

APPENDIX B

THE CORRECTION FOR SPECTRAL RESPONSE OF THE SPECTROMETER-PMT SYSTEM

The spectrometer used in my photoluminescence study is a SPEX 1404 double grating spectrometer which has two ruled gratings with 1200 gr/mm and 500 nm blaze [85]. As a rule of thumb, the grating efficiency reaches 50 % of the blaze efficiency at two-thirds of the blaze wavelength and at two times the blaze wavelength for single grating. The blaze efficiency is 77 %. The detector used is a HAMAMATSU R943-02 photomultiplier tube (PMT). This PMT has a GaAs(Cs) cathode with a wide spectral response ranging from 160 nm to 930 nm. All lenses used are made of optical fused quartz.

To determine the spectral response of our spectrometer-detector system, I used a standard Quartz Tungsten Halogen (QTH) lamp No. EN-23 from The Eppley Laboratory as a calibration source. The spectral irradiance of this QTH lamp at 7.90 A current was given in power unit by the company [86]. For photon counting electronics, we have to convert the irradiance in the unit of photon rate. I denote the spectral irradiance of the QTH in the unit of photon rate as $E(\lambda)$ which is shown in Fig. 36. The conversion relation is

$$I_{power} = \frac{hc}{\lambda} I_{photon} \qquad (B1)$$

where I is the irradiance, h is the Planck's constant, c is the velocity of light, and λ is the wavelength. Table VII shows the corresponding values in two units.

Using the QTH lamp as the light source and through the spectrometer, scanning from 360 nm to 660 nm, I measured the spectral distribution of the signal from the PMT. The measured spectral distribution of intensity is shown in Figure 37, denoted as R(λ). Comparing Fig. 36 and Fig. 37, the spectrum is significantly distorted by the spectral response of our spectrometer-detector system. We can simply relate the input E(λ) and output R(λ) by the spectral response of our system, S(λ), which is defined as

$$R(\lambda) = S(\lambda)\, E(\lambda) \qquad (B2)$$

The spectral response of our system for unpolarized light is then plotted from 360 nm to 660 nm in Fig. 38. The blaze efficiency was normalized to 60 %, a calibrated value given by Milton Roy company [85]. The values of the spectral response S(λ) from 360 nm to 660 nm are listed in table VIII.

My photoluminescence data were then corrected by this S(λ).

TABLE VII

THE SPECTRAL IRRADIANCE OF THE QTH LAMP

λ (μm)	.350	.400	.450	.500	.555	.600	.655
I_{power}	7.301	19.98	40.90	68.04	101.6	129.0	159.0
I_{photon}	2.56	7.99	18.4	34.0	56.4	77.4	104

where the units of I_{power} is μw cm^{-2} nm^{-1} and the units of I_{photon} is 1/hc cm^{-2} nm^{-1}, both at 50 cm distance.

TABLE VIII

THE SPECTRAL RESPONSE OF THE SPECTROMETER SYSTEM

λ(nm)	360	370	380	390	400	410	420	430
S(λ)	.125	.139	.158	.198	.248	.289	.341	.390
λ(nm)	440	450	460	470	480	490	500	510
S(λ)	.449	.592	.527	.553	.582	.600	.595	.588
λ(nm)	520	530	540	550	560	570	580	590
S(λ)	.575	.560	.545	.525	.508	.478	.453	.419
λ(nm)	600	610	620	630	640	650	660	
S(λ)	.385	.353	.322	.302	.274	.251	.225	

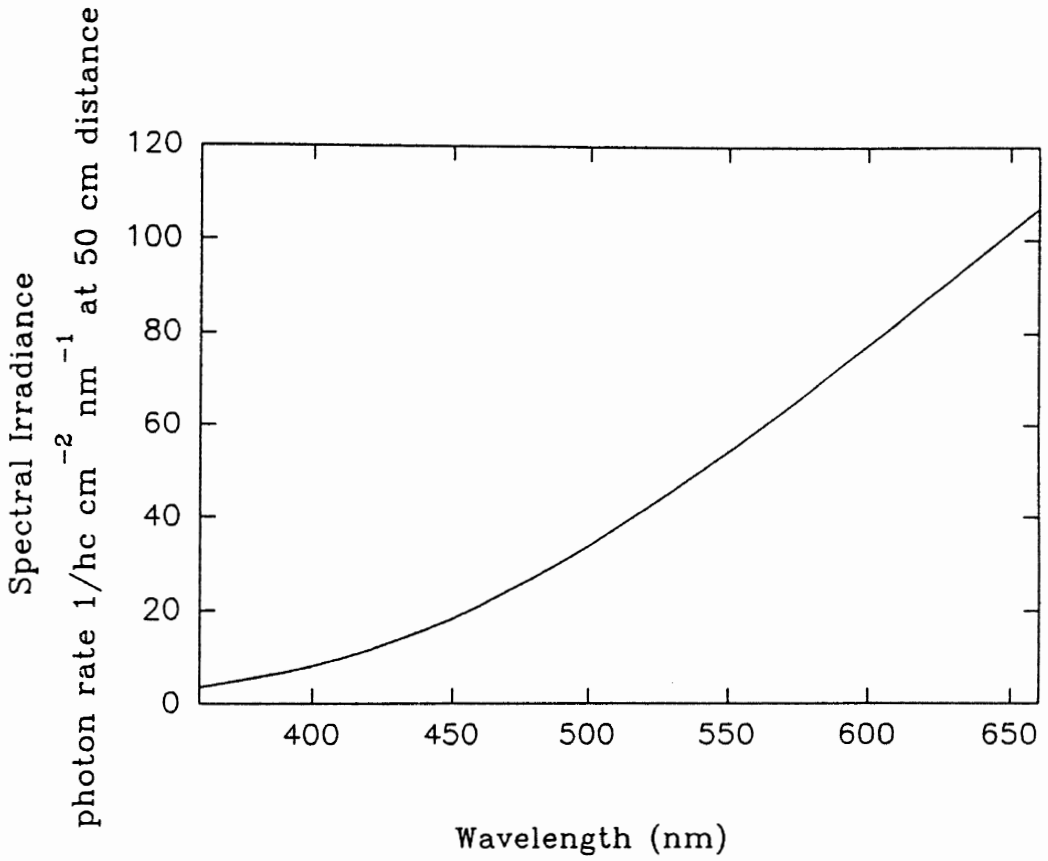

Figure 36. Spectral Irradiance of Calibrated Quartz Tungsten Halogen (QTH) Lamp.

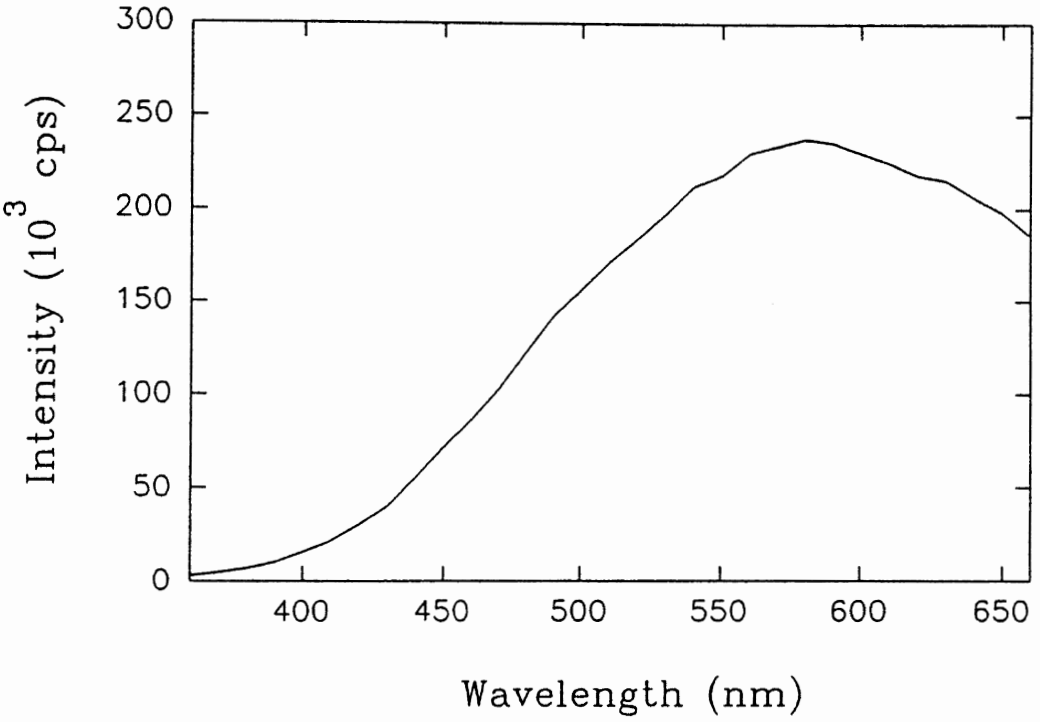

Figure 37. The Measured Spectral Distribution of the QTH Lamp Through the Spectrometer.

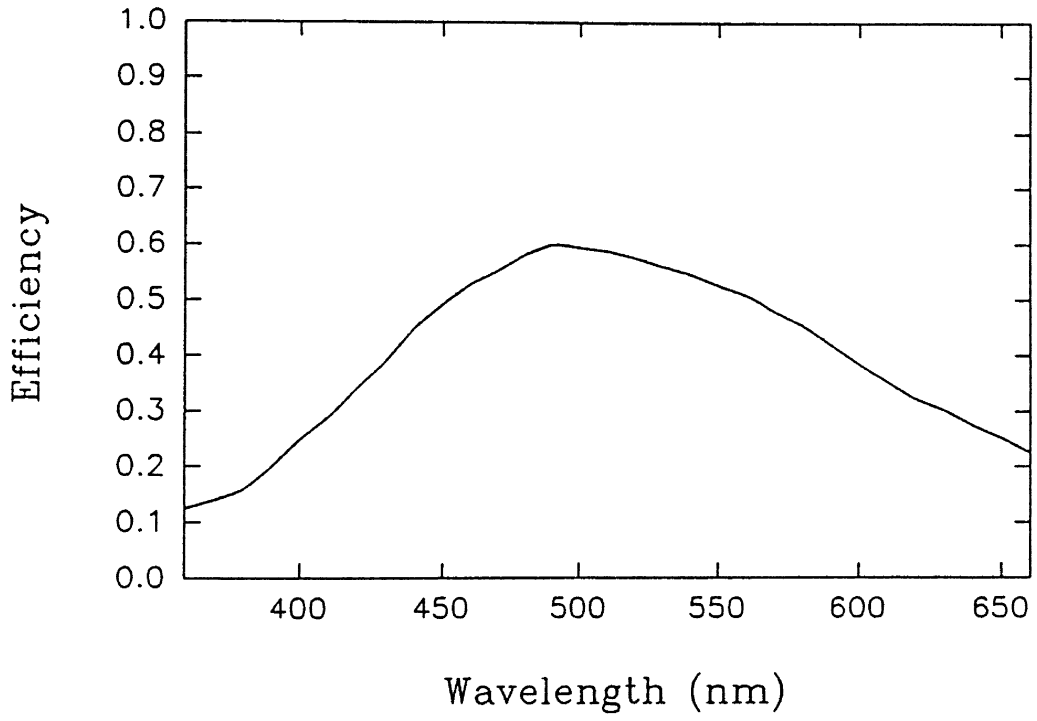

Figure 38. The Spectral Response of the Spectrometer for Unpolarized Light.

VITA

ZHENGDA PAN

Candidate for the Degree of

Doctor of Philosophy

Thesis: RAMAN AND PHOTOLUMINESCENCE STUDIES OF POLY (P-PHENYLENE SULFIDE) FILMS

Major Field: Physics

Biographical:

Personal Data: Born in Shanghai, China, January 26, 1944, the son of Xinghuang Pan and Xigu Zhu.

Education: Graduated from Shanghai School (senior) in July, 1962; received Bachelor of Science degree in Engineering Physics from Tsing Hua University, Beijing, China, in February, 1968; received the Master of Science from Oklahoma State University in December, 1989; completed the requirements for the Doctor of Philosophy Degree at Oklahoma State University in December, 1992.

Professional Experience: Engineer, Jianshi Chemical Fertilizer Plant, Hubei, China, July 1968 to December 1977; Instructor, Physics Department, Huazhong Institute of Technology, January 1978 to March 1979; Lecturer, Optical Engineering Department, Huazhong University of Science and Technology, April 1979 to August 1986; Graduate Teaching Assistant, Oklahoma State University, August 1986 to June 1988; Graduate Research Assistant, Oklahoma State University, July 1988 to present. Member of the Chinese Institute of Electronics. Member of the American Physical Society.